Online Fault Detection for High Temperature Proton Exchange Membrane Fuel Cells

A Data Driven Impedance Approach

Jeppesen, Christian

DOI (link to publication from Publisher):
10.5278/vbn.phd.eng.00002

Publication date:
2017

Document Version
Publisher's PDF, also known as Version of record

ONLINE FAULT DETECTION FOR HIGH TEMPERATURE PROTON EXCHANGE MEMBRANE FUEL CELLS

- A DATA DRIVEN IMPEDANCE APPROACH

BY
CHRISTIAN JEPPESEN

DISSERTATION SUBMITTED 2017

AALBORG UNIVERSITY
DENMARK

Online Fault Detection for High Temperature Proton Exchange Membrane Fuel Cells

- A Data Driven Impedance Approach

Ph.D. Dissertation
Christian Jeppesen

Dissertation submitted March 16th 2017

Dissertation submitted: March 16th 2017

PhD supervisors: Prof. Søren Knudsen Kær
Aalborg University

Søren Juhl Andreasen, PhD
SerEnergy A/S

PhD committee: Associate Professor Zhenyu Yang (chairman)
Aalborg University

Professor Daniel Hissel
University of Franche-Comte

Dr. Holger Janssen
Research Center Jülich

PhD Series: Faculty of Engineering and Science, Aalborg University

ISSN (online): 2446-1636
ISBN (online): 978-87-7112-918-2

Published by:
Aalborg University Press
Skjernvej 4A, 2nd floor
DK – 9220 Aalborg Ø
Phone: +45 99407140
aauf@forlag.aau.dk
forlag.aau.dk

Printed in Denmark by Rosendahls, 2017

List of Publications

The main body of this dissertation is based on the contents of the following papers:

A Christian Jeppesen , Pierpaolo Polverino , Søren Juhl Andreasen , Samuel Simon Araya , Simon Lennart Sahlin , Cesare Pianese , Søren Knudsen Kær. "Impedance Characterization of High Temperature Proton Exchange Membrane Fuel Cell Stack under the Influence of Carbon Monoxide and Methanol Vapor" Submitted to *International Journal of Hydrogen Energy* December 2016. Status: Under Review.

B Christian Jeppesen, Samuel Simon Araya, Simon Lennart Sahlin, Søren Juhl Andreasen, Søren Knudsen Kær. "Investigation of Current Pulse Injection as an On-line Characterization Method for PEM fuel cell stack". Submitted to *International Journal of Hydrogen Energy* January 2017. Status: Under Review.

C Christian Jeppesen, Mogens Blanke, Fan Zhou, Søren Juhl Andreasen. "Diagnosis of CO Pollution in HTPEM Fuel Cell using Statistical Change Detection". *IFAC-PapersOnLine* 48-21 (2015) 547–553. DOI: 10.1016/j.ifacol.2015.09.583

D Christian Jeppesen, Samuel Simon Araya, Simon Lennart Sahlin, Sobi Thomas, Søren Juhl Andreasen, Søren Knudsen Kær. "Fault Detection and Isolation of High Temperature Proton Exchange Membrane Fuel Cell Stack under the Influence of Degradation" Submitted to *Journal Power Sources* January 2017. Status: Under Review.

This dissertation has been submitted for assessment in partial fulfillment of the PhD degree. The dissertation is based on the submitted or published scientific papers which are listed above. Parts of the papers are used directly or indirectly in the extended summary of the dissertation, and referred to as e.g. paper A. As part of the assessment, co-author statements have been made available to the assessment committee and are also available at the Faculty.

In addition to the papers, the following conferences presentations have been conducted:

- "Fuel Cell Equivalent Electric Circuit Parameter Mapping". *CARISMA 2014*, Cape Town, South Africa. December 1st 2014. Poster Presentation.
- "Diagnosis of CO Pollution in HTPEM Fuel Cell using Statistical Change Detection". *9th IFAC Symposium on Fault Detection, Supervision and Safety for Technical Processes* (SafeProcess 2015), Paris, France. September 3rd 2015. Oral presentation.
- "Fuel cell characterization using current pulse injection". *Fuel Cells Science and Technology 2016*, Glasgow, United Kingdom. April 13th 2016. Oral presentation.

The following publications have also been published or submitted during the PhD period, however, are not part of the appended papers included in the partial fulfilment of the requirements for the Ph.D. degree:

- Samuel Simon Araya, Fan Zhou, Vincenzo Liso, Simon Lennart Sahlin, Jakob Rabjerg Vang, Sobi Thomas, Xin Gao, Christian Jeppesen, Søren Knudsen Kær. "A comprehensive review of PBI-based high temperature PEM fuel cells". *International Journal of Hydrogen Energy* 41 (2016) 21310–21344. DOI: 10.1016/j.ijhydene.2016.09.024
- Sobi Thomas, Christian Jeppesen, Samuel Simon Araya, Søren Knudsen Kær. "New operational strategy for longer durability of HTPEM fuel cell" Submitted to *Electrochimica Acta* Status: Under Review.

Abstract

An increasing share of fluctuating energy sources are being introduced in the Danish electricity grid. This is a result of a pursuit of greener energy system, where renewable energy sources produce the electricity. However, this introduces new problems related to balancing the supply and demand, at all times. In Denmark, this problem has so far been addressed by building new high voltage electricity transmission lines to surrounding countries, but with an increasing amount of renewable energy this solution is not feasible in long term. One possible solution could be to introduce electricity storage solutions, that can store the energy from surplus capacity periods and use it in low capacity periods. One way of storing electricity is to produce hydrogen using electrolyzers and utilize it in fuel cells to produce electricity whenever electricity is needed.

For fuel cells to become ready for large scale commercialization, prices need to come down and the durability needs to be improved. One method to improve durability and availability is by designing fault detection and isolation (FDI) algorithms, which can commence mitigation strategies for preventing down time and to ensure smooth fuel cell operation with minimal degradation.

In this dissertation, FDI algorithms for detecting five common faults in high temperature proton exchange membrane fuel cells are investigated. The five faults investigated are related to anode and cathode gas supply. For the anode, the considered faults are carbon monoxide (CO) contamination, methanol vapor contamination and hydrogen starvation. For the cathode, oxidant starvation and too high flow of oxidant are considered.

The FDI algorithms are based on a data-driven impedance approach, where databases containing data from healthy and non-healthy operations are constructed. The fault detection and isolation process has been divided in to three steps: characterization, feature extracting and change detecting & isolation.

For characterization of the fuel cell impedance, two techniques are considered, electrochemical impedance spectroscopy (EIS) and current pulse injection (CPI).

In the CPI method, small current pulses are added to the DC fuel cell current, and based on the corresponding voltage, the parameters of a simple

equivalent electrical circuit (EEC) model can be estimated. The parameters of the EEC model can be used as features for fault detection. The advantage of this method is that it can be implemented simply, using a transistor and a resistor, and although the estimated EEC model is more simple, it might be useful for some FDI applications.

When using the EIS method for fuel cell impedance characterization, a small sinusoidal current is superimposed on the DC current, and based on the corresponding phase shift and amplitude difference, the impedance can be estimated. Based on the fuel cell impedance, two feature extraction methods are analyzed in this dissertation. First, fitting an EEC model to the impedance spectrum and utilizing the EEC model parameters as features. Second, extracting internal relationships of the impedance spectrum, such as angles and magnitudes as features. Knowing the behavior of the features in healthy and non-healthy operation, algorithms are designed for FDI.

For change detection and isolation of the faults, two methods are considered in this dissertation. Firstly, based on an extracted feature, a squared error is calculated and compared to a threshold. Based on this a general likelihood ratio test is designed for detecting an increased level of CO in the anode gas, for a change in the value of a resistor in the EEC model. The algorithm demonstrated the ability to detect CO contamination with very low probability of false alarm. As a second method, an artificial neural network classifier is trained based on a database containing healthy and non-healthy data. This approach is demonstrated in this dissertation, resulting in a global accuracy of 94.6 %, and the algorithm is reported to yield a good detectability for four of the five faults investigated, with the exception of methanol vapor contamination in the anode gas, where it showed difficulties distinguishing between healthy operation and the faulty operation, for the investigated methanol vapour concentration.

Resumé

En stigende andel af fluktuerende energikilder bliver implementeret i det danske elektricitetsnet. Dette er som resultat af et mål om en grønnere elektricitets produktion, hvor vedvarende energikilder spiller en større rolle. Dette introducerer nye problemer, hvor et af dem er at balancere elektricitetsnettet, så udbud og efterspørgsel hele tiden er i balance. I Danmark, er det hidtil løst ved at bygge højspændingstransmissionslinjer til nabolande, men med en stigende andel af produktion fra vedvarende energikilder, forbliver denne løsning ikke holdbar. En mulig løsning kan være at introducere energilagering, der kan lagere energien fra højproduktionsperioder, til senere tidspunkter hvor produktionen fra vedvarende energikilder er lav. Dette kan implementeres ved at producere brint ved elektrolyse, når det er nødvendigt, og brinten kan derved bruges i brændselsceller til at producere elektricitet.

For at brændselsceller kan blive klar til kommercialiseringen i stor skala, er det nødvendigt, at prisen sænkes og at levetiden øges. En måde at øge levetiden og forsyningssikkerheden er ved at designe fejldetektions og isolerings (FDI) algoritmer, som kan iværksætte forebyggende strategier, der forebygger nedetid og sikre et minimum af brændselscelledegradering.

Denne afhandling omhandler FDI algoritmer af høj temperatur PEM brændselsceller, som skal detektere fem typiske fejl. De fem typiske fejl som bliver undersøgt, er relateret til anode og katode gasforsyningen. For fejlene der er relateret til anode gasforsyningen, undersøges karbonoxid (CO) forgiftning, metanoldamp forgiftning og brintmangel. For fejlene der er relateret til katode gasforsyningen, undersøges iltmangel og iltoverskud.

De FDI algoritmer der undersøges, er baseret på den empirisk bestemte brændselscelleimpedans. FDI algoritmerne er designet ud fra databaser, der er sammensat af data fra normal og fejlbaseret drift. FDI processen er opdelt i tre trin: karakterisering, feature udvinding samt forandringsdetektering og -isolering.

For at udføre karakteriseringen af brændselscelleimpedansen, anvendes to forskellige metoder: elektrokemisk impedans spektroskopi (EIS) samt strømpuls injektion (CPI).

Ved anvendelse af CPI teknikken, trækkes små ekstra strømpulse ud over den eksisterende DC brændselscellestrøm, og baseret på den resulterende spænding, kan parametre i en simpel ækvivalent elektrisk kredsløbs (EEC) model estimeres. EEC model parametrene kan bruges som features til fejldetektering. Fordelen ved denne metode er, at den nemt kan implementeres med en transistor og en modstand, og selvom EEC modellen er simpel, kan den muligvis bruges til nogle FDI applikationer.

Ved anvendelse af EIS metoden til at karakterisere brændselscelleimpedansen, overlejres DC brændselscelle strømmen med en sinusformet AC strøm. Baseret på den tilsvarende faseforskydelse af spændingen og amplitude forholdet, kan impedansen estimeres. Baseret på impedancen af brændselscellen kan to metoder anvendes til at beregne features. Ved den ene metode tilpasses en EEC model til impedansspektret, og værdierne fra EEC modelen kan anvendes som features. Ved den anden metode udregnes features baseret på det interne forhold for spektret, såsom vinkler og modulus. Med viden om opførslen af disse features for normal og fejlbaseret drift kan FDI algoritmer designes.

For detektering af fejl på brændselsceller, er to metoder taget anvendt i denne afhandling. Den ene metode er baseret på at udregne kvadratet af afvigelse mellem den karakteriserede feature og den forventede feature. Værdien sammenlignes med en grænsetærskel, hvorved normal- eller fejldrift bestemmes. Denne metode er demonstreret med en GLR-test for en EEC model modstandsværdi, som kan detektere et øget niveau af CO forgiftning i anodegassen. Det er vist at algoritmen kan detektere CO forgiftning med en lav sandsynlighed for falsk alarm. Den anden metode, er baseret på en udvælgelse via et kunstigt neuralt netværk, som er trænet baseret på en database som indeholder normal og fejlbaseret driftsdata. I afhandlingen demonstreres det, at metoden resulterer i en 94.6 % samlet præcision, og derudover er problemer med adskillelse mellem normal drift og fejlstadiet med metanol.

Preface

This dissertation has been submitted to the Faculty of Engineering and Science at Aalborg University in partial fulfilment of the requirements for the degree of Doctor of Philosophy in Energy Technology, and is submitted in the form of collection papers. The work has been carried out at the Department of Energy Technology at Aalborg University. The work is conducted in the frame of the 4M Center research project (Mechanisms, Material, Manufacturing and Management – Interdisciplinary Fundamental Research to Promote Commercialization of HT-PEMFC), which is funded by Innovation Fund Denmark. The PhD project has been carried out in close collaboration with SerEnergy A/S.

This is the end of three years study, and now after 7265 electrochemical impedance spectroscopy measurements, it seems that I have reached the end of the road. It has been a journey, where I have faced many ups and downs, which I would not have overcome if it was not for the encouragement and support of my co-workers, friends and family.

Firstly, I would like to thank my supervisors, Søren Juhl Andreasen and Professor Søren Knudsen Kær, for their ongoing support, guidance and for trusting me with the freedom to go in the directions that I found interesting. Likewise, I would like to thank Associate Professor Samuel Simon Araya for deep discussions and thorough review of my manuscripts.

Thanks go also to Professor Cesare Pianese for inviting me to do my study abroad stay in his group at University of Salerno. A special thanks to Dr. Pierpaolo Polverino for arranging my stay, for enthusiastic discussions and for acting as my Italian interpreter.

Furthermore, thanks to my office mates Kristian, Simon and Sobi, for many long and detailed discussions on both academic and non-academic topics.

Finally, I would like to express my deepest gratitude to friends, family and my girlfriend Thea, without whom I would never have reached the end of the PhD journey. They have always supported me in both ups and downs, and never doubted me.

Christian Jeppesen
Aalborg University, March, 2017

Contents

Chapter 1

Introduction

In recent decades, there has been an increasing focus by researchers and the public on the effects of the emissions from energy production from fossil fuels, which have dramatically increased, since the first industrial revolution [1]. The emission types of focus, is mainly CO_2 and particle matter. In recent years, many politicians have finally changed their interpretation what is caused by man-made, and what is due to changes natural cycles, and opened their eyes for the consequences of this topic [2, 3].

The consequence of the increased emissions of CO_2 are by the Intergovernmental Panel on Climate Change (IPCC) [1] linked to climate change and global warming. By monitoring the global temperature a clear indication on global warming is seen for the last decades, where 2015 and 2016 had the warmest recorded earth surface temperatures, since modern surface temperature records began in 1880 [4, 5].

Climate change has severe effects on human health, such as the spread of disease, reduced access to drinking water, air pollution etc., which is also confirmed by the World Health Organization (WHO) estimates that approx. 150,000 lives have been claimed annually by climate change [6]. In addition to costing lives climate change also causes more extreme weather conditions, and according to estimates by the European Environment Agency, the cost of weather extremes due to climate change, was € 33 billion (in 2015 value) in the period 1980-2015, and varying from annual € 7.5 billion in 1980-1989 to annual € 13.3 billion in the period 2010-2015 [7].

Another consequence of the energy production from fossil fuels, is emissions and formation of particle matter (PM_{10} and $PM_{2.5}$). Besides creating visual smog conditions in larger cities all over the world, such as Beijing, Moscow,

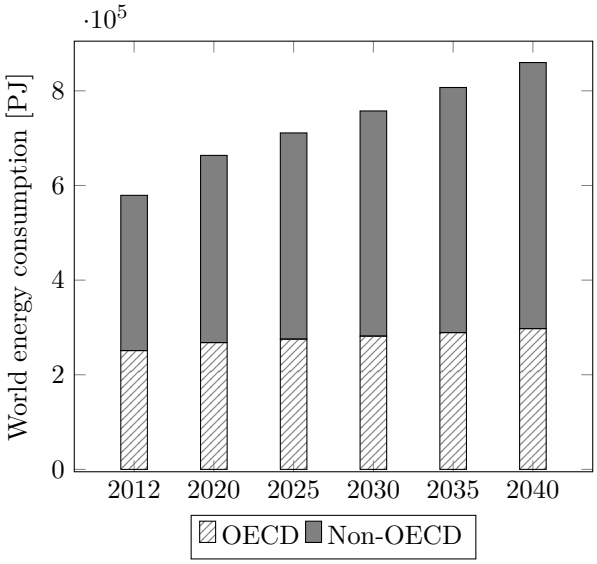

Figure 1.1: Forcast for the worlds energy consumption in Peta joule. Devised by the U.S. Energy Information Administration [18].

Los Angeles, London, Paris and Naples, the particle matter also constitutes a health risk such as premature death, increasing risk for heart or lung disease, etc. [8–12]. Particle matter also contributes to environmental damages, such as depleting the nutrients in soil, making lakes acidic, damaging farm crops, etc. [13–15].

In a study by WHO, it was estimated that globally in 2012, 3 million premature deaths were due to air pollution world wide [16]. A different study by the Health Effects Institute [1] found that 366.000 premature deaths in China were due to air pollution, in 2013 alone [17].

If the global society continues down this lane, producing the majority of energy from fossil fuels, the above problems are only going to grow. In a study by the U.S. Energy Information Agency (EIA) [18], the global energy consumption will increase dramatically with a growing middleclass in developing countries. In Figure 1.1 a prognosis of the worlds energy consumption, in the coming years toward 2040 will increase by 48 % with respect to 2012 values, provided no change in politics and business as usual [18].

Globally most countries are committed to implement changes. As an example, China have committed to spend $ 360 billion on renewable energy before

[1] Receives funding from the U.S. Environmental Protection Agency and U.S. based motor vehicle industry.

2020, and to supply 15 % of their total energy consumption by renewable energy by the year 2020 [19, 20].

In Denmark, the Danish government in 2012 approved the official Danish targets of being fossil free by 2050. A wide range of investments will accomplish this, by improving energy efficiency and installing renewable energy systems. The intermediate goal is to have more than 35 % renewable energy share of total energy consumption by 2020, and to supply approximately 50 % of the electricity from wind turbines, 7.6 % reduction in net energy consumption and to reduce greenhouse gas emisions by 34 % compared to 1990 [21, 22]. The latest prognosis for 2020 from the Danish Department of Energy, Distribution, and Climate, reports that the 2020 goals for the electricity sector will be accomplished, and that wind share in the grid will be 53-59 % [23].

To reach these goals, a broad variety of solutions, such as wind and solar is needed. As a result electricity, will play a larger role in 2050.

1.1 An electrochemical part of the solution

Most renewable energy sources fluctuate, "as the wind blows and the sunshines" so to say. In the Danish energy system, the aim is that more than 50 % electricity should be supplied by wind turbines, on average in 2020. This results in periods with more than 100 % supplied from wind turbines, and periods with negligible supply from wind turbines. In some periods, this becomes a problem since the grid needs to be balanced and the Danish electricity consumers also need electricity when wind production is low [23].

In production periods with more than 100 % electricity supply from wind turbines, this problem has been solved by exporting electricity to the surrounding countries. This is made possible through several established high power transmission lines, through which surrounding countries can purchase electricity when Denmark produces more than needed, or sell when Denmark is in need. [24]

This solution is only feasible when the surrounding countries can purchase, however the surrounding countries do also invest in wind power, and therefore have surplus wind power production, in the same hours as Denmark [25]. With an increasing installment of wind power in Denmark, and surrounding countries a more flexible demand and supply is needed. A flexible demand could be achieved by implementing storage solutions for balancing between energy supply and demand [26].

This storage solution could be achieved by producing hydrogen using elec-

trolyzers, and thereby storing the energy as hydrogen. When grid electricity is in shortage, the hydrogen can be used in fuel cells to generate electricity to balance the electrical grid. Alternatively, the hydrogen could be used in the transport sector for fuel cell electric cars, in micro combined heat and power plants in households, or be used as a building block in the production of synthetic fuels such as methanol [27–29].

1.1.1 Fuel cells

A fuel cell is an electrochemical device, that converts potential chemical energy to electricity. The principle was first described by Grove [30], in 1843, as a gas battery, and has the advantage compared to batteries, that it continuously can produce electricity, as long as it is supplied with fuel and oxidant.

The most common type of fuel cell is the proton exchange membrane (PEM) fuel cell, which uses hydrogen as fuel and oxygen as oxidant, and produces electricity, heat and water. A PEM fuel cell consists of two electrodes, the anode and cathode. In between the anode and cathode, a PEM is located, which only conducts protons. The working principle of a PEM fuel cell is illustrated in Figure 1.2. On the anode side of the PEM, hydrogen is distributed through a gas diffusion layer (GDL) and undergoes the reaction as shown in Equation 1.1. Protons (H^+) move through the PEM to the cathode and the electrons move as electricity through an external load. On the cathode side, an oxygen molecule reacts with four electrons and four protons, and form water, as shown in Equation 1.2. Normally, the cathode side is supplied by atmospheric air, where of approx. 21 % is oxygen.

$$\text{Anode}: \quad 2H_2 \rightarrow 4H^+ + 4e^- \tag{1.1}$$

$$\text{Cathode}: \quad O_2 + 4e^- + 4H^+ \rightarrow 2H_2O \tag{1.2}$$

The two GDLs, two catalyst layers and the PEM are collectively named a membrane electrode assembly (MEA). The MEA is compressed between flow plates, which distributes the hydrogen and the oxygen. One fuel cell MEA has an operation voltage in the range 0.5 V to 0.8 V, which is too low for most applications. Therefore, the MEAs are stacked together for achieving a higher voltage.

There are two types of PEM fuel cells, a low temperature PEM (LTPEM) fuel cell and a high temperature PEM (HTPEM) fuel cell. The most common fuel cell type, is the low temperature PEM fuel cell, which uses Nafion as

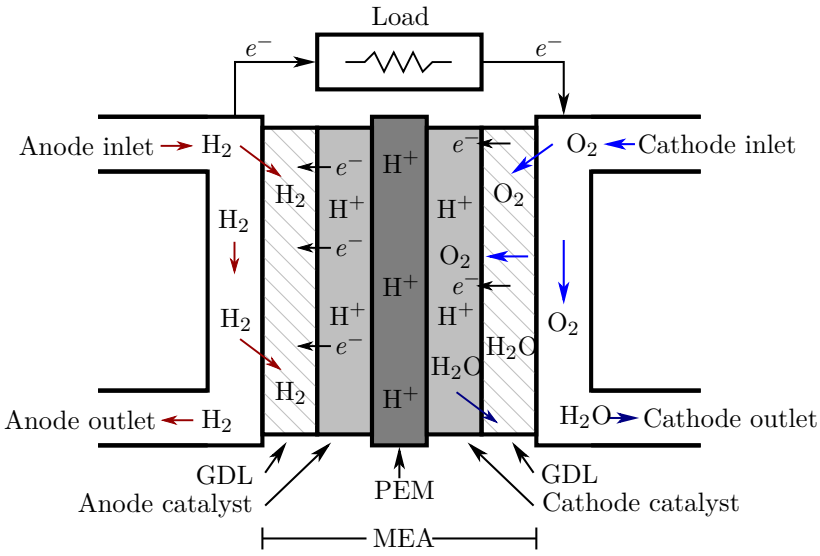

Figure 1.2: Working principle of a PEM fuel cell. Based on illustration from [31].

membrane material, which is operated at temperatures below 100 °C. The other type of PEM fuel cell, is the HTPEM, which uses polybenzimidazole (PBI) doped with phosphoric acid, as membrane material. HTPEM fuel cells operate between 130-220 °C [32, 33]. LTPEM fuel cells require high hydrogen purity of more than 99.9 % [34]. HTPEM fuel cells can tolerate a higher share of impurities in the anode gas, compared to LTPEM fuel cells, and as an example up to 3 % CO at 160 °C is reported in the literature [35, 36]. This is mainly due to lower CO adsorption rates at higher temperatures, and electro-oxidation of some CO into CO2 at higher temperature. In addition, since HTPEM is operated at above 100 °C, problems with flooding never occurs, and water management are thereby more simple. Furthermore, the waste heat quality of a HTPEM fuel cell is higher compared to LTPEM fuel cells.

The disadvantage of HTPEM fuel cells, are that start-up time is longer, efficiency is lower and the lifetime is shorter compared to LTPEM fuel cells [33, 37]. This is also natural since HTPEM fuel cells have been under development for a shorter period, and the gap between them is closing.

Since HTPEM fuel cells can be operated with a higher share of impurities in the anode gas, they can be deployed together with a reformer and run on reformate gas, without a gas purification system.

1.1.2 Reformed methanol fuel cell systems

In most fuel cell applications the cathode oxygen is supplied by a fan using the surrounding atmospheric air. The anode gas is most often supplied from a high pressure hydrogen vessel, using a pressure from 20 – 70 MPa. This storage method requires a very carefully designed hydrogen vessel and the energy density is lower compared to gasoline. Other applications store the hydrogen in liquid form (-253 °C), or using metal hydrides [38]. However, these methods are expensive and heavy.

Alternatively, hydrogen can be stored in liquid form at room temperature, as a alchohols such as methanol (CH_3OH) or ethanol (CH_4OH). The advantage is higher energy density compared to compressed hydrogen and more ease of transportation and storage. For fitting in the fossil free synergy described in the beginning of chapter 1, the fuel must be produced based on electricity from renewable sources and CO_2 [39].

One promising fuel is methanol, which can be used directly in direct methanol fuel cells (DMFC). Alternatively, methanol can be converted into a hydrogen rich gas through methanol steam reforming [40], which can be used in hydrogen PEM fuel cells. Instead of methanol, ethanol could also be used in a steam reformer, however this requires higher reforming temperatures.

The Danish chemist J. A. Christiansen described methanol steam reforming in a study from 1921, conducted at University of Copenhagen, where he discovered that by running a water and methanol mix across a reduced copper surface at 250 °C, it would convert to a gas containing hydrogen and CO_2 [41–43].

The methanol steam reforming reaction can be seen in Equation 1.3:

$$CH_3OH + H_2O \rightarrow 3H_2 + CO_2 \qquad \Delta H^0 = +49.4 \left[\frac{\text{kJ}}{\text{mol}}\right] \tag{1.3}$$

If oxygen is available, an exothermic reaction between methanol and oxygen can occur as a partial oxidation as shown in Equation 1.4. The reaction occurs in the temperature range 180 – 300 °C.

$$CH_3OH + \tfrac{1}{2}O_2 \rightarrow 2H_2 + CO_2 \qquad \Delta H^0 = -192.2 \left[\frac{\text{kJ}}{\text{mol}}\right] \tag{1.4}$$

In a likewise temperature range a decomposition of methanol also occurs as shown in reaction scheme 1.5, which outputs two parts hydrogen and one part CO.

$$CH_3OH \rightarrow 2H_2 + CO \qquad \Delta H^0 = 198 \left[\frac{\text{kJ}}{\text{mol}}\right] \tag{1.5}$$

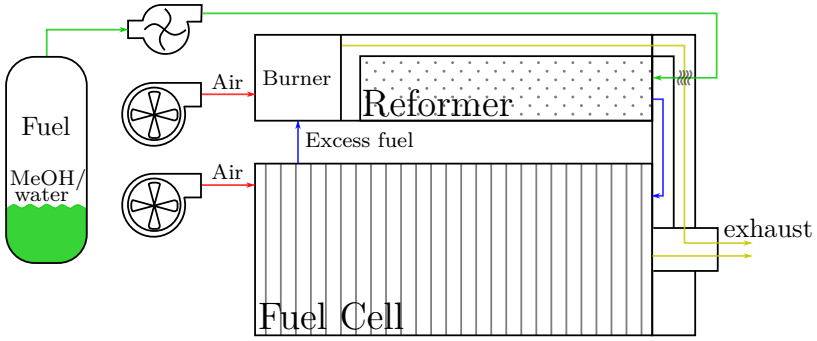

Figure 1.3: A simplified schematic diagram illustrating the principle of a reformed methanol fuel cell system [44]. Blue lines display syngas, red lines air, green lines methanol and water fuel mix and the brown lines display movement of warm gases.

Parts of the CO produced by methanol decomposition are removed by a water gas shift reaction:

$$CO + H_2O \rightarrow H_2 + CO_2 \qquad \Delta H^0 = -41.1 \left[\frac{\text{kJ}}{\text{mol}}\right] \tag{1.6}$$

Designing the reformer with a good trade-off between steam reforming and partial oxidation, the reforming reactions can be self-sustaining, without any external heat supply. The water gas shift reaction can be controlled by adjusting the temperatures, and thereby the concentration of CO in the output gas.

A reformed methanol fuel cell (RMFC) system could be composed as shown in Figure 1.3, which is the working principle of a commercially available RMFC system [44]. The RMFC system in this configuration was first suggested by Kurpit [45], in 1975. The RMFC system configuration as shown in Figure 1.3, utilizes the anode exhaust gas in a burner. The burner is thermally connected with the reformer and fuel evaporator, and thereby provides necessary heating for the system process.

The reformer output gas flow therefore needs to be controlled in such a manner that it never brings the fuel cell in hydrogen starvation, and must never create temperature spikes in the burner. Control of the reformer output gas flow, is a process linked with large time delays, and that is why the control of a RMFC system is an interesting task for control engineers.

A RMFC system in the configuration shown in Figure 1.3, is not able to start-up, but need an external source of heating, such as electric heaters. In some configurations the external heat source is a combination of electric heaters in the burner and the methanol/water fuel being feed into the burner.

In the RMFC system configuration as shown in Figure 1.3, the reformer output gas is connected directly to the anode input on the fuel cell, without any gas purification system. The fuel cell therefore needs to be robust toward impurities such as CO and methanol vapor. As mentioned in the end of section 1.1.1, HTPEM fuel cells can operate with a higher share of impurities compared to LTPEM, and they are well-suited for this type of application.

Faults on RMFC systems

One of the advantages of RMFC systems, such as the concept illustrated in Figure 1.3, is a potentially higher reliability and availability compared to its internal combustion engine counterpart. However, the reliability and availability of RMFC systems can be jeopardized by several faults occurring on sensors, actuators or on the control system.

The Department of Energy (US) has in their program, set a target for the lifetime of fuel cell applications, which needs to be fulfilled for fuel cell systems' commercial competitiveness, compared to other available electricity generators. This target has been the global target for fuel cells systems, and demands 40,000 h for stationary and 5,000 h for automotive, before degrading to 80 % of rated power [46]. For this reason it is desirable to detect and isolate faults on fuel cell systems, in order to commence a mitigation strategy.

Any fault on the RMFC system, will result in a fault on the most expensive component; the fuel cell stack. A fault on the fuel cell stack will easily lead to an increased degradation which would yield a decreased lifetime of the fuel cell. The different faults lead to different degradation mechanisms, which leads to a degraded fuel cell. Most degradation mechanisms lead to a decrease in electrochemical surface area, while some leads to membrane degradation or loss of carbon support. The loss of electrochemical surface area is related to a reduction on platinum catalyst or adsorption of impurities on the catalyst sites. The membrane degradation is a result of e.g. leaching of phosphoric acid or membrane tinning and pin hole formation, because of hotspots. The loss of carbon support, can also lead to membrane tinning, but are most often related to change in the gas diffusion layer or the carbon support in the catalyst layer [47, 48].

The input and output of the fuel cell stack is the anode and cathode gases, and the coolant. In this dissertation, the considered faults, will be limited to faults occurring based on abnormalities in anode and cathode gases, and can be summarized as five different faults (ϕ_1-ϕ_5).

Faults related to the air delivery system, can be divided into two cases:

ϕ_1 A decrease in cathode stoichiometry (λ_{Air}). The occasion could be a faulty fan/compressor, or a gas channel blockade or reduction. Alternatively, the system could be deployed at high altitude, without control adjustments.

ϕ_2 An increase in cathode stoichiometry (λ_{Air}). The occasion could be a change in fan/compressor characteristics or a software error.

Faults related to the anode gas delivery system, can be divided into three cases:

ϕ_3 An increase of carbon monoxide in the anode gas. The occasion could be a change in the temperature profile of the reformer, or a degradation on the reformer catalyst.

ϕ_4 An increase of methanol vapor in the anode gas. The occasion could be a change in the temperature profile of the reformer, or a degradation on the reformer catalyst. Alternatively, it could be due to more methanol delivered by the methanol pump than expected or a fault on the methanol evaporation system.

ϕ_5 A decrease in the anode stoichiometry (λ_{H_2}). The occasion could be a decrease in methanol delivered by the methanol pump or due to a degradation on the reformer catalyst. Alternatively, a gas channel blockade or reduction.

1.2 Project objective

The primary objective of this PhD study is to advance the fundamental knowledge about fault detection and isolation on HTPEM fuel cell stacks, which are deployed in RMFC systems. The faults considered is limited to faults related to anode and cathode supplies.

It is a requirement specified prior the project, that the fault detection and isolation algorithms must not rely on additional sensors, and only depend on available measured signals.

Chapter 2

Diagnostics of Fuel Cells

To extend the life time of fuel cells, effort must be put into research improving MEA materials, design of bipolar flow plates and optimal control of the fuel cell operation. In addition to this, proper fault detection and isolation (FDI) algorithms must be designed, to prevent them from causing an increased degradation of the fuel cell.

In the final construction, the diagnostic algorithm will be a part of a health management system, which has the purpose of maintaining the fuel cell operation in a reliable way to extend the lifetime [49].

For FDI algorithms to be successful, they must be able to function in-situ in a non-intrusive manner. Furthermore, it is desired that the algorithm can function without any additional sensors, and must therefore rely on fuel cell voltage, current and temperature, as measured signals. This requirement is desired for reducing the cost of the fuel cell system, reducing the complexity and most importantly for increasing the reliability.

This chapter aims at describing the state of the art within the research areas of FDI of fuel cells.

Most available fault detection (FD) algorithms for fuel cells function as shown in Figure 2.1. The characterization is based on direct measurements, conducted on the fuel cell system or a specific characterization technique such as e.g. estimating the fuel cell impedance, the total harmonic distortion or the like. The feature extraction could be based on e.g.: calculating a residual between a model and the measured signal, estimating a model parameter, calculating a maximum phase for the impedance spectra or the like. The selected feature is then used for determining whether the fuel cell is in normal operation, and could be based on e.g. comparing to a threshold, a machine learning approach

Figure 2.1: "*Flow chart of most available methods for fuel cell fault detection.*" Paper B

or the like.

In general FD of fuel cells can be accomplished quite straight forward by monitoring the fuel cell voltage. An example of this is given in Figure 2.2, where in the left column ((a),(c),(e)) a high CO in the anode gas fault (0.5 % to 2.5 %), is analyzed and in the right column ((b),(d),(f)) the occurrence of a low cathode stoichiometry ($\lambda_{\text{Air}} = 4$ to $\lambda_{\text{Air}} = 1.5$) fault is analyzed. In both columns, the fault occurs at 150 s (marked by a vertical black line in the two top plots in Figure 2.2). The voltage data illustrated in the top row of Figure 2.2, is collected in the initial phase of experiments for Paper D.

For illustrating how fault detection can be performed using the voltage as characterization method, two feature extraction methods are used for detecting the two faults above. In Figure 2.2.c and 2.2.d, the squared error of the above voltage signal is illustrated. The squared error is calculated as the square of the residual between the expected value of the voltage and the actual voltage. It is clearly seen that the voltage drops when the fault is introduced. The squared error can then be compared to a threshold (horizontal dashed line in Figure 2.2.c and 2.2.d) for determining if the fuel cell is in non-healthy operation.

In Figure 2.2.e and 2.2.f, the standard deviation of the voltage signal is shown. The standard deviation is calculated based on a moving window of length 10. It is clearly seen that the standard deviation of the voltage signal increases when the two faults are introduced. The standard deviation can again be compared to a threshold, for determining if the fuel cell is in non-healthy operation.

These two simple methods can be used for fault detection of a fuel cell, alternatively the voltage variance or voltage gradient could be used in a similar way. The advantages of these methods are that they are easy to implement, are low in computational cost and can be performed at a low sampling rate of the voltage. Even though the methods above are suitable for fault detection of fuel cells, it is questionable whether the methods can be used for full fault identification, meaning determining what kind of fault, the amplitude and the location of the fault.

One evident method for isolating the faults that occur on a fuel cell system, is installing additional sensors for monitoring extra states of the system. It could be obvious to install e.g. flow meters, advanced humidity sensors, gas

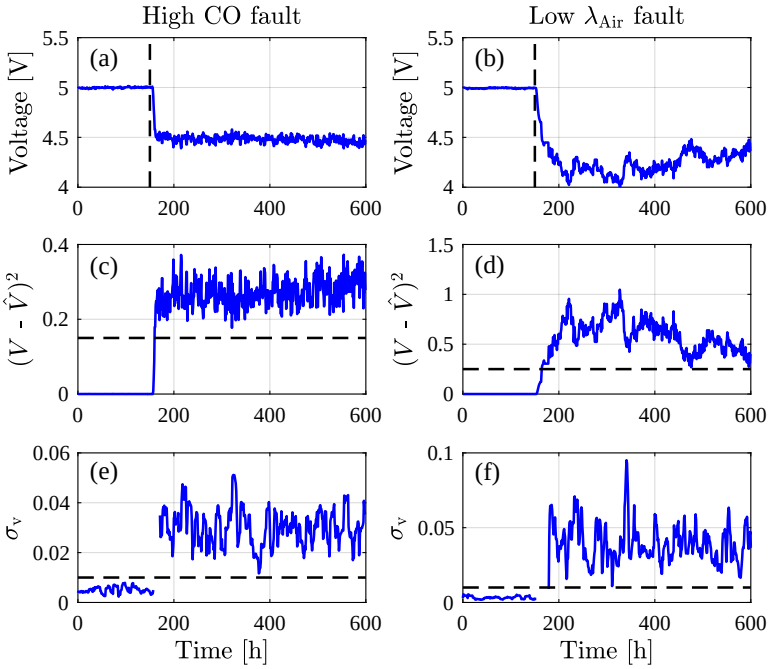

Figure 2.2: **(a)** Fuel cell voltage during a high CO in the anode gas fault. **(b)** Fuel cell voltage at the occurrence of a low cathode stoichiometry (λ_{Air}) fault. Both faults occurs at 150 s. **(c)** and **(d)** The squared error of the above signal. **(e)** and **(f)** Standard deviation of the voltage signal above (moving window of size 10). The data is collected in the initial phase of experiments for Paper D.

analyzers, however, this would increase the cost of the fuel cell system and reduce the power density of the system. Therefore, if additional sensors are to be installed, it is important that they are at low cost and size. Several studies have addressed this approach such as in the work by Lee and Lee [50], a metallic micro sensor was described for the detection and isolation of anode and cathode starvation. In a similar manner, Lee et al. [51] installed micro-electro-mechanical sensor, for estimating the flow, temperature and voltage, inside a HTPEM fuel cell. Alternatively, many studies have investigated small differential pressure sensors, for detecting a flooding state of LTPEM fuel cells [52–54], or other types of sensors for detecting flooding and drying of LTPEM fuel cells, such as hot wires [55, 56] or acoustic emission sensors [57]. But, as mentioned earlier in this section, adding additional sensors is not desired. Therefore, different methods needs to be addressed for fault detection and isolation for fuel cells, which will be addressed in the following section.

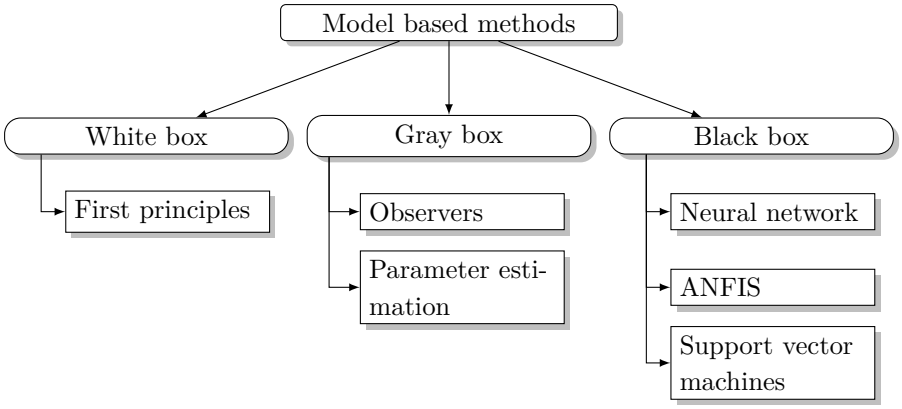

Figure 2.3: Different available model based diagnostic methods for fuel cell applications. Inspired by [62]

2.1 State of the Art on Fuel Cell FDI

Even though FD on fuel cells are straight forward, isolating what fault occurred is more challenging. This is why, many fuel cell researchers focus on experimental characterization and mathematical modeling and fault diagnostics of fuel cells, for accomplishing FDI of fuel cells. Activities on online diagnosis of fuel cells started in the early 2000s [52, 58, 59], and are now spread-out around the world. The studies done on fault detection and isolation often focus on low temperature PEM fuel cells, and are often related to water management problems [60, 61]. The studies done within HTPEM fuel cells are limited, and the literature study in section 2.1.1 and 2.1.2 will therefore include studies on all types of fuel cells, where the two sections will focus on model based and non-model based methods, respectively. Section 2.1.3 will focus on state of the art of diagnostics of HTPEM.

2.1.1 Model based

Model based FDI of fuel cells can be divided into three categories; white box, gray box and black box based models, as shown in Figure 2.3. These three categories, can then be divided into different subcategories.

White box model based FDI approaches often rely on a set of non-linear first principle algebraic and differential equations, which mathematically describe the behavior of fuel cells. For fuel cells, this yields a multiscale, multidimensional and multiphysical model, with a wide span of time constants. The time scales vary from micro second range of electrical power and electrochemical

reactions, to temperature changes of minutes.

For diagnostic purposes, the white box model is simulated online with the same inputs as the physical system, and the model output is used for calculating a residual between the model and output of the physical system. There are a few studies in the literature pursuing this direction, as in Escobet et al. [63], where a relative fault sensitivity method is used for detecting faults on auxiliary components of a LTPEM fuel cell system. In the studies by Rosich et al. [64, 65] and Yang et al. [66, 67], a structural model approach was presented for FDI on auxiliary components of a LTPEM fuel cell system. In the work by Polverino et al. [68], a white box model based on first principles was used for calculating residuals for binary decision, isolating the faults using a fault signature matrix. Simulating a complex white box model is in many cases too computationally intensive for online use, and are therefore, not suitable for online FDI of fuel cell systems. A similar approach is attempted in Polverino et al. [69], using static scalar values for describing the nominal operation conditions and without a model of the fuel cell. For this reason, the presented algorithm will not function, under the influence of degradation.

Gray box models are in general built on first principle equations but are supported with prior knowledge or are heavily simplified. Often, gray box models are based on a set of linear equations, which e.g. can be put on a state space form, and used in cooperation with an observer. In the study by De Lira et al. [70, 71] a Luenberger observer is designed based on a linear parameter varying dynamic model, which is able to detect four typical sensor fault scenarios, and utilizes an adaptive threshold for robustness of the proposed algorithm. For FDI on the actual fuel cells, this approach is only useful if a dynamic linear model is available in the literature, which is not the case for any type of fuel cell. Fuel cell models build on first principle equations are often very complicated on a microscopic scale, and not suited for linearization. Alternatively, the models that are simple and fast executable are empirical data driven and far away from physical relations.

Another gray box model FDI approach is parameter estimation, which can be performed on a low cost micro controller during the operation of the fuel cell. The estimated parameter, which is related to a specific behavior of the fuel cell can then be compared to the normal value. If the value differs from the normal value and it can be linked to a specific fault, the fault can thereby be isolated.

A well described powerful method for characterization of fuel cells is electrochemical impedance spectroscopy (EIS) [72–75]. The method empirically determines the impedance for a given range of frequencies, and yields an instant

of the dynamic behavior. The method will be further described in section 3.2. A common approach for quantifying the impedance is to estimate parameters of an equivalent electrical circuit (EEC) model [76–79]. For the application of FDI of fuel cells, the parameters of the EEC model can be used as features for determining whether the fuel cell is in healthy or non-healthy operation. The EEC model used for FDI propose is most often a modified version of the Randles circuit [80, 81], or a series of RC circuits [82, 83].

In the study by Fouquet et al. [81], a Randles-like EEC model was fitted to the acquired EIS measurements, and the three resistances of the EEC model were used for FDI of flooding, drying and normal operation. The isolation is shown graphically but no explicit algorithm or threshold for online implementation is suggested, which is common for early publications for fuel cell FDI. In the study by Tant et al. [84], the EEC model parameters were used to detect flooding and drying. In a study by Mousa et al. [85] a LTPEM fuel cell is characterized by EIS for hydrogen leaking cells into the cathode side, and quantified by the parameters of a simple Randles EEC model, and in a later paper [86], the findings are coupled with a set of fuzzy rules, for online implementation of the algorithm. In the work, no other faults were considered. In the study by Konomi and Saho [87],[88], a Fast Fourier Transform of a LTPEM fuel cell voltage was used to estimate the fuel cell impedance, and an EEC model of three RC circuits was fitted to the impedance. In the work seven faults were investigated and the faults were isolated based on a fault signature matrix and a set of rules, using the resistors of an EEC model as fault features.

In the work by Génevé et al. [82], a time-constant spectrum is estimated by applying small current steps, and thereby a series of RC circuits. Génevé et al. [82] then utilized the peak amplitude of the resistance and time constant as features for comparing them to a threshold for fault detection. In the work only flooding is considered.

In some of the above references, EIS is used for the characterization of the fuel cell. EIS measurements on laboratory scale are traditionally performed by expensive potentiostats and spectrum analyzers. The online implementation of EIS measurements on the DC/DC converter was suggested by Narjiss et al. [89] and Bethoux et al. [90], and investigated in depth by the two EU projects D-code[1] and Health code[2]. In this dissertation, all EIS measurements are performed by a commercial potentiostat, but it is assumed that the EIS measurements can be performed online by a DC/DC converter.

The advantage of white and gray box models is their ability to adapt and

[1]Fuel Cells and Hydrogen Joint Undertaking (FCH JU) under grant agreement No 256673.
[2]Fuel Cells and Hydrogen Joint Undertaking (FCH JU) under grant agreement No 671486.

detect faults that are not previously seen, by linking a physical parameter directly to a new fault. However, the problem with model based FDI of fuel cells is that the quality, accuracy and robustness are directly linked to the model performance, and a very large number of parameters are needed for fuel cell modelling. This is most likely also why all white box model FDI approaches have focused on auxiliary components. No model based FDI studies have yet described a method, which take degradation of the fuel cell into account, which is needed for the method to function during the entire lifetime of the fuel cell.

The third category on Figure 2.3 of model based FDI of fuel cell, is a black box approach. Black box models are a data driven approach to establish a relationship between inputs and outputs, and do not rely on any physical relations. Black box models are well suited for online implementation and for modelling of complex non-linear systems such as fuel cells. The down side of the method is that it requires a large data foundation and that the implementation of new functionality requires new experiments. The three most common black box models for fuel cells are Artificial Neural Networks (ANN) [91–93], Support Vector Machines (SVM) [94–96] and Adaptive Neuro-Fuzzy inference system (ANFIS) [97–99], and all of them can be static or dynamic models.

In the study by Steiner et al. [100], an ANN model was used to model the pressure drop over a LTPEM fuel cell stack, using fuel cell current, stack temperature, cathode gas dew point and cathode gas volume flow. The modelled pressure drop was then compared to the measured pressure drop and a residual was calculated as fault feature, and the method was successfully demonstrated. The study was extended by the same authors [101], where in addition to the above model, the ANN model was trained to also have the voltage as output. By comparing the two outputs to the measured signal, two residuals can be calculated as fault features, and by comparing the two residuals to thresholds a rule decision based FDI algorithm can distinguish between flooding, drying and normal operation of a LTPEM fuel cell. The same approach was used by Sorrentino et al. [102], where a black box static model of the voltage of a solid oxide fuel cell (SOFC), using 12 inputs of fuel cell current and different temperatures and flows was utilized to detect 4 different faults, operation under high temperature gradients and anode re-oxidation at degraded and non-degraded operation. The accuracy of detection of the faults varied from 32.81 % to 88.75 %. The work concludes high accuracy and reliability, but it neither comments on false alarm or false detection, nor mentions the implementation of the method for online use.

To summarize, the model based FDI approaches for fuel cells rely on calculating a residual based on a model of one or more of the fuel cell states or an

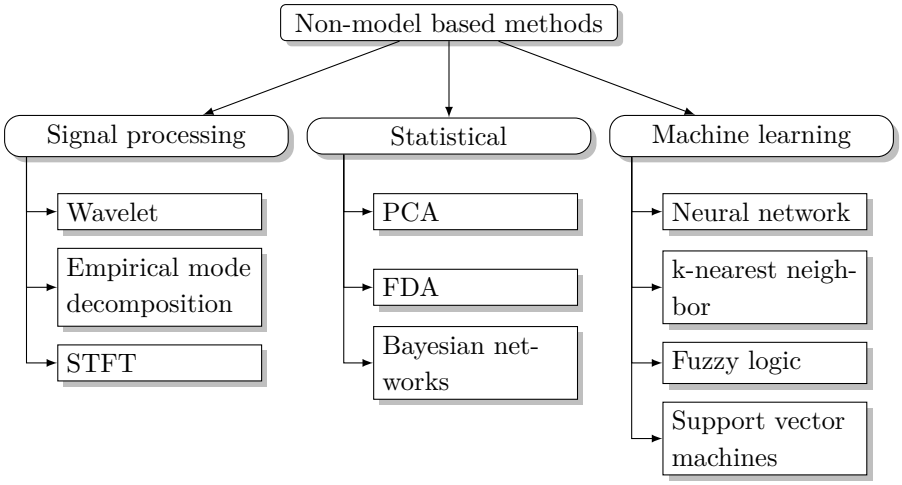

Figure 2.4: Different available non-model based diagnostic methods for fuel cell applications. Inspired by [103]

estimated parameter, which is compared to a threshold. For fault isolation, a fault feature matrix is most often used for linking different feature signatures to a specific fault.

2.1.2 Non-model based

Non-model based FDI methods of fuel cells are also often divided into three categories: Signal processing, Statistical and Machine learning, as shown in Figure 2.4. These three categories can then be divided into different subcategories.

Signal processing non-model based FDI approaches for fuel cells use signal processing methods of raw measured signals to detect and isolate faults on fuel cell systems, often over a sliding window. The methods detect a change of signal oscillations or harmonics when the fuel cell go into non-healthy operation. There are many different approaches and methods to signal processing [104] for FDI, but the most described in the literature are Wavelet transform (WT), Short time fourier transform (STFT) (in different formulations), Singularity spectrum (SS) and Empirical mode decomposition (EMD).

Wavelet transform (WT) is a method for feature extraction of a measured signal. The WT method reconstructs the measured signal, by a series of superpositioned wavelets, of which the set of decomposition signals can be used as fault features. For isolation of the faults, the WT must be utilized in co-

operation with a fault classifier, such as an ANN, SVM or a fault signature matrix.

For using the WT for FDI of fuel cells often the measured signal is the fuel cell voltage, but examples of the WT of the pressure drop across the fuel cell stack is also reported. In the study by Ibrahim et al. [105], WT of the measured LTPEM fuel cell voltage was used to distinguish between normal operation, flooding and drying. In the work, a comparison between the continuous WT and the discrete WT was performed, and they concluded that the discrete WT was superior based on evaluation time and the localization of the beginning and end of the faulty mode. In the work no classifier was suggested for fault isolation. In the study by Rubio et al. [106], the WT of the measured LTPEM fuel cell voltage under steady state operation, was utilized for detecting three faults: flooding, drying and the cathode stoichiometry. A Chebyshev distance residual was used for comparing the normal operation conditions, and a fault signature matrix was used for fault isolation.

In the study by Pahon et al. [107], using the WT of the air pressure drop across the fuel cell stack, for detecting three faults: an emulated electrical short circuit fault, high air stoichiometry fault and a cooling system fault. In the study, the authors claim that the faults can be isolated, but do not demonstrate it or propose a classifier algorithm.

An extended feature extraction method to the WT is the Wavelet Transform Modulus Maxima as suggested by Benouioua et al. [108], for using as fault feature for FDI of fuel cells. In the work by the same authors [109], the same method was applied for FDI of five faults on a LTPEM fuel cell, using a k-nearest neighbor (kNN) and support vector machines (SVM) as fault classifier, which yielded a 91 % global accuracy, with 25 % probability of false alarm. The authors described a small computational time of the method. Wavelet leader was used as features on the same dataset in a study by the same authors [110], in which it was investigated the performance of the classifiers for different number of extracted features, where the best global accuracy was 90 % by kNN [111].

There are several different methods available for converting a signal from the time domain to the frequency domain. The most common ones are based on different versions of the Fourier Transform, such as Fast Fourier Transform (FFT) or the Short-Time Fourier Transform (STFT). By this transformation, the signal is represented as a series of magnitude and phase components, which can be used as fault features. The Fourier Transform is therefore, a feature extraction method comparable to the wavelet transform, and needs a fault classifier for isolation of faults. In most cases, this method is used for analyz-

ing the fuel cell voltage, where the system is excited by a small AC current perturbation, superpositioned on the fuel cell DC current. This is also known as EIS measurement, which is referred to in subsection 2.1.1. It is demonstrated that FFT can be implemented on the DC in the study by e.g. Katayama and Kogoshi [112] and others. However, the FFT can also be used as features extraction of the measured differential pressure drop across the gas channels, as demonstrated by Chen and Zhou [113], for detection of flooding states. In the study by Dotelli et al. [114], the Fourier transform of the voltage signal, was used to detect flooding and drying, by changing the switching mode of the DC-DC converter in order to create non-sinusoidal current harmonics. The resulting frequency spectrum is then used as fault feature, where the high and low frequency spectrum is used to distinguish between normal, flooding and drying states. In the work, no classifier algorithm is proposed.

In the study by Damour et al. [115], empirical mode decomposition (EMD), is investigated for FDI of flooding and drying of a LTPEM fuel cell. EMD is based on a small number of Intrinsic Mode Functions that admit a series of well-behaved Hilbert transforms. The described method relies only on the measured LTPEM fuel cell voltage, and do not require any excitation signal, such as EIS do. Fault isolation is managed by a fault signature matrix and a set of rules, with a global accuracy of 98.6 %, based on two Intrinsic Mode Functions as features. The method promises low computational time, and is therefore well suited for online implementation.

The statistical non-model based FDI methods for fuel cells use large datasets to extract the most dominant features that are related to non-healthy operation. Often, many signals are measured on fuel cell systems, which cannot be used for FDI since many signals are correlated. However, by applying statistical methods the number of dimensions can be reduced. The reduced dimensions can then be used as features for fault detection, and a classifier is needed for FDI.

The most common dimensional reduction methods in the literature is Principle Component analysis (PCA) and Fisher Discriminant analysis (FDA), and their nonlinear kernel versions KPCA and KFDA. Studies of fuel cell FDI, have been carried out using PCA [57, 116] and FDA [117–119], for reducing the dimensions of the measured signals. In an extensive study by Li et al. [120], PCA, FDA, KPCA and KFDA are compared for reducing the dimension of 20 individual cell measurements of a LTPEM fuel cell stack, for detecting flooding, drying and normal operation, with kNN, SVM and Gaussian Mixture Model (GMM) as FDI classifiers. The result is that FDA in cooperation with SVM classifier yields the best performance, and the lowest computational cost.

Bayesian Networks (BN) are a class of statistical classifiers which have been used for FDI of fuel cell. They are sets of probabilistic graphical models, which are constructed in a network, for representing a set of random variables that describe a static system. Using a BN consists of two parts: setting the network structure and calculating conditional probabilities using a data driven approach.

In the study by Riascos et al. [121, 122], a BN is suggested for detecting four faults on a fuel cell system: fault in the cathode supply, cooling system fault, increase in hydrogen crossover fault and hydrogen pressure fault. The authors report an early FDI and demonstrate online implementation. In the study by Wasterlain et al. [123], six impedance points at six frequencies are used as input to a BN, for detection of flooding, drying and normal operation of a LTPEM fuel cell, where more degrees of flooding and drying were included. The study reported a 91 % global accuracy. In the study by Wang et al. [124], a BN was constructed using 6 operating variables as input, and trained based on data from two different SOFC stack, installed in two different test benches. The method was trained for six different faults which yielded a 67 % global accuracy. BNs are an alternative classifier to the Machine learning and fault signature rule based methods, which is described in the literature of fuel cell FDI.

Most signal processing methods, such as PCA and FDA presented on Figure 2.4 are for the purpose of feature extraction. The methods in the machine learning (ML) category shown on Figure 2.4, are in the content of non-model based FDI of fuel cells, for fault classification. The application of FDI using ML can be divided into two categories, supervised and unsupervised learning. The most commonly described method is supervised learning, where a database of healthy and non-healthy data, which is labeled by the state, is used for training. One of the ML methods mentioned in Figure 2.4, is then deployed online, for fuel cell FDI. Even though supervised learning is the most common approach to FDI of fuel cells, examples of unsupervised ML approaches are also available [125]. The most common methods for classification of the fault isolation of fuel cells are Artificial Neural Network (ANN), k-Nearest Neighbor (kNN), Fuzzy Logic (FL) and Support Vector Machines (SVM).

In the literature, there are two approaches described for attempting FDI of fuel cells, one is to use directly measured signals for dimensional reduction in cooperation with a ML classifier, and another one is to use extracted features from the impedance spectrum as features for ML classifiers.

In five studies with Z. Li as main author [117–119, 126, 127], individual cell measurements were used as measurement space and FDA for reducing the

dimensions. In all the five studies, the authors use SVM or a subvariant of SVM as fault classifier. In most cases the reported accuracy is larger than 90 %. In one of the studies the authors propose an online incremental learning of the classifier [118, 127], for retraining the classifier to adapt to new and unknown faults during the life time of the fuel cell. However, the accuracy of the new unknown fault is less than 40 %. The authors demonstrate that the method can be applied for different stack sizes after retraining [119].

Using the individual cell voltages as measurement space requires that these are measured online, which is not the case for some fuel cell systems. Alternatively, EIS measurements can be used for characterization of the fuel cell in operation, and based on the EIS measurement, the fuel cell impedance can be estimated. In the study by Debenjak et al. [128], three points of the impedance are used as features for distinguishing between flooding, drying and normal operation of a LTPEM fuel cell. The faults are isolated by a fault signature matrix and a set of rules, and the method is demonstrated on a commercial fuel cell system.

As an alternative to using impedance points directly, features can be calculated and extracted based on internal relations of the impedance spectra, such as, the maximum phase of the impedance spectra, high frequency crossing of the real axis, maximum impedance amplitude, etc. In the work by Onanena et al. [129], kNN was used as a classifier in cooperation with two different feature extraction methods from the impedance spectrum, the first was specific impedance points and the second feature extraction method is based on the high frequency crossing of the real axis, the difference between the high and low frequency crossing of the real axis and the maximum phase. The authors reported a fault detection accuracy of 99.6 % for the former feature extraction method and 94.3 % accuracy for the latter feature extraction method. In the work by Zheng et al. [130][131], extracted features based on internal relations of the impedance spectrum were used as input to a fuzzy clustering classification algorithm for detecting three different degrees of drying, air starvation and normal operation. The paper reported the combination of fuzzy clustering and fuel cell impedance data is well suited for FDI of LTPEM fuel cells, but must be extended to include more fault states.

To summarize non-model based methods use different signal processing and statistical methods for feature extraction of measured signals, and fault signature matrix based on rules or machine learning classifiers for fault isolation. The main disadvantage for the FDI methods described in the literature is the need for a large database of healthy and non-healthy operational data. Furthermore, most of the methods lack the ability for adapting new unseen faults

for online deployment. None of the described model based or non-model based methods for FDI of fuel cells account for the degradation of the fuel cell, which is needed for real life fuel cell FDI applications.

2.1.3 State of the Art on HTPEM fuel cell diagnostics

As can be seen from the literature survey in subsection 2.1.1 and subsection 2.1.2, the majority of available studies within the area of FDI of fuel cells, treat the topic of water management of LTPEM fuel cells. However, this dissertation treats the topic of FDI of HTPEM fuel cell systems, where the water management problem, known from LTPEM fuel cells is not a problem, since water vaporizes at the operational temperature for HTPEM fuel cells and do not rely on the presence of liquid water in the polymer membrane for proton conduction.

As stated in the beginning of section 2.1, limited work has been done in the field of FDI of fuel cells. In several studies, HTPEM fuel cells have been characterized for changes in temperature, CO contamination of anode gas, anode and cathode stoichiometry [74, 75, 77, 79, 132], wherein the EIS characterization method has been proven a powerful tool. Only one study available in literature has pursued characterization of small levels (less than 2 % Vol.) of methanol vapor in the anode gas [83], but more studies focus on methanol vapor (above 3 % Vol.) influence on the degradation of fuel cells [133–135]. The study investigating small levels of methanol vapor in the anode gas [83], did not combine the characterization of different CO and current levels.

The topic of FDI of HTPEM fuel cells is almost nonexistent in literature, and algorithms needs to be further developed. However, some studies have focused on FD on HTPEM fuel cells. In a study by Jensen et al. [136], a method for estimating the CO contamination concentration of the anode gas of a single HTPEM fuel cell is pursued, based on a mapping of the impedance using EIS as characterization method, using three methods of feature extraction. The method considers six different temperatures and only one current set point. The work reported an estimation error less than 1.5 %, using the real values of the impedance at 100 Hz and the temperature as features. In the study, the authors do not take fuel cell degradation into consideration for the algorithm.

In the work by Thomas et al. [137], a method for detection of anode and cathode starvation of a HTPEM fuel cell stack is purposed. The work utilizes the total harmonic distortion (THD), during an EIS measurement for characterizing the linearity of the fuel cell. The authors investigate how the THD

increases at different frequencies for starvation of anode and cathode gases. The authors report that THD at 15 Hz is linked to anode starvation and THD at 25 and 15 Hz is linked to cathode starvation, but do not propose any algorithm to distinguish between healthy and non-healthy operation.

In the work by de Beer et al. [138], the use of EIS to characterize a HTPEM fuel cell at different levels of CO contamination, by fitting an EEC model to the impedance spectrum was investigated. The authors propose to use the parameters of the EEC model as features for fault detection, but do not propose any algorithm for online implementation. In the study by the same authors [132], the characterization was extended to include anode and cathode starvation, phosphoric acid leaching, loss of catalyst and CO contamination. Based on the characterization, the authors propose a fault signature matrix for fault detection, but do not report any suggestions for an online implementation and do not suggest any mitigation strategy for the phosphoric acid leaching and loss of catalyst faults.

The same authors suggest a method for fuel cell characterization, based on small current pulses injecting (CPI) and estimating an EEC model for the responding signal [139], and tested the method on a power supply with an electric circuit in series. In a later study [140] the authors tested the method on a HTPEM fuel cell with offline data processing, but do report that the method is capable of detecting a change in the fuel cell dynamics when CO contamination is introduced in the anode gas.

To summarize, only few studies have been performed in the field of FD of HTPEM fuel cells, with focus on CO contamination of the anode gas and starvation of the anode and cathode. None of the studies have purposed an algorithm for online implementation for FD, and no studies have attempted to perform fault isolation, for the full degree of FDI for HTPEM fuel cells.

2.2 Main contributions

As it can be seen in the literature study above, the field of FDI of fuel cells is active and has been growing rapidly for the past half decade. Most of the published work within FDI of fuel cells is on LTPEM fuel cells, and the field of diagnostics of HTPEM needs to be expanded. In the literature study above, it has been proven that impedance spectroscopy is a power full tool for characterization of fuel cells, and different feature extraction methods can be applied for FDI. Hence, in this dissertation the method will be used as the preferred characterization technique. However, there is a lack of understanding of how the impedance behaviour of a HTPEM fuel cell is, for small concentrations of

methanol vapor and CO in the anode gas, which will be investigated in this work, and quantified by the parameters of an EEC model.

In literature, the most common method for estimating the fuel cell impedance is EIS measurements, which is time consuming and complicated to implement online. As an alternative to EIS measurements, CPI can be used for estimating the impedance based on time domain signals. This method is not well described as a method for online implementations, and a parameter estimation method which is suited for online implementation is needed. This will be described in this dissertation, and the CPI method will be benchmarked against EIS measurements.

No studies found in the literature, reports any method for online FD, of CO contamination in the anode gas for a HTPEM fuel cell. Hence, in this dissertation, a method for FD of CO contamination of the anode gas is proposed, based on a model based statistical change detection approach. No studies available on FDI of fuel cells address the issue that the static and dynamic characteristic of fuel cells change, during degradation at normal operation. This issue will be addressed in this dissertation, and a FDI method, which can detect and isolate common faults in HTPEM fuel cells and is robust towards fuel cell degradation will be proposed.

All studies presented in this dissertation will be based on an experimental data driven methodology, and aim to advance the fundamental understanding of HTPEM fuel cell behavior under healthy and non-healthy operation.

Chapter 3

Impedance Characterization of HTPEM Fuel Cells

As shown in the beginning of chapter 2 in Figure 2.1, fuel cell diagnostics is often divided into characterization, feature extraction and change detection. In this dissertation the characterization will be based on impedance driven methods, as stated in section 2.2. Impedance based FDI methods have been proven powerful in the literature, and can provide information on the fuel cell dynamic behavior, which when known both for healthy and non-healthy fuel cell operation, can be used to diagnose the fuel cell.

3.1 Experimental Setup

This dissertation is based on a data driven approach for FDI of HTPEM fuel cells. A set of experimental data is therefore needed for the development and assessment of the FDI algorithms. The experimental work for this dissertation is conducted solely for the propose for this dissertation. For all experiments, the purpose has been to reproduce the operation of a methanol reformer system, such as the one shown in Figure 1.3.

The experimental work is conducted on two different GreenLight fuel cell test stations, where the operational parameters can be controlled and different fault scenarios can be emulated. Test on single cell level is conducted on a GreenLight G60 test station with an 800 W electric load. For single cell testing the cell assembly is heated by electric heaters which is installed in the endplates. The short stack testing is conducted on a GreenLight G200 test station with a 12 kW electric load. For heating and cooling of the HTPEM short

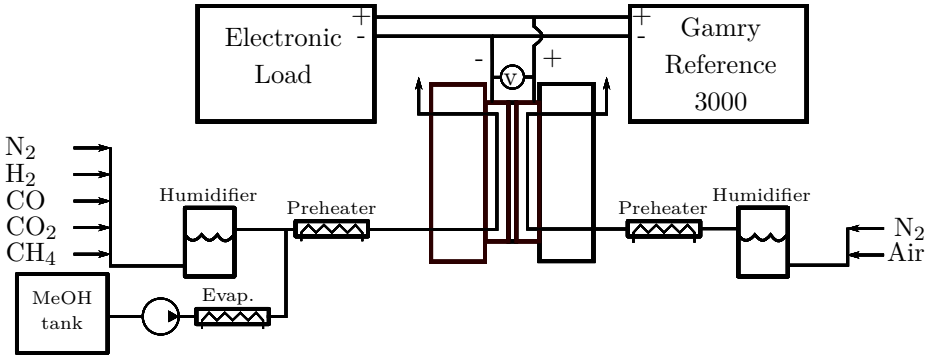

Figure 3.1: Flow schematic of the two GreenLight fuel cell test stations used for the experimental work in this dissertation.

stack, an external cooling cart running an oil circuit is used. For humidification of the gases, both test stations use a bubbler principle, where the temperature of the water can be controlled. It is assumed that the size of the bubbler tank is sufficient for the gas to obtain the same dew point temperature as the temperature of the water in the bubbler tank. The humidification can be bypassed, for using dry gas. For estimation of the impedance a commercial Gamry Reference 3000 potentiostat is utilized. When conducting the impedance measurements, 7.5% of the DC value is used as AC amplitude, with a maximum AC current amplitude of ± 3 A.

For the experimental work in paper B, the GreenLight test station was modified, using an external electrical load and an external National Instrument compact RIO system for controlling the electrical load and for fast data logging.

3.2 Electrochemical Impedance Spectroscopy

Electrochemical impedance spectroscopy (EIS) is an in-situ characterization method frequently used for fuel cells. The method can be conducted in steady state operation, and is well suited for online operation. Electrochemists widely use the method for gaining information on the dynamic operation of the fuel cell, and how changing different materials or operational conditions influences the fuel cell. The method works by superimposing a sinusoidal signal onto the current or the voltage, and measuring the responding voltage or current. The impedance can then be estimated based on the ratio between the signal

amplitudes and the phase shift (φ):

$$Z = \frac{\Delta V}{\Delta I} \quad e^{j\varphi} \tag{3.1}$$

The estimation of the amplitude difference and the phase shift is often base on Fast Fourier Transform (FFT) or sine correlation [141]. This is then repeated for a range of frequencies, for yielding the impedance spectrum. For this dissertation, the frequency range for all impedance measurements are from 10 kHz to 0.1 Hz. The impedance spectrum is often illustrated using Nyquist plots or bode plots.

Generally, when using EIS for fuel cell diagnosis, there are two ways to extract features for change detection, model based and non-model based. For the model based approach, the impedance spectrum is fitted to a EEC model whereof the parameters are used as features. For the non-model based approach, internal relations of the impedance spectrum, such as different angles or magnitudes are extracted as features for change detection.

3.2.1 Model based feature extraction

In paper A and C a model based approach was used for extracting features to analyse different operational conditions. In the literature, different EEC models are used for fitting the impedance of LTPEM and HTPEM fuel cells. Most often, the impedance reassembles two to three capacitive semicircles by two to three RC loops and a series resistance [77, 79] or an EEC model as shown in Figure 3.2, e.g. in combination with an additional RC loop [142].

The fitting of the EEC model to the impedance spectrum is often automated by an optimization algorithm using a least squares cost function. Many available programs rely on gradient based optimization algorithms, which converge fast but not necessarily to the global minimum, since the task of fitting an EEC model to the impedance spectrum is a highly non-linear problem. Therefore, researchers aim to fit the EEC model to the impedance spectrum, using non-gradient based algorithms such as the Nelder–Mead Simplex algorithm. However, for ensuring that the algorithms converge fast, an initial guess is needed. In the study by Tant et al. [84], initial guess values were extracted from the polarization curve. An alternative approach to initial guesses for the optimization algorithm was suggested by Petrone [143], who proposed a geometrical first guess algorithm, which is based on extracted values from a geometrical representation of the impedance spectrum.

In this dissertation, all EEC model parameters fitting were performed using a series of matlab scripts developed during the duration of this PhD study. The

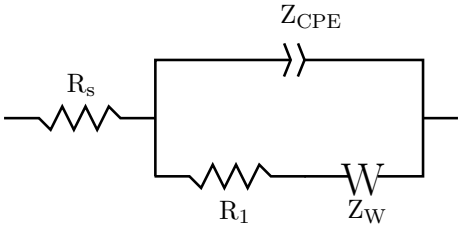

Figure 3.2: The Equivalent electrical circuit model used in Paper A.

routine is based on a differential evolution optimization algorithm [144] and a complex least squares cost function. This algorithm is not well suited for online implementation on low cost micro controllers, but ensures a higher probability of finding the global minimum [145]. The alternative non-gradient based algorithms such as the Nelder–Mead Simplex algorithm, can be implemented on floating points DSP, however, the fitting of EEC model parameters will be computationally intensive and time consuming. Implementation on DSP microcontrollers is necessary for industrial products, since full size computers are too expressive, too energy inefficient and physically too large, for real life systems.

For the study in paper A, the EEC model shown in Figure 3.2, was used for quantifying the impedance of a short HTPEM fuel cell stack, at varying load current, CO anode contamination and methanol vapor anode contamination. A complete mapping of contamination levels of CO in the range 0-1.5 % and methanol vapor in the range 0-0.5 % was measured at 21 different current loads.

An EEC model parameter mapping, as the one conducted in paper A, could potentially be used for designing a fault signature matrix, for isolating different faults on a HTPEM fuel cell. The experiment in paper A is conducted for realistic reformer output values, and the value of the EEC model parameters is therefore not too distinct. However, the data clearly indicates a change of EEC model parameters, and the data can be used for FD, for both CO and methanol vapor contamination. The correlation between EEC model parameters and increasing levels of CO and methanol vapor contamination is illustrated in Table 3.1. It is shown that the same parameters vary for both a change in CO and methanol vapor contamination, and a unique fault signature matrix is therefore not possible.

In paper C, a more simple circuit based on one R-CPE loop in series with a resistor is utilized for FD of CO contamination in the anode gas. The simpler EEC model was adapted for faster fitting times and low variance of the

Table 3.1: "*The correlation between increasing levels of CO and methanol vapor contamination of the anode gas and the EEC model parameters.*" Paper A

	R_1	R_2	α	Q_1	T_1	R_W
CO	↑	↑	↓	↑	-	↑
CH_3OH	↑	↑	↓	↑	-	↑

estimated EEC model parameters. The parameter resistance in the R-CPE loop and the α coefficient of the CPE element were proven to be good fault indicators, when CO was mixed into the anode gas. Although the simple EEC model was proven efficient to detect CO, it would be difficult to find unique parametric signatures for new faults, and therefore, it is not possible to isolate new faults.

3.2.2 Non-model based feature extraction

As an alternative to fitting an EEC model to the impedance spectrum, features can be extracted based on internal relations in the impedance spectrum. This can be done, by directly choosing k of the d dimensions which contain the most information needed for the fault classification, where d is the measurement space [128, 146]. As an alternative, a set of features can be calculated, based on the shape of the impedance spectrum, such as angles and magnitudes.

In Figure 3.3, a typical impedance spectrum of a PEM fuel cell is illustrated, together with four (a-d) extracted features for fuel cell FDI, which are often found in the literature. The first (a) is the internal or series resistance, which often is estimated as the high frequency intercept with the real axis [129], the second (b) is the span of the impedance spectrum, often referred to as the sum of the charge transfer and mass transport resistance, and calculated as the difference between the internal resistance and the low frequency intercept with the real axis [130, 147]. The third is the low frequency intercept with the real axis or the maximum magnitude of the impedance spectrum, which is often referred to as the polarizing resistance [130, 131]. The fourth is the maximum angle of the impedance spectrum [129, 131] or the frequency at the maximum angle [130].

Based on an analysis performed in paper D, it is seen that the proposed features (a)-(d) change during degradation of the fuel cell. For the FDI algorithm to be consistent during the entire lifetime of the fuel cell, it is necessary that the features do not change with degradation. This is important because if change detection can be based on features, with a low variance that do not change during the fuel cell life time, the thresholds could be designed more

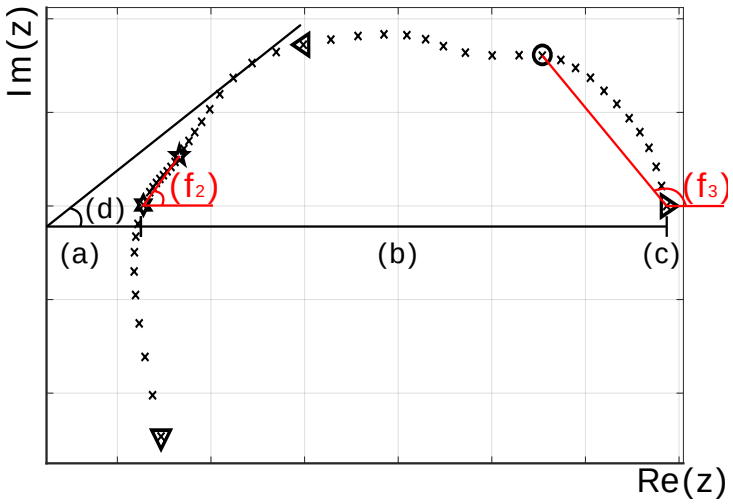

Figure 3.3: Typically non-model based features found in the literature ((a)-(d)) and the two features (f_2 , f_3) used in Paper D.

aggressively. If thresholds are designed more aggressively, faults at lower amplitudes can be detected. Further, when the features change during the fuel cell life time, the FDI algorithm becomes more prone to giving false alarm or false detection.

In paper D, two alternative features are suggested, which are shown to be independent to fuel cell degradation. The two proposed features are the angle between the 1 kHz and 100 Hz marker and the angle between the 1 Hz and 0.1 Hz marker, which are suggested together with the DC component of the current. In paper D, these three features are proven suitable for detecting the faults listed in section 1.1.2.

3.2.3 EIS feature extraction discussion

In this dissertation both model based and non-model based feature extraction has been applied. Based on this, a series of observations have been made, which led to some recommendations.

As stated in the previous section, the model based method for feature extraction is a result of a gray box model approach, where many researchers give physical meaning to the different parameters of the EEC model. However, the physical meaning of the parameters is often different from study to study, and based on observations made during this PhD project, a change in one operational parameter, which in theory should only be reflected in one part of the

impedance spectrum, often causes more parts of the spectrum to change. This makes the physical meaning of the EEC model parameters ambiguous. This is further underlined by the fact that different EEC models might fit the same impedance spectrum and support the initial statement that this is a gray box model approach.

An additional problem is illustrated in Figure 3.4, which is impedance spectra from paper A, at different load currents using pure hydrogen. For low currents, the spectrum is shaped as one semicircle and when the load current increases, the shape of the impedance spectrum changes. By investigating the other Nyquist plots seen in paper A, it can be seen that for high concentrations of CO and methanol vapor, a third semicircle appears. This change in the shape of the impedance spectra, is hard to capture with one generic EEC model, when working with large data sets. Furthermore, it is often seen that the impedance spectrum changes shape when a fault is introduced.

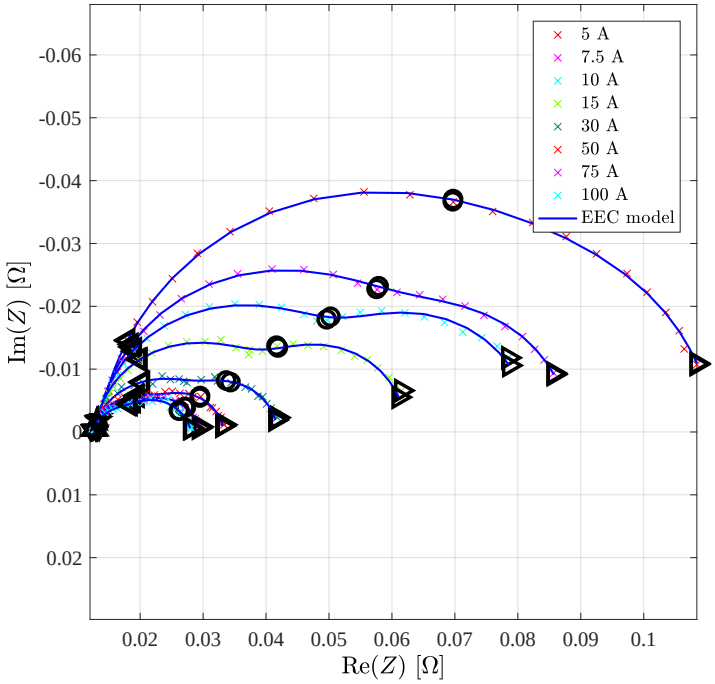

Figure 3.4: Nyquist impedance plot at different current loads, using pure hydrogen for the anode gas. The black markers indicate the frequency decades {1k,100,10,1,0.1} Hz. The blue line indicates the EEC model fit for each EIS measurement, using the EEC model shown in Figure 3.2. Data from Paper A

One downside of the gray box model approach to feature extraction of

the impedance spectrum is, as mentioned in section 3.2.1, that the fitting algorithms are computationally intensive compared to extraction by means of internal angles and magnitudes of the impedance spectrum. During this PhD study, substancial amount of time has been spent to adjust EEC model fitting scripts and changing parameter constrains, and the same can be expected if an EEC model based feature extraction method should be implemented online.

For non-model based feature extraction methods, the downside is that they often only rely on few points in the impedance spectrum, which makes them more sensitive towards noise. Extracting a feature based on an impedance point which is highly influenced by noise, will result in a larger probability of false alarm or false detection.

Furthermore, for the non-model based approach, it is not possible to predict or identify new and previously unseen faults. To include new faults in the FDI algorithm a large new dataset of faulty data will be required. This will to some extent also be the case with the model based feature extraction method, but it is considered to be less data demanding.

An advantage of the non-model based method is that only parts of the spectrum could be necessary for extracting features for FDI algorithms. Thus, the characterization time of the fuel cell operation will be shorter.

Based on the above discussion, it is recommended that for new studies on impedance based FDI algorithms the non-model based feature extraction approach is pursued.

3.3 Current Pulse Injection

An alternative method to EIS fuel cell characterization is current pulse injection (CPI), which is analyzed in paper B. When using the CPI method, small current pulses are added to the DC current, and based on the responding voltage signal, the fuel cell dynamic behavior can be estimated. This dynamic behavior can be modeled using a EEC model, whereas the EEC model parameters were estimated in the frequency domain for EIS they are estimated in the time domain when using the CPI characterization method.

One of the disadvantages of EIS measurements are that the method is most often demonstrated on lab scale. On lab scale the method is often implemented by expensive commercial potentiostats, which are not suited for online implementation. Therefore, researchers suggest to implement the EIS method in the DC/DC converter [89, 90], however, this sets strict requirements for the bandwidth of the DC/DC converter. This can be accomplished, but demands some development and a set requirements to the output of the DC/DC converter.

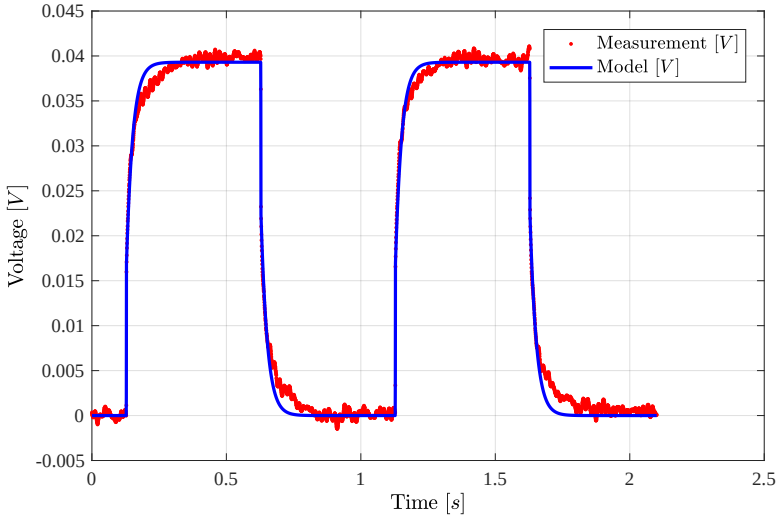

Figure 3.5: "*Selected time series data of 1 Hz (duty cycle=0.5) pulses, including the simple R-RC EEC model, at a 1 A current pulse amplitude.*" Paper B

The advantage of the CPI method is that the implementation is simple, and only requires two components: a transistor and a resistor.

The EEC model which can be obtained using the CPI method, is in general simpler than what can be obtained using EIS. For some applications, this simpler EEC model might be sufficient for fuel cell FDI. In Figure 3.5, a normalized voltage response is illustrated, for two current pulses of 1 A amplitude, together with the model fit of a R-RC EEC model. The advantage of fitting a simpler EEC model to the experimental data, is lower fitting times, and a lower variance of the parameters of the EEC model. In paper B, a non-recursive least squares parameter estimation method is proposed, which is well suited for online implementation on a low cost floating point DSP micro controller.

When comparing the EEC model, which is estimated using EIS characterization and CPI characterization, it can be seen that the low frequency information of the impedance spectrum is lost in the CPI method, as illustrated on Figure 3.6. The low frequency part of the impedance spectrum holds information on phenomena which are related to mass transport and the gas channel geometry [79]. When using the CPI characterization method, the gas oscillations in the gas channel in not excited as when using the EIS method for fuel cell characterization, and the low frequency part of the impedance spectrum is therefore not captured [148–151]. When comparing the EIS method to the CPI method, the low frequency part of the spectrum is therefore not fitted to

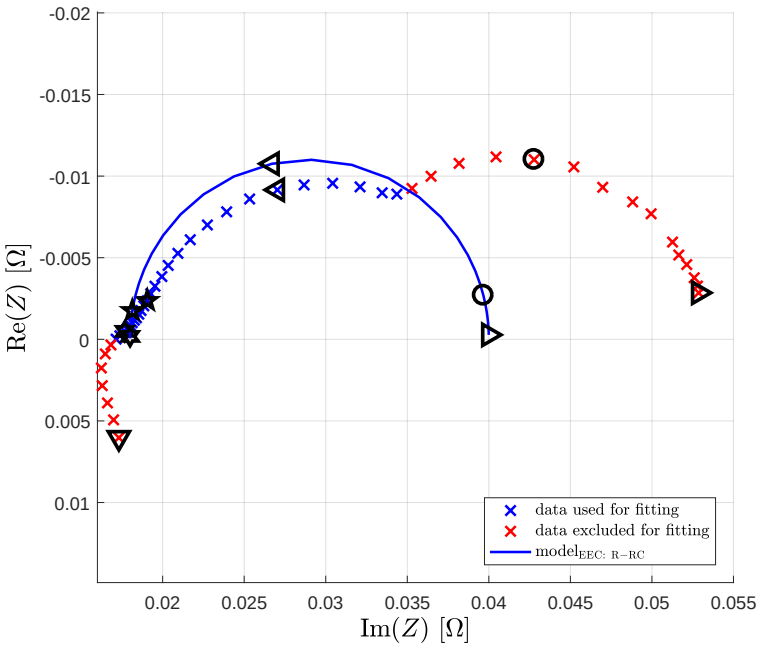

Figure 3.6: "*Simple R-RC EEC model fitted to high and intermediate frequencies. EIS data collected at 0.2* Acm^{-2} *load current density. The black markers indicate the frequency decades* $\{10k, 1k, 100, 10, 1, 0.1\}$ Hz." Paper B

the EEC model, as shown in Figure 3.6. In Figure 3.6, an R-RC EEC model is fitted to the impedance spectrum of all the negative imaginary points until 2 Hz. The resulting EEC model parameters are shown in Table 3.2, were compared to the EEC model parameters obtained using the CPI method. It can be concluded that the CPI method captures the same EEC model parameters as the ones obtained using EIS, within a reasonable band of uncertainty.

In this dissertation, the CPI fuel cell characterization method has not been investigated for non-healthy operation. The method has therefore not been evaluated directly for fuel cell FDI. Based on the simplicity of fitting and ease

Table 3.2: "*Comparing the estimated EEC parameters using the CPI method and the EIS method at 0.2* Acm^{-2} *DC fuel cell output current.*" Paper B

	1 A CPI	**EIS**	
$\mathbf{R}_s$	16.5 $m\Omega$	16.9 $m\Omega$	2.3 %
$\mathbf{R}_1$	22.8 $m\Omega$	23.6 $m\Omega$	3.4 %
$\mathbf{C}_1$	1.05 F	0.99 F	6 %

of implementation, this method can be considered suitable for fault detection of fuel cells. However, since the low frequency information of the impedance spectrum is lost, as seen in Figure 3.6, the fault isolation property of the method is considered to be unlikely for a wide range of faults, such as the case study in section 1.1.2.

Chapter 4

Diagnostics of HTPEM Fuel Cells

Based on the extracted features, such as the ones described in chapter 3, an algorithm for change detection and fault isolation can be designed. These algorithms are often divided into model based and non-model based methods, but this refers to the feature extraction method. By principle, the same algorithms for change detection and fault isolation can be applied for both model based and non-model based feature extraction methods. To summarize from section 2.1, the most common change detection and fault isolation methods for data driven fuel cell FDI, is Bayesian networks, various machine learning approaches and fault signature matrices using thresholds.

4.1 Threshold design

When a set of features have been selected and analyzed at healthy and non-healthy operating conditions, the last step, which is shown in Figure 2.1, has to be completed. One approach is to compare the characterized feature to a reference value, and then deciding the condition based on a threshold. The value of the threshold could be chosen arbitrarily during the initial phase of the fuel cell system life time, to a value which shows a promising result. Alternatively, the threshold could be designed based on the statistical properties of the features, of which the probability of false alarm and false detection could be calculated. This topic is discussed in paper C.

In Figure 4.1, the probability density function of the feature R_2, for healthy ($\mathcal{H}_0$) and non-healthy ($\mathcal{H}_1$) operation in one set point is illustrated, where non-healthy operation is when there is CO present in the anode gas. It can be shown that the EEC model parameter R_2 follows a Gaussian distribution, both

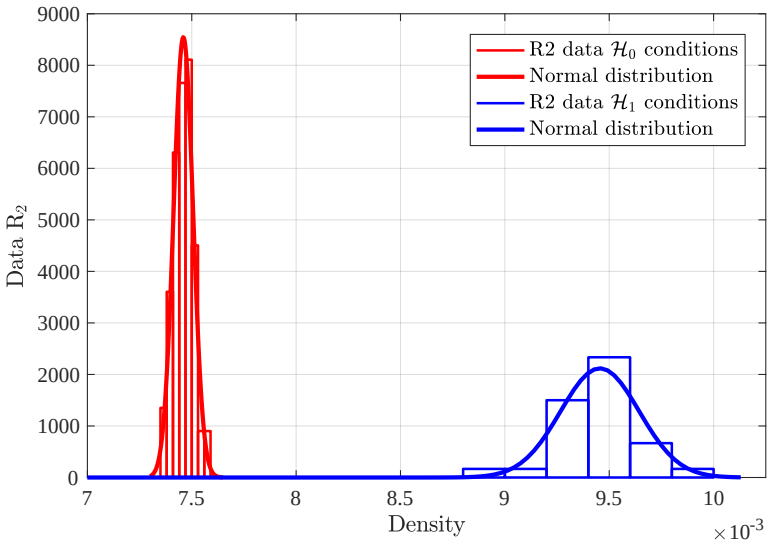

Figure 4.1: "*Histogram of the R_2 EEC parameter in non-faulty and faulty operation. The non-faulty operation R_2 data follows a normal distribution with mean of $\mu_0 = 7.459 \cdot 10^{-3}$ and a variance of $\sigma^2 = 2.179 \cdot 10^{-9}$. The faulty operation R_2 data follows a normal distribution with mean of $\mu_0 = 9.45 \cdot 10^{-3}$ and a variance of $\sigma^2 = 0.188 \cdot 10^{-3}$.*" Paper C

in healthy and non-healthy operation. There is a clear change from healthy to non-healthy operation, and non-healthy operation can therefore be detected as a change in the amplitude of the parameter R_2.

Detecting a change in amplitude of unknown amplitude, of a parameter, can be formulated as a one-sided hypothesis test. The null-hypothesis ($\mathcal{H}_0$) as the healthy operation and the alternative hypothesis ($\mathcal{H}_1$) as the non-healthy operation:

$$\mathcal{H}_0 : R_2 = \mu_0(\bar{I})$$
$$\mathcal{H}_1 : R_2 > \mu_0(\bar{I})$$

Since this detecting algorithm in paper C aims to detect a change in R_2 of unknown amplitude for an unknown amplitude of CO contamination in the anode gas, the detecting algorithm will be a Composite hypothesis test. For Composite hypothesis testing without prior knowledge on the CO contamination likelihood, a Neumann-Pearson approach using a Generalized Likelihood Ratio Test (GLRT) [141] can be applied. When the GLRT algorithm is applied for detecting a change of a parameter amplitude, the GLRT algorithm is based on the maximum likelihood estimation (MLE) approach. The MLE of a Gaussian signal can be calculated as the mean of the signal [152]. The GLRT

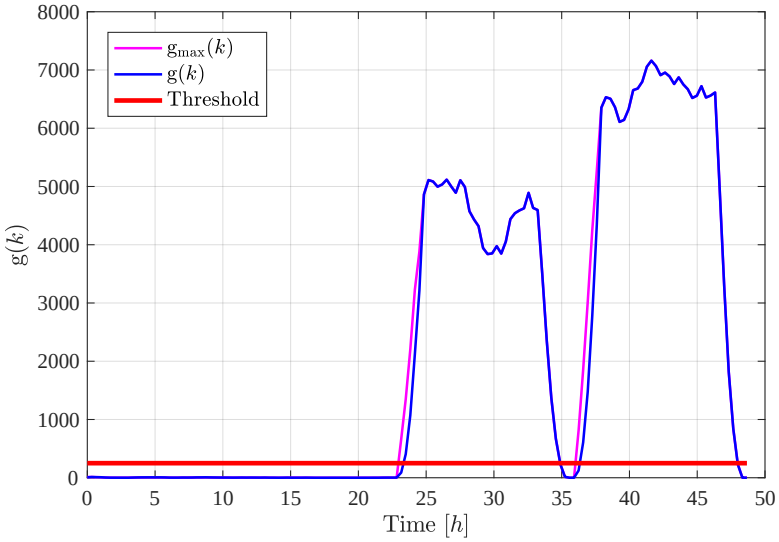

Figure 4.2: "*The GLRT decision algorithm $g(k)$ detecting a change in the mean value of R_2.*" Paper C

algorithm can be formulated as [153]:

$$g(k) = \frac{1}{2\sigma^2 M}\left[\sum_{i=k-M+1}^{k}(R_2(i) - \mu_0(\bar{I}))\right]^2 \tag{4.1}$$

The output of the GLRT algorithm, when 0.5 % and 1 % CO is present in the anode gas, is shown in Figure 4.2. The value can be determined based on the test statistics of the GLRT algorithm output for normal operation. In paper C, the GLRT algorithm output during normal operation is proven to follow an exponential distribution. Based on this, the threshold can calculated for a tradeoff between probability of false alarm and probability of false detecting.

For the study in paper C, the CO contamination fault is introduced as step. In a real-life application, this would not be the case, but since the proposed method detects a change in amplitude of the EEC model parameter R_2, the algorithm is robust toward incipient faults.

Using this method for designing thresholds, the probabilities for false alarm and false detecting are only valid at the present state of degradation. Furthermore, the method only takes into consideration a change in the load current, and is not robust toward fault isolation, such as the ones listed in section 1.1.2. Detection and isolation of other faults could be approached using a fault signature matrix, with a similar approach for threshold design. However, based on

Table 4.1: The five faults described in section 1.1.2, which is analyzed for FDI in paper D, at the listed amplitudes.

Nr.	Fault	Normal	Abnormal
ϕ_1	Low λ_{Air}	2.5 [-]	1.5 [-]
ϕ_2	High λ_{Air}	2.5 [-]	4 [-]
ϕ_3	High CO	0.5 % Vol.	2.5 % Vol.
ϕ_4	High MeOH vapor	0 % Vol.	5 % Vol.
ϕ_5	Low λ_{H_2}	1.4 [-]	1.15 [-]

the experience from paper D this would require a more complex EEC model, than the one suggested in paper C.

4.2 Fault isolation using artificial neural network

As an alternative to comparing a feature to a reference value and then checking the state based on a threshold, a Machine learning approach such as an artificial neural network (ANN) can be used for the same purpose. For using ANN for FDI of fuel cells, a data set under healthy and non-healthy operation is needed for the training of the ANN. This is both an advantage and a disadvantage. It is an advantage, because almost no time is spent on modelling, and it is a disadvantage because time is spent on collecting experimental data.

In paper D, the five faults described in section 1.1.2 are experimentally analyzed and an ANN FDI algorithm is proposed. In Table 4.1, the amplitudes of the five faults analyzed in paper D are listed.

In paper D, the proposed FDI algorithm is split into four steps, as shown in Figure 4.3. The first step is to acquire an EIS measurement of the fuel cell system, as it runs online in the field. The experiments conducted for paper D are on a lab scale, using a commercial potentiostat, in a controlled environment. However, for real life applications, the EIS measurements should be implemented on the onboard DC/DC converter, as disused earlier in this dissertation. The second step of the FDI algorithm, is the preprocessing of the EIS measurement. The main purpose of the preprocessing is noise rejection. Using one impedance point to extract a feature, which are highly influenced by noise, could lead to a false detection or a false alarm. In paper D, a zero phase implementation of a Butterworth filter is suggested, which requires a full impedance spectrum. In the paper, it was pointed out that an advantage of the

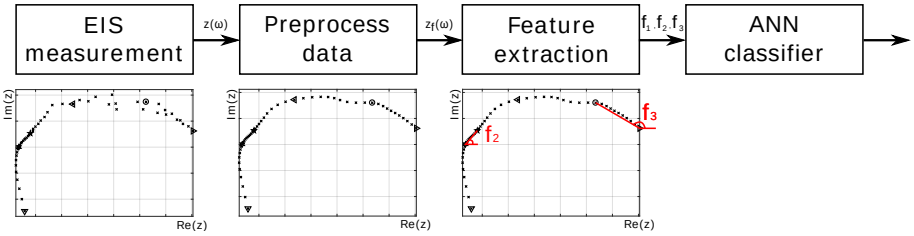

Figure 4.3: "*Flow chart of the artificial neural network fault detection and isolation methodology.*" Paper D.

method is that it only requires parts of the impedance spectrum. In the case when only parts of the spectrum are acquired, the preprocessing step must be changed. This could be done by taking multiple impedance measurements at the relevant points.

The third step of the algorithm, is feature extraction. For the work in paper D the value of the DC current, and two internal angles of the impedance spectrum is utilized as feature extracting. As mentioned in section 3.2.2, the two angles are robust toward degradation, which is important for reducing the number of cases of false alarms. However, other extracted features could have been used for the purpose. As the fourth step of the FDI algorithm, the extracted features (f_1-f_3) are used as inputs to the ANN classifier, which selects one of the 6 different cases (ϕ_0- ϕ_6), where ϕ_0 is healthy operation.

The ANN classifier is constructed as a feed forward on standard form, and consists of one hidden layer with 10 neurons, with a tansig transfer function. The output layer consists of one outlet for each of the six cases, with a softmax transfer function.

The ANN is trained based on an experimental database, where data for healthy and non-healthy operations are represented and labeled. The training process is thereby a supervised procedure. The data set is divided into three parts: training, validation and test. The training part of the data set is used for the training of the ANN classifier neurons and transfer functions. The validation data set is used as stop criteria for the training algorithm. The test part of the data set is used for testing the performance of the algorithm, on data which has not yet been used during the training and validation of the ANN algorithm. The majority of the database consists of healthy data, which is over represented compared to non-healthy data. The test data set, is selectively chosen to contain an equal amount of data points for each fault. The remainder of the data set was randomly divided between training and validation, but in theory one fault case could be under represented. A method to overcome this,

Table 4.2: "*The result of the test data, listed in a confusion matrix. The results are listed in %. Global accuracy is 94.6 %.*" Paper D. The faults ϕ_1 - ϕ_6 is described in section 1.1.2.

		Target class					
		ϕ_0	ϕ_1	ϕ_2	ϕ_3	ϕ_4	ϕ_5
ANN output class	ϕ_0	98	0	0	0	70	0
	ϕ_1	0	100	0	0	0	0
	ϕ_2	0	0	100	0	0	0
	ϕ_3	0	0	0	100	0	0
	ϕ_4	2	0	0	0	30	0
	ϕ_5	0	0	0	0	0	100

could be to implement a K-fold cross validation of the ANN, for the training process, meaning splitting the complete training and validation data set into K parts, and running the training K number of iterations.

The performance of the ANN classifier based FDI algorithm proposed in paper D, is illustrated in Table 4.2. A good accuracy of four out of the five faults is reported, yielding a 100 % detectability. It was found that the algorithm had difficulties distinguishing between healthy operation (ϕ_0) and the methanol fault (ϕ_4), yielding in only 30 % detection of ϕ_4 data instances. The global accuracy of the algorithm is 94.6 %. For FDI of HTPEM fuel cells, no studies have been reported in the literature, but the global accuracy is in good alignment with similar studies for LTPEM fuel cells [129, 130, 147].

Chapter 5

Final remarks

In this dissertation, the study of developing fault detection and isolation algorithms for high temperature proton exchange membrane fuel cells has been investigated. Throughout the dissertation, a data driven approach has been used, with the fuel cell impedance as the characterized parameter. The faults that have been investigated are related to anode and cathode gasses. For the anode, the considered faults have been carbon monoxide (CO) and methanol vapor contamination and hydrogen starvation. For the cathode, oxidant starvation and too high flow of oxidant is considered. The fault detection and isolation process has been divided in to three steps: characterization, feature extraction and change detection and isolation.

For characterization of the fuel cell impedance, two methods have been considered: electrochemical impedance spectroscopy (EIS) and current pulse injection (CPI). For EIS a sinusoidal current is superimposed on the DC current and the phase shift and amplitude difference for the corresponding voltage is measured. By repeating this for a range of frequencies, the impedance spectrum can be characterized. EIS has been proven to be a powerful characterization method throughout the project, to distinguish between healthy and non-healthy fuel cell operation.

With inspiration from the battery field, an alternative method to EIS is investigated, namely CPI. For CPI, a small current pulse is drawn in addition to the DC current, and the resulting voltage transient is measured. In this PhD study, a procedure for estimating the parameters of an equivalent electrical circuit based on the transient voltage response is suggested, which is suited for online implementation. The method was proven to be effective on experimental data, however, with a loss of information in the low frequency part,

compared to what can be obtained using EIS as characterization method. The CPI method yielded consistent results with low variance for different current pulse amplitudes. The CPI characterization method could be useful in some fault detecting algorithms for fuel cells, but this has not been investigated in the frame of this dissertation.

For extraction of features based on the impedance spectrum acquired from EIS measurements, two general methods have been investigated during the PhD study: model and non-model based feature extraction methods. For the model based approach an EEC model is fitted to the impedance spectrum, and the parameters of the EEC model are used as features for change detection. The fitting process is computationally intensive and time consuming. Furthermore, the choice of model structure is not trivial, as a fuel cell could be represented using different model structures for different operating conditions. The EEC model complexity needs to be high, to be able to isolate multiple faults. However, increasing the complexity of the EEC model lowers the consistency of the fitting accuracy.

As an alternative to model based feature extraction, non-model based feature extraction could be applied. For the non-model based feature extraction, internal relations of the impedance spectrum are calculated, such as angles and amplitude. The computational cost of this is significantly lower than the model based approach, and no information is lost.

Based on the work done on model and non-model based feature extraction in this PhD project, it can be concluded that non-model based feature extraction of the impedance spectra is best suited for online fault detection and isolation of high temperature proton exchange membrane fuel cells.

During normal degradation, the impedance spectrum spreads and is slightly shifted. This is a problem when using the impedance as a feature for fault detection, since the thresholds need to be designed less aggressively and the algorithms become more prone towards false alarm. In this PhD study the impedance during the first 800 hours of fuel cell operation is investigated and a new set of non-model based features that are independent of degradation was suggested.

A complete mapping of the fuel cell impedance using EIS, quantified by equivalent electrical circuit (EEC) model parameters was also presented. The mapping spanned seven points of CO contamination in the anode gas in the range 0 – 1.5 % vol. and three points of methanol vapor contamination in the anode gas, in the range 0 – 0.5 % vol. The different combinations of gas compositions were evaluated for 21 current set points in the range 5 – 100 A. Based on the study, it can be concluded that it is not possible to isolate whether

CO or methanol vapor is present in the anode gas based on the EEC model parameters for the suggested EEC model.

The General likelihood ratio test is proposed for change detection of a resistor in an EEC model, for distinguishing between healthy data and CO contamination in the anode gas. Using this method, an analysis of probability of false alarm is given.

For isolating five common faults, which occurs on high temperature proton exchange membrane fuel cells, an artificial neural network (ANN) classifier is proposed. It is trained through a supervised procedure based on an experimental database containing healthy and non-healthy data. The ANN classifier method was concluded to be effective for the application of fault detection and isolation in fuel cells, however, with problems of distinguishing between healthy operation and methanol vapor contamination in the anode gas. A global accuracy of 94.6 % was demonstrated.

5.1 Future work

As with most other scientific research projects, the result of this study show many results, but also open new areas of investigation.

In order to improve the algorithms suggested in this study, it could be helpful to diagnose the amplitude or the degree of the faults. This could be extended by adding additional measurements points to the database, and retraining the algorithm. Alternatively, the change detecting algorithm could be changed to a fuzzy based methodology.

The fault detecting and isolating algorithms rely on a set of characteristic features extracted from the impedance. However, the impedance is known to vary from fuel cell stack to fuel cell stack. This is a matter of reliable fuel cells production, which in term of impedance is not yet investigated for high temperature proton exchange membrane fuel cells.

Moreover, the experimental studies performed for this project are conducted on single cell level or using a 10 cell short stack. Testing the suggested algorithms on full size stacks or complete systems could give a good idea regarding the robustness of the algorithms and the possibilities of their implementation in real life systems, with integrated methanol reformer. This would require that the EIS measurement technique is implemented as a part of the system, for example on the on-board DC/DC converter. This in turn opens many tasks to be investigated, such as the bandwidth of the DC/DC converter for controlling the current by a sinusoidal wave form, and making sure that the output of the DC/DC converter can handle a fluctuating voltage/current. Furthermore, the

algorithm must also be retrained with impedance data from the new fuel cell stack.

This study has been focused on FDI of fuel cells, using the fuel cell impedance as indicator of the fuel cell state of health. It could be interesting to study the fuel cell FDI, including indicators from surrounding components. The surrounding components, for the fuel cell in a reformed methanol fuel cell system, are the reformer, burner and cooling system. Such indicators could include, temperatures, temperature gradients, flows, etc., and could be in combination with or without the fuel cell impedance.

Future studies could also include new fault cases, such as: cell reversal, phosphoric acid washout, coolant leakage into anode and cathode gas channels, anode or cathode gas channel blockage, pin hole formation, presence of hot spots, etc. In the future, analysis of the mean time between faults for each fault case could be assessed for evaluating which faults have higher priority to be included in a fuel cell FDI algorithm.

Finally, expanding the fault detecting and isolation algorithms to the full class of health management and prognostics system topology could be of great interest for future studies. This involves developing mitigation strategies for each fault classes, and incorporating them in fault tolerant control systems on heuristic systems control level. Furthermore, the health management system must be expanded to include prognostic functions for estimating the remaining useful life time of the system.

If the methods suggested in this dissertation, and some of the initiatives suggested in this chapter is implemented in real life fuel cell systems, it will lead to more robust and reliable operation, which have the potential to increase the life time. For HTPEM fuel cells stacks which are deployed in reformed methanol systems, this will contribute to commercialization and bring down the maintenance cost.

References

[1] IPCC. Climate Change 2014 Synthesis Report Summary Chapter for Policymakers. Technical report, Intergovernmental Panel on Climate Change, 2014.

[2] United Nations/Framework Convention on Climate Change. Paris Agreement. 2015.

[3] Barack Obama. The irreversible momentum of clean energy. *Science*, 6284(January), 2017. doi: 10.1126/science.aam6284.

[4] NOAA. ENSO: Recent Evolution, Current Status and Predictions. Technical Report November, U.S. National Oceanic and Atmospheric Administration, 2016. URL `http://www.cpc.ncep.noaa.gov/products/analysis{_}monitoring/lanina/enso{_}evolution-status-fcsts-web.pdf`.

[5] Gavin A Schmidt and Thomas R Karl. Annual Global Analysis for 2015 NASA 2016 Global Temperature. Technical Report January, National Aeronautics & Space Administration, 2017.

[6] Jonathan A. Patz, Diarmid Campbell-Lendrum, Tracey Holloway, and Jonathan A. Foley. Impact of regional climate change on human health. *Nature*, 438(7066):310–317, 2005. ISSN 0028-0836. doi: 10.1038/nature04188.

[7] EEA. Economic losses from climate-related extremes. Technical report, European Environment Agency, 2017. URL `http://www.eea.europa.eu/data-and-maps/indicators/direct-losses-from-weather-disasters-3/assessment`.

[8] O. Raaschou-Nielsen, R. Beelen, M. Wang, G. Hoek, Z. J. Andersen, B. Hoffmann, M. Stafoggia, E. Samoli, G. Weinmayr, K. Dimakopoulou, M. Nieuwenhuijsen, W. W. Xun, P. Fischer, K. T. Eriksen, M. S{o}rensen, A. Tjanneland, F. Ricceri, K. de Hoogh, T. Key, M. Eeftens, P. H. Peeters, H. B. Bueno-de Mesquita, K. Meliefste, B. Oftedal, P. E. Schwarze, P. Nafstad, C. Galassi, E. Migliore, A. Ranzi, G. Cesaroni, C. Badaloni, F. Forastiere, J. Penell, U. De Faire, M. Korek, N. Pedersen, C. G. Åstenson, G. Pershagen, L. Fratiglioni, H. Concin, G. Nagel, A. Jaensch, A. Ineichen, A. Naccarati, M. Katsoulis, A. Trichpoulou, M. Keuken, A. Jedynska, I. M. Kooter, J. Kukkonen, B. Brunekreef, R. S. Sokhi, K. Katsouyanni, and P. Vineis. Particulate matter air pollution components and risk for lung cancer. *Environment International*, 87(November 2015):66–73, 2016. ISSN 18736750. doi: 10.1016/j.envint.2015.11.007.

[9] Richard T. Burnett, C. Arden Pope, Majid Ezzati, Casey Olives, Stephen S. Lim, Sumi Mehta, Hwashin H. Shin, Gitanjali Singh, Bryan Hubbell, Michael Brauer, H. Ross Anderson, Kirk R. Smith, John R. Balmes, Nigel G. Bruce, Haidong Kan, Francine Laden, Annette Prüss-Ustün, Michelle C. Turner, Susan M. Gapstur, W. Ryan Diver, and Aaron Cohen. An integrated risk function for estimating the global burden of disease attributable to ambient fine particulate matter exposure. *Environmental Health Perspectives*, 122(4):397–403, 2014. ISSN 15529924. doi: 10.1289/ehp.1307049.

[10] K.E. Brown, D.K. Henze, and J.B. Milford. How accounting for climate and health impacts of emissions could change the US energy system. *Energy Policy*, 102, 2017. doi: 10.1016/j.enpol.2016.12.052.

[11] Steve H L Yim, Gideon L Lee, In Hwan, Jonathan I Levy, May K Woo, Stefani L Penn, Iny Jhun, Brent A Coull, Joel Schwartz, Matthew D Turner, Daven K Henze, and Shannon L Capps. Impact of the Volkswagen emissions control defeat device on US public health. *Environ.Res.Lett.*, 10, 2005. doi: 10.1088/1748-9326/10/11/114005.

[12] George D Thurston, Richard T Burnett, Michelle C Turner, Yuanli Shi, Daniel Krewski, Ramona Lall, Kazuhiko Ito, Michael Jerrett, Susan M Gapstur, W Ryan Diver, and C Arden Pope Iii. Ischemic Heart Disease Mortality and Long-Term Exposure to Source-Related Components of U.Sl Fine Particle Air Pollution. *Environmental Health Perspectives*, 124 (6):785–795, 2016. doi: 10.1289/ehp.1509777.

[13] Micaela E. Ellison and Michael T. Brett. Particulate phosphorus bioavailability as a function of stream flow and land cover. *Water Research*, 40 (6):1258–1268, 2006. ISSN 00431354. doi: 10.1016/j.watres.2006.01.016.

[14] Maaike Steenhof, Ilse Gosens, Maciej Strak, Krystal J Godri, Gerard Hoek, Flemming R Cassee, Ian S Mudway, Frank J Kelly, Roy M Harrison, Erik Lebret, Bert Brunekreef, Nicole A H Janssen, and Raymond H H Pieters. In vitro toxicity of particulate matter (PM) collected at different sites in the Netherlands is associated with PM composition, size fraction and oxidative potential–the RAPTES project. *Particle and fibre toxicology*, 8(1):26, 2011. ISSN 1743-8977. doi: 10.1186/1743-8977-8-26.

[15] Guor Cheng Fang, Cheng Nan Chang, Chia Chium Chu, Yuh Shen Wu, Peter Pi Cheng Fu, I. Lin Yang, and Ming Hsiang Chen. Characterization of particulate, metallic elements of TSP, PM2.5 and PM2.5-10 aerosols at a farm sampling site in Taiwan, Taichung. *Science of the Total Environment*, 308(1-3):157–166, 2003. ISSN 00489697. doi: 10.1016/S0048-9697(02)00648-4.

[16] WHO. World Health Statistics 2016. Technical report, World Health Organization, 2016.

[17] GBD MAPS Working Group and Bob O'Keef. Burden of Disease Attributable to Coal-Burning and Other Air Pollution Sources in China. Technical Report August, Special Report 20. Boston, MA - Health Effects Institute, 2016. URL `https://www.healtheffects.org/system/files/GBDMAPS-ReportEnglishFinal1.pdf`.

[18] U.S. Energy Information Administration. International Energy Outlook 2016. Technical Report May 2016, EIA, 2016. URL `www.eia.gov/forecasts/ieo/pdf/0484(2016).pdf`.

[19] NEB. " Thirteen Five-Year " period the total investment in renewable energy will reach 2 . 5 trillion yuan. Technical report, China National Energy Board, 2017.

[20] Michael Forsythe. China Aims to Spend at Least $ 360 Billion on Renewable Energy by 2020. *New York Times*, 2017. URL `https://www.nytimes.com/2017/01/05/world/asia/china-renewable-energy-investment.html?smid=fb-share{&}{_}r=0`.

[21] Energistyrelsen. Aftale om den danske energipolitik 2012-2020. Technical report, Energistyrelsen, 2012. URL http://www.ens.dk/sites/ens.dk/files/politik/dansk-klima-energipolitik/politiske-aftaler-paa-energiomraadet/energiaftalen-22-marts-2012/Aftale{_}22-03-2012{_}FINAL{_}ren.doc.pdf.

[22] ENS. Accelerating green energy towards 2020. Technical Report March, Danish Ministry of Climate, Energy and Building, 2012. URL https://ens.dk/sites/ens.dk/files/EnergiKlimapolitik/accelerating{_}green{_}energy{_}towards{_}2020.pdf.

[23] EFKM. Energipolitisk redegørelse 2016. Technical report, Energi-, forsynings- og klimaministerens redegørelse til Folketinget om energipolitikken, 2016. URL http://old.efkm.dk/sites/kebmin.dk/files/EnergipolitiskRede/energipolitisk{_}redegoerelse{_}2016.pdf.

[24] Energinet.dk. System Plan 2015 - Electricity and Gas in Denmark. Technical report, Energinet.dk, 2015. URL http://www.energinet.dk/SiteCollectionDocuments/Engelskedokumenter/Omos/SystemPlan2015.pdf.

[25] H. Lund and E. Münster. Management of surplus electricity-production from a fluctuating renewable-energy source. *Applied Energy*, 76(1-3):65–74, 2003. ISSN 03062619. doi: 10.1016/S0306-2619(03)00048-5.

[26] Martin I. Hoffert, Ken Caldeira, Gregory Benford, David R. Criswell, Christopher Green, Howard Herzog, Atul K. Jain, Haroon S. Kheshgi, Klaus S. Lackner, John S. Lewis, H. Douglas Lightfoot, Wallace Manheimer, John C. Mankins, Michael E.Mauel, L. John Perkins, Michael E. Schlesinger, Tyler Volk, and Tom M. L. Wigley. Advanced Technology Paths to Global Climate Stability: Energy for a Greenhouse Planet. *Science*, 298(5595):981–987, 2002. URL http://www.jstor.org/stable/3832889.

[27] M. Becherif, H. S. Ramadan, K. Cabaret, F. Picard, N. Simoncini, and O. Bethoux. Hydrogen Energy Storage: New Techno-Economic Emergence Solution Analysis. *Energy Procedia*, 74(0):371–380, 2015. ISSN 18766102. doi: 10.1016/j.egypro.2015.07.629.

[28] John Andrews and Bahman Shabani. Re-envisioning the role of hydrogen in a sustainable energy economy. *International Journal*

of Hydrogen Energy, 37(2):1184–1203, 2012. ISSN 03603199. doi: 10.1016/j.ijhydene.2011.09.137.

[29] S. Pacala and R. Socolow. Stabilization Wedges : Solving the Climate Problem for the Next 50 Years with Current Technologies. *Science*, 305 (5686):968–972, 2004. URL `http://www.jstor.org/stable/3837555`.

[30] W. Grove. On the Gas Voltaic Battery. Experiments Made with a View of Ascertaining the Rationale of Its Action and Its Application to Eudiometry. *Philosophical Transactions of the Royal Society of London*, 133(1843):91–112, 1843. doi: 10.1098/rstl.1843.0009.

[31] James Larminie and Andrew Dicks. *Fuel Cell Systems Explained*. Wiley, 2nd edition, 2003.

[32] Qingfeng Li, Ronghuan He, Jo Jensen, and Nj Bjerrum. Approaches and recent development of polymer electrolyte membranes for fuel cells operating above 100 C. *Chemistry of materials*, pages 4896–4915, 2003. ISSN 0897-4756. doi: 10.1021/cm0310519.

[33] Samuel Simon Araya, Fan Zhou, Vincenzo Liso, Simon Lennart Sahlin, Jakob Rabjerg Vang, Sobi Thomas, Xin Gao, Christian Jeppesen, and Søren Knudsen Kær. A comprehensive review of PBI-based high temperature PEM fuel cells. *International Journal of Hydrogen Energy*, 41(46): 21310–21344, 2016. ISSN 03603199. doi: 10.1016/j.ijhydene.2016.09.024.

[34] Xuan Cheng, Zheng Shi, Nancy Glass, Lu Zhang, Jiujun Zhang, Datong Song, Zhong Sheng Liu, Haijiang Wang, and Jun Shen. A review of PEM hydrogen fuel cell contamination: Impacts, mechanisms, and mitigation. *Journal of Power Sources*, 165(2):739–756, 2007. ISSN 03787753. doi: 10.1016/j.jpowsour.2006.12.012.

[35] Gia Nguyen, Simon Sahlin, Søren Juhl Andreasen, Brendan Shaffer, and Jack Brouwer. Dynamic modeling and experimental investigation of a high temperature PEM fuel cell stack. *International Journal of Hydrogen Energy*, 41(8):4729–4739, 2016. ISSN 03603199. doi: 10.1016/j.ijhydene.2016.01.045.

[36] Susanta K. Das, Antonio Reis, and K. J. Berry. Experimental evaluation of CO poisoning on the performance of a high temperature proton exchange membrane fuel cell. *Journal of Power Sources*, 193(2):691–698, 2009. ISSN 03787753. doi: 10.1016/j.jpowsour.2009.04.021.

[37] R.E. Rosli, A.B. Sulong, W.R.W. Daud, M.A. Zulkifley, T. Husaini, M.I. Rosli, E.H. Majlan, and M.A. Haque. A review of high-temperature proton exchange membrane fuel cell (HT-PEMFC) system. *International Journal of Hydrogen Energy*, pages 1–22, 2016. ISSN 03603199. doi: 10.1016/j.ijhydene.2016.06.211.

[38] D. J. Durbin and C. Malardier-Jugroot. Review of hydrogen storage techniques for on board vehicle applications. *International Journal of Hydrogen Energy*, 38(34):14595–14617, 2013. ISSN 03603199. doi: 10.1016/j.ijhydene.2013.07.058.

[39] George A. Olah, Alain Goeppert, and G. K Surya Prakash. Chemical recycling of carbon dioxide to methanol and dimethyl ether: From greenhouse gas to renewable, environmentally carbon neutral fuels and synthetic hydrocarbons. *Journal of Organic Chemistry*, 74(2):487–498, 2009. ISSN 00223263. doi: 10.1021/jo801260f.

[40] S. T. Yong, C. W. Ooi, S. P. Chai, and X. S. Wu. Review of methanol reforming-Cu-based catalysts, surface reaction mechanisms, and reaction schemes. *International Journal of Hydrogen Energy*, 38(22):9541–9552, 2013. ISSN 03603199. doi: 10.1016/j.ijhydene.2013.03.023.

[41] Jens Anton Christiansen. A reaction between methanol and water and some related reactions. *J. Am. Chem. Soc.*, 43:1670, 1921.

[42] Jens Anton Christiansen and J. R. Huffman. The reaction between methanol and steam as an example of heterogeneous catalysis. *Z. Phys. Chem.*, 34(A151):269–302, 1930.

[43] Jens Anton Christiansen. Use of the method of stationary velocities for the reaction CH3OH + H2O -> 3H2 + CO2. *Z. Phys. Chem.*, pages 69–77, 1931.

[44] SerEnergy. SerEnergy Methanol Fuel Cell Systems, 2017. URL `http://serenergy.com/applications/systems/`.

[45] S. S. Kurpit. 1.5 and 3KW indirect methanol-air fuel cell power plants. In *Annual Intersociety Energy Conversion and Engineering Conference*, pages 222–228, Newark, Del., 1975. URL `http://adsabs.harvard.edu/abs/1975iece.conf..222K`.

[46] DoE. The Fuel Cell Technologies Office Multi-Year Research, Development, and Demonstration Plan. Technical report, U.S. Department of Energy, 2016. URL `https://energy.gov/eere/fuelcells/fuel-cells`.

[47] Samuel Simon Araya. *High Temperature PEM Fuel Cells - Degradation and Durability*. PhD thesis, Aalborg University, 2012.

[48] N. Yousfi-Steiner, Ph Moçotéguy, D. Candusso, and D. Hissel. A review on polymer electrolyte membrane fuel cell catalyst degradation and starvation issues: Causes, consequences and diagnostic for mitigation. *Journal of Power Sources*, 194(1):130–145, 2009. ISSN 03787753. doi: 10.1016/j.jpowsour.2009.03.060.

[49] D. Hissel and M.C. Pera. Diagnostic & health management of fuel cell systems: Issues and solutions. *Annual Reviews in Control*, 42:201–211, 2016. ISSN 13675788. doi: 10.1016/j.arcontrol.2016.09.005.

[50] Chi Yuan Lee and Yu Ming Lee. In-situ diagnosis of local fuel cell performance using novel micro sensors. *International Journal of Hydrogen Energy*, 37(5):4448–4456, 2012. ISSN 03603199. doi: 10.1016/j.ijhydene.2011.11.098.

[51] Chi-Yuan Lee, Fang-Bor Weng, Yzu-Wei Kuo, Yen-Ting Cheng, Chih-Kai Cheng, Chao-Hsuan Tsai, and Ti-Ju Lee. Persistent effect test for high temperature resistant integrated microsensor embedded in high temperature proton exchange membrane fuel cell stack. *Sensors and Actuators A: Physical*, 250:202–209, 2016. ISSN 0924-4247. doi: http://dx.doi.org/10.1016/j.sna.2016.09.026.

[52] Wensheng He and Trung Van Nguyen. A New Diagnostic Tool for Liquid Water Management in PEM Fuel Cells Using Interdigitated Flow Fields. In *Electrochemical society meeting 2002*, 2002.

[53] F. Barbir, H. Gorgun, and X. Wang. Relationship between pressure drop and cell resistance as a diagnostic tool for PEM fuel cells. *Journal of Power Sources*, 141(1):96–101, 2005. ISSN 03787753. doi: 10.1016/j.jpowsour.2004.08.055.

[54] Rupak Banerjee, Danielle Howe, Valentina Mejia, and Satish G. Kandlikar. Experimental validation of two-phase pressure drop multiplier as a diagnostic tool for characterizing PEM fuel cell performance. *International Journal of Hydrogen Energy*, 39(31):17791–17801, 2014. ISSN 03603199. doi: 10.1016/j.ijhydene.2014.08.118.

[55] Torsten Berning. A method for the ad hoc and real-time determination of the water balance in a PEMFC. *International Jour-*

nal of Hydrogen Energy, 39(1):449–458, 2014. ISSN 03603199. doi: 10.1016/j.ijhydene.2013.09.126.

[56] Torsten Berning and Saher Al Shakhshir. Applying hot-wire anemometry to directly measure the water balance in a proton exchange membrane fuel cell for a pre-humidified hydrogen stream. *International Journal of Hydrogen Energy*, 41(10):5315–5320, 2016. ISSN 03603199. doi: 10.1016/j.ijhydene.2016.01.136.

[57] B. Legros, P. X. Thivel, Y. Bultel, M. Boinet, and R. P. Nogueira. Acoustic emission: Towards a real-time diagnosis technique for Proton exchange membrane fuel cell operation. *Journal of Power Sources*, 195(24):8124–8133, 2010. ISSN 03787753. doi: 10.1016/j.jpowsour.2010.07.045.

[58] D. Hissel, S. Jemeï, V. Hubert, X. François, M.C. Péra, and J.M. Kauffmann. A diagnosis-oriented model of a fuel cell power generator dedicated to automotive applications. In *ISNGVT'01 4th international symposium on next generation vehicle technology*, pages 49–57´4, 2001.

[59] D Hissel, M.C Péra, and J.M Kauffmann. Diagnosis of automotive fuel cell power generators. *Journal of Power Sources*, 128(2):239–246, 2004. ISSN 03787753. doi: 10.1016/j.jpowsour.2003.10.001. URL `http://www.sciencedirect.com/science/article/pii/S0378775303010127`.

[60] O. Lottin, B. Antoine, T. Colinart, S. Didierjean, G. Maranzana, C. Moyne, and J. Ramousse. Modelling of the operation of Polymer Exchange Membrane Fuel Cells in the presence of electrodes flooding. *International Journal of Thermal Sciences*, 48(1):133–145, jan 2009. ISSN 12900729. doi: 10.1016/j.ijthermalsci.2008.03.013.

[61] Jianlu Zhang, Yanghua Tang, Chaojie Song, Zetao Xia, Hui Li, Haijiang Wang, and Jiujun Zhang. PEM fuel cell relative humidity (RH) and its effect on performance at high temperatures. *Electrochimica Acta*, 53(16):5315–5321, 2008. ISSN 00134686. doi: 10.1016/j.electacta.2008.02.074.

[62] R. Petrone, Z. Zheng, D. Hissel, M. C. Péra, C. Pianese, M. Sorrentino, M. Becherif, and N. Yousfi-Steiner. A review on model-based diagnosis methodologies for PEMFCs. *International Journal of Hydrogen Energy*, 38(17):7077–7091, jun 2013. ISSN 0360-3199. doi: 10.1016/j.ijhydene.2013.03.106.

[63] T. Escobet, D. Feroldi, S. de Lira, V. Puig, J. Quevedo, J. Riera, and M. Serra. Model-based fault diagnosis in PEM fuel cell systems.

Journal of Power Sources, 192(1):216–223, 2009. ISSN 03787753. doi: 10.1016/j.jpowsour.2008.12.014.

[64] Albert Rosich, Fatiha Nejjari, and Ramon Sarrate. *Fuel cell system diagnosis based on a causal structural model*, volume 42. IFAC, 2009. ISBN 9783902661463. doi: 10.3182/20090630-4-ES-2003.00089.

[65] A. Rosich, R. Sarrate, and F. Nejjari. On-line model-based fault detection and isolation for PEM fuel cell stack systems. *Applied Mathematical Modelling*, 38(11-12):2744–2757, 2014. ISSN 0307904X. doi: 10.1016/j.apm.2013.10.065.

[66] Q Yang, A Aitouche, and B Ould Bouamama. Structural Analysis for Air Supply System of Fuel Cell. *International Renewable Energy Congress \\emph{IREC'09}*, 2009. URL `https://hal.archives-ouvertes.fr/hal-00804098`.

[67] Q Yang, A Aitouche, and B Ould Bouamama. Structural Analysis for Fault Detection and Isolation in Fuel Cell Stack System. In *Sustainability in Energy and Buildings: Proceedings of the International Conference in Sustainability in Energy and Buildings (SEB'09)*, pages 239–254. Springer Berlin Heidelberg, 2009.

[68] Pierpaolo Polverino, Cesare Pianese, Marco Sorrentino, and Dario Marra. Model-based development of a fault signature matrix to improve solid oxide fuel cell systems on-site diagnosis. *Journal of Power Sources*, 280: 320–338, 2015. ISSN 03787753. doi: 10.1016/j.jpowsour.2015.01.037.

[69] Pierpaolo Polverino, Angelo Esposito, Cesare Pianese, Bastian Ludwig, Boris Iwanschitz, and Andreas Mai. On-line experimental validation of a model-based diagnostic algorithm dedicated to a solid oxide fuel cell system. *Journal of Power Sources*, 306:646–657, 2016. ISSN 03787753. doi: 10.1016/j.jpowsour.2015.12.046.

[70] S. De Lira, V. Puig, and J. Quevedo. LPV model-based fault diagnosis using relative fault sensitivity signature approach in a PEM fuel cell. *IFAC Proceedings Volumes (IFAC-PapersOnline)*, pages 528–533, 2009. ISSN 14746670. doi: 10.3182/20090630-4-ES-2003.0335.

[71] S. De Lira, V. Puig, and J. Quevedo. Robust LPV model-based sensor fault diagnosis and estimation for a PEM fuel cell system. *Conference on Control and Fault-Tolerant Systems, SysTol'10 - Final Program and Book of Abstracts*, pages 819–824, 2010. doi: 10.1109/SYSTOL.2010.5676000.

[72] Saeed Asghari, Ali Mokmeli, and Mahrokh Samavati. Study of PEM fuel cell performance by electrochemical impedance spectroscopy. *International Journal of Hydrogen Energy*, 35(17):9283–9290, 2010. ISSN 03603199. doi: 10.1016/j.ijhydene.2010.03.069.

[73] Carmelo Brunetto, Antonino Moschetto, and Giuseppe Tina. PEM fuel cell testing by electrochemical impedance spectroscopy. *Electric Power Systems Research*, 79(1):17–26, 2009. ISSN 03787796. doi: 10.1016/j.epsr.2008.05.012.

[74] Søren Juhl Andreasen, J. L. Jespersen, E. Schaltz, and S. K. Kær. Characterisation and modelling of a high temperature PEM fuel cell stack using electrochemical impedance spectroscopy. *Fuel Cells*, 9(4):463–473, 2009. ISSN 16156846. doi: 10.1002/fuce.200800137.

[75] Jesper Lebæk Jespersen, Erik Schaltz, and Søren Knudsen Kær. Electrochemical characterization of a polybenzimidazole-based high temperature proton exchange membrane unit cell. *Journal of Power Sources*, 191(2): 289–296, 2009. ISSN 03787753. doi: 10.1016/j.jpowsour.2009.02.025.

[76] Seyed Mohammad Rezaei Niya and Mina Hoorfar. Study of proton exchange membrane fuel cells using electrochemical impedance spectroscopy technique - A review. *Journal of Power Sources*, 240:281–293, 2013. ISSN 03787753. doi: 10.1016/j.jpowsour.2013.04.011.

[77] Søren Juhl Andreasen, Rasmus Mosbæk, Jakob Rabjerg, Søren Knudsen Kær, and Samuel Simon Araya. Eis Characterization Of The Poisoning Effects Of Co And Co 2 On A Pbi Based Ht-Pem Fuel Cell. In *Proceedings of the ASME 2010 Eighth International Fuel Cell Science, Engineering and Technology Conference*, 2010.

[78] Xiaozi Yuan, Haijiang Wang, Jian Colin Sun, and Jiujun Zhang. AC impedance technique in PEM fuel cell diagnosis–A review. *International Journal of Hydrogen Energy*, 32(17):4365 – 4380, 2007. ISSN 0360-3199. doi: DOI: 10.1016/j.ijhydene.2007.05.036.

[79] Søren Juhl Andreasen, Jakob Rabjerg Vang, and Søren Knudsen Kær. High temperature PEM fuel cell performance characterisation with CO and CO2 using electrochemical impedance spectroscopy. *International Journal of Hydrogen Energy*, 36(16):9815–9830, 2011. ISSN 03603199. doi: 10.1016/j.ijhydene.2011.04.076.

[80] J. E. B. Randle. KINETICS OF RAPID ELECTRODE REACTIONS. *Discussions of the Faraday Society*, 1:11–19, 1947. doi: DOI: 10.1039/DF9470100011.

[81] N. Fouquet, C. Doulet, C. Nouillant, G. Dauphin-Tanguy, and B. Ould-Bouamama. Model based PEM fuel cell state-of-health monitoring via ac impedance measurements. *Journal of Power Sources*, 159(2):905–913, 2006. ISSN 03787753. doi: 10.1016/j.jpowsour.2005.11.035.

[82] Thomas Génevé, Jérémi Régnier, and Christophe Turpin. Fuel cell flooding diagnosis based on time-constant spectrum analysis. *International Journal of Hydrogen Energy*, 41(1):516–523, 2016. ISSN 03603199. doi: 10.1016/j.ijhydene.2015.10.089.

[83] Samuel Simon Araya, Ionela Florentina Grigoras, Fan Zhou, Søren Juhl Andreasen, and Søren Knudsen Kær. Performance and endurance of a high temperature PEM fuel cell operated on methanol reformate. *International Journal of Hydrogen Energy*, 39(32):18343–18350, oct 2014. ISSN 03603199. doi: 10.1016/j.ijhydene.2014.09.007.

[84] S. Tant, S. Rosini, P.-X. Thivel, F. Druart, A. Rakotondrainibe, T. Geneston, and Y. Bultel. An algorithm for diagnosis of proton exchange membrane fuel cells by electrochemical impedance spectroscopy. *Electrochimica Acta*, 135:368–379, 2014. ISSN 00134686. doi: 10.1016/j.electacta.2014.04.108.

[85] G. Mousa, J. Devaal, and F. Golnaraghi. Diagnosis of hydrogen crossover and emission in proton exchange membrane fuel cells. *International Journal of Hydrogen Energy*, 39(35):20116–20126, 2014. ISSN 03603199. doi: 10.1016/j.ijhydene.2014.09.116.

[86] Ghassan Mousa, Farid Golnaraghi, Jake Devaal, and Alan Young. Detecting proton exchange membrane fuel cell hydrogen leak using electrochemical impedance spectroscopy method. *Journal of Power Sources*, 246:110–116, 2014. ISSN 03787753. doi: 10.1016/j.jpowsour.2013.07.018.

[87] T. Konomi and I. Saho. Research of diagnosis technique on PEFC running condition (over voltage analysis and diagnosis of PEFC by FFT). *Nihon Kikai Gakkai Ronbunshu, B Hen/Transactions of the Japan Society of Mechanical Engineers, Part B*, 72(2), 2006.

[88] T. Konomi, A. Kawakami, and H. Tachibana. Effects of internal leak current on PEFC output voltage (Internal leak current at open circuit

and close circuit in smaller current density region). *Nihon Kikai Gakkai Ronbunshu, B Hen/Transactions of the Japan Society of Mechanical Engineers, Part B*, 71(712), 2005.

[89] Abdellah Narjiss, Daniel Depernet, Denis Candusso, Frederic Gustin, and Daniel Hissel. Online diagnosis of PEM fuel cell. *2008 13th International Power Electronics and Motion Control Conference, EPE-PEMC 2008*, pages 734–739, 2008. doi: 10.1109/EPEPEMC.2008.4635354.

[90] O. Bethoux, M. Hilairet, and T. Azib. A new on-line state-of-health monitoring technique dedicated to PEM fuel cell. *IECON Proceedings (Industrial Electronics Conference)*, pages 2745–2750, 2009. ISSN 1553-572X. doi: 10.1109/IECON.2009.5415422.

[91] S. Jemeï, D. Hissel, M. C. Péra, and J. M. Kauffmann. On-board fuel cell power supply modeling on the basis of neural network methodology. *Journal of Power Sources*, 124(2):479–486, 2003. ISSN 03787753. doi: 10.1016/S0378-7753(03)00799-7.

[92] Samir Jemeï, Daniel Hissel, Marie-Cécile Péra, and Jean Marie Kauffmann. A New Modeling Approach of Embedded Fuel-Cell Power Generators Based on Artificial Neural Network. *IEEE Transactions on Industrial Electronics*, 55(1):437–447, 2008. ISSN printan. doi: 10.1109/TIE.2007.896480.

[93] Koan-Yuh Chang. The optimal design for PEMFC modeling based on Taguchi method and genetic algorithm neural networks. *International Journal of Hydrogen Energy*, 36(21):13683–13694, 2011. ISSN 0360-3199. doi: 10.1016/j.ijhydene.2011.07.094.

[94] Zhi Dan Zhong, Xin Jian Zhu, and Guang Yi Cao. Modeling a PEMFC by a support vector machine. *Journal of Power Sources*, 160(1):293–298, 2006. ISSN 03787753. doi: 10.1016/j.jpowsour.2006.01.040.

[95] Zhi Dan Zhong, Xin Jian Zhu, Guang Yi Cao, and Jun Hai Shi. A hybrid multi-variable experimental model for a PEMFC. *Journal of Power Sources*, 164(2):746–751, 2007. ISSN 03787753. doi: 10.1016/j.jpowsour.2006.11.030.

[96] Chun Hua Li, Xin Jian Zhu, Guang Yi Cao, Sheng Sui, and Ming Ruo Hu. Identification of the Hammerstein model of a PEMFC stack based on least squares support vector machines. *Journal of Power Sources*, 175 (1):303–316, 2008. ISSN 03787753. doi: 10.1016/j.jpowsour.2007.09.049.

[97] Yasemin Vural, Derek B. Ingham, and Mohamed Pourkashanian. Performance prediction of a proton exchange membrane fuel cell using the ANFIS model. *International Journal of Hydrogen Energy*, 34(22):9181–9187, 2009. ISSN 03603199. doi: 10.1016/j.ijhydene.2009.08.096.

[98] Yi-ping Liu, Gang Niu, and Jing Wang. Design of capacitance sensor system for void fraction measurement. *Journal of Zhejiang University SCIENCE A*, 6A(12):1424–1429, 2005. ISSN 1673-565X. doi: 10.1631/jzus.2005.A.

[99] Kristian Kjær Justesen, Søren Juhl Andreasen, and Simon Lennart Sahlin. Modeling of a HTPEM fuel cell using Adaptive Neuro-Fuzzy Inference Systems. *International Journal of Hydrogen Energy*, 40(46): 16814–16819, 2015. ISSN 03603199. doi: 10.1016/j.ijhydene.2015.08.061.

[100] N. Yousfi Steiner, D. Candusso, D. Hissel, and P. Mooteguy. Model-based diagnosis for proton exchange membrane fuel cells. *Mathematics and Computers in Simulation*, 81(2):158–170, 2010. ISSN 03784754. doi: 10.1016/j.matcom.2010.02.006.

[101] N. Yousfi Steiner, D. Hissel, Ph. Moçotéguy, and D. Candusso. Diagnosis of polymer electrolyte fuel cells failure modes (flooding & drying out) by neural networks modeling. *International Journal of Hydrogen Energy*, 36(4):3067–3075, 2011. ISSN 03603199. doi: 10.1016/j.ijhydene.2010.10.077.

[102] M. Sorrentino, D. Marra, C. Pianese, M. Guida, F. Postiglione, K. Wang, and A. Pohjoranta. On the Use of Neural Networks and Statistical Tools for Nonlinear Modeling and On-field Diagnosis of Solid Oxide Fuel Cell Stacks. *Energy Procedia*, 45:298–307, 2014. ISSN 18766102. doi: 10.1016/j.egypro.2014.01.032.

[103] Z. Zheng, R. Petrone, M. C. Péra, D. Hissel, M. Becherif, C. Pianese, N. Yousfi Steiner, and M. Sorrentino. A review on non-model based diagnosis methodologies for PEM fuel cell stacks and systems. *International Journal of Hydrogen Energy*, 38(21):8914–8926, 2013. ISSN 03603199. doi: 10.1016/j.ijhydene.2013.04.007.

[104] Alan V. Oppenheim and Ronald W. Schafer. *Discrete-Time Signal Processing*. Prentice-Hall Signal Processing Series, 3rd edition, 2014.

[105] Mona Ibrahim, Ursula Antoni, Nadia Yousfi Steiner, Samir Jemei, Celestin Kokonendji, Bastian Ludwig, Philippe Moçotéguy, and Daniel

Hissel. Signal-Based Diagnostics by Wavelet Transform for Proton Exchange Membrane Fuel Cell. *Energy Procedia*, 74:1508–1516, 2015. ISSN 18766102. doi: 10.1016/j.egypro.2015.07.708.

[106] M.A. Rubio, K. Bethune, A. Urquia, and J. St-Pierre. Proton exchange membrane fuel cell failure mode early diagnosis with wavelet analysis of electrochemical noise. *International Journal of Hydrogen Energy*, 41(33): 14991–15001, 2016. ISSN 03603199. doi: 10.1016/j.ijhydene.2016.05.292.

[107] E Pahon, N Yousfi-Steiner, S Jemei, D Hissel, and P Moçoteguy. A Non-Intrusive Signal-Based Method for a Proton Exchange Membrane Fuel Cell Fault Diagnosis. *Fuel Cells*, page 62319, 2012. ISSN 1615-6854. doi: 10.1002/fuce.201600070.

[108] D. Benouioua, D. Candusso, F. Harel, and L. Oukhellou. Fuel cell diagnosis method based on multifractal analysis of stack voltage signal. *International Journal of Hydrogen Energy*, 39(5):2236–2245, 2014. ISSN 03603199. doi: 10.1016/j.ijhydene.2013.11.066.

[109] D. Benouioua, D. Candusso, F. Harel, and L. Oukhellou. PEMFC stack voltage singularity measurement and fault classification. *International Journal of Hydrogen Energy*, 39(36):21631–21637, 2014. ISSN 03603199. doi: 10.1016/j.ijhydene.2014.09.117. URL `http://dx.doi.org/10.1016/j.ijhydene.2014.09.117`.

[110] D. Benouioua, D. Candusso, F. Harel, and L. Oukhellou. The dynamic multifractality in PEMFC stack voltage signal as a tool for the aging monitoring. *International Journal of Hydrogen Energy*, pages 2–7, 2016. ISSN 03603199. doi: 10.1016/j.ijhydene.2016.04.033.

[111] D. Benouioua, D. Candusso, F. Harel, and L. Oukhellou. Multifractal Analysis of Stack Voltage Based on Wavelet Leaders: A New Tool for PEMFC Diagnosis. *Fuel Cells*, pages 1–8, 2016. ISSN 16156854. doi: 10.1002/fuce.201600029.

[112] Noboru Katayama and Sumio Kogoshi. Real-Time Electrochemical Impedance Diagnosis for Fuel Cells Using a DC-DC Converter. *IEEE Transactions on Energy Conversion*, 30(2):707–713, 2014. ISSN 08858969. doi: 10.1109/TEC.2014.2376529.

[113] Jixin Chen and Biao Zhou. Diagnosis of PEM fuel cell stack dynamic behaviors. *Journal of Power Sources*, 177(1):83–95, 2008. ISSN 03787753. doi: 10.1016/j.jpowsour.2007.11.038.

[114] Giovanni Dotelli, Roberto Ferrero, Paola Gallo Stampino, Saverio Latorrata, and Sergio Toscani. PEM Fuel Cell Drying and Flooding Diagnosis With Signals Injected by a Power Converter. *IEEE Transactions on Instrumentation and Measurement*, 64(8):2064–2071, 2015. ISSN 00189456. doi: 10.1109/TIM.2015.2406051.

[115] Cédric Damour, Michel Benne, Brigitte Grondin-Perez, Miloud Bessafi, Daniel Hissel, and Jean Pierre Chabriat. Polymer electrolyte membrane fuel cell fault diagnosis based on empirical mode decomposition. *Journal of Power Sources*, 299:596–603, 2015. ISSN 03787753. doi: 10.1016/j.jpowsour.2015.09.041.

[116] Jianfeng Hua, Jianqiu Li, Minggao Ouyang, Languang Lu, and Liangfei Xu. Proton exchange membrane fuel cell system diagnosis based on the multivariate statistical method. *International Journal of Hydrogen Energy*, 36(16):9896–9905, 2011. ISSN 03603199. doi: 10.1016/j.ijhydene.2011.05.075.

[117] Zhongliang Li, Rachid Outbib, Daniel Hissel, and Stefan Giurgea. Online diagnosis of PEMFC by analyzing individual cell voltages. In *2013 European Control Conference (ECC)*, pages 2439–2444, Zürich, Switzerland, 2013. ISBN 9783952417348.

[118] Zhongliang Li, Stefan Giurgea, Rachid Outbib, and Daniel Hissel. Fault diagnosis and novel fault type detection for PEMFC system based on spherical-shaped multiple-class support vector machine. *IEEE/ASME International Conference on Advanced Intelligent Mechatronics, AIM*, pages 1628–1633, 2014. doi: 10.1109/AIM.2014.6878317.

[119] Zhongliang Li, Rachid Outbib, Stefan Giurgea, Daniel Hissel, and Yongdong Li. Fault detection and isolation for Polymer Electrolyte Membrane Fuel Cell systems by analyzing cell voltage generated space. *Applied Energy*, 148:260–272, 2015. ISSN 03062619. doi: 10.1016/j.apenergy.2015.03.076.

[120] Zhongliang Li, Rachid Outbib, Daniel Hissel, and Stefan Giurgea. Data-driven diagnosis of PEM fuel cell: A comparative study. *Control Engineering Practice*, 28:1–12, 2014. ISSN 09670661. doi: 10.1016/j.conengprac.2014.02.019.

[121] Luis Alberto M Riascos, Marcelo G. Simoes, and Paulo E. Miyagi. A Bayesian network fault diagnostic system for proton exchange mem-

brane fuel cells. *Journal of Power Sources*, 165(1):267–278, 2007. ISSN 03787753. doi: 10.1016/j.jpowsour.2006.12.003.

[122] Luis Alberto M Riascos, Marcelo G. Simoes, and Paulo E. Miyagi. Online fault diagnostic system for proton exchange membrane fuel cells. *Journal of Power Sources*, 175(1):419–429, 2008. ISSN 03787753. doi: 10.1016/j.jpowsour.2007.09.010.

[123] Sebastien Wasterlain, Denis Candusso, Fabien Harel, Xavier Francois, and Daniel Hissel. Diagnosis of a fuel cell stack using electrochemical impedance spectroscopy and Bayesian Networks. *2010 IEEE Vehicle Power and Propulsion Conference*, pages 1–6, 2010. doi: 10.1109/VPPC.2010.5729184.

[124] K. Wang, M. C. Péra, D. Hissel, N. Yousfi Steiner, A. Pohjoranta, and S. Pofahl. SOFC modelling based on discrete Bayesian network For system diagnosis use. *IFAC Proceedings Volumes (IFAC-PapersOnline)*, 8 (PART 1):675–680, 2012. ISSN 14746670. doi: 10.3182/20120902-4-FR-2032.00118.

[125] Raïssa Onanena, Latifa Oukhellou, Etienne Côme E, and Samir Jemei. Fuel Cell Health Monitoring Using Self Organizing Maps. *Chemical Enginering Transactions*, 33:1021–1026, 2013. doi: 10.3303/CET1333171.

[126] Z. Li, S. Giurgea, R. Outbib, and D. Hissel. Online diagnosis of PEMFC by combining support vector machine and fluidic model. *Fuel Cells*, 14 (3):448–456, 2014. ISSN 16156854. doi: 10.1002/fuce.201300197.

[127] Zhongliang Li, Rachid Outbib, Stefan Giurgea, and Daniel Hissel. Diagnosis for PEMFC Systems: A Data-Driven Approach With the Capabilities of Online Adaptation and Novel Fault Detection. *IEEE Transactions on Industrial Electronics*, 62(8):5164–5174, 2015. ISSN 02780046. doi: 10.1109/TIE.2015.2418324.

[128] Andrej Debenjak, Matej Gašperin, Boštjan Pregelj, Maja Atanasijević-Kunc, Janko Petrovčič, and Vladimir Jovan. Detection of flooding and drying inside a PEM fuel cell stack. *Strojniski Vestnik/Journal of Mechanical Engineering*, 59(1):56–64, 2013. ISSN 00392480. doi: 10.5545/sv-jme.2012.640.

[129] R. Onanena, L Oukhellou, E Côme, D Candusso, D Hissel, P Aknin, and P Aknin R. Onanena, L Oukhellou, E Côme, D Candusso, D Hissel. Fault-diagnosis of PEM fuel cells using electrochemical spectroscopy

impedance. *Power Plants and Power Systems Control*, 45(21):651–656, 2012. ISSN 14746670. doi: 10.3182/20120902-4-FR-2032.00114.

[130] Zhixue Zheng, Marie Cécile Péra, Daniel Hissel, Mohamed Becherif, Kréhi Serge Agbli, and Yongdong Li. A double-fuzzy diagnostic methodology dedicated to online fault diagnosis of proton exchange membrane fuel cell stacks. *Journal of Power Sources*, 271:570–581, 2014. ISSN 03787753. doi: 10.1016/j.jpowsour.2014.07.157.

[131] Z. Zheng, R. Petrone, M. C. Pera, D. Hissel, M. Becherif, and C. Pianese. Diagnosis of a commercial PEM fuel cell stack via incomplete spectra and fuzzy clustering. *IECON Proceedings (Industrial Electronics Conference)*, pages 1595–1600, 2013. doi: 10.1109/IECON.2013.6699371.

[132] Chris de Beer, Paul Barendse, Pragasen Pillay, Brian Bullecks, and Raghunathan Rengaswamy. Classification of High Temperature PEM Fuel Cell Degradation Mechanisms Using Equivalent Circuits. *IEEE Transactions on Industrial Electronics*, 0046(c):1–1, 2014. ISSN 0278-0046. doi: 10.1109/TIE.2015.2393292.

[133] SS Araya, SJ Andreasen, and SK Kær. Experimental characterization of the poisoning effects of methanol-based reformate impurities on a PBI-based high temperature PEM fuel cell. *Energies*, 5:4251—-4267, 2012. doi: doi:10.3390/en5114251.

[134] Marta Boaventura, Isabel Alves, Paulo Ribeirinha, and Adélio Mendes. The influence of impurities in high temperature polymer electrolyte membrane fuel cells performance. *International Journal of Hydrogen Energy*, 1:2–11, 2016. ISSN 03603199. doi: 10.1016/j.ijhydene.2016.06.201.

[135] Sobi Thomas, Jakob Rabjerg Vang, Samuel Simon Araya, and Søren Knudsen Kær. Experimental study to distinguish the effects of methanol slip and water vapour on a high temperature PEM fuel cell at different operating conditions. *Applied Energy*, pages –, 2016. ISSN 0306-2619. doi: http://dx.doi.org/10.1016/j.apenergy.2016.11.063.

[136] Hans-christian B Jensen, Søren Juhl, Søren Knudsen, and Erik Schaltz. Estimation of CO concentration in high temperature PEM fuel cells using electrochemical impedance spectroscopy. *Proceedings of the 5th International Conference on Fundamentals and Development of Fuel Cells, FDFC2013*, pages 4623 – 4630, 2013.

[137] Sobi Thomas, Sang C. Lee, A.K. Sahu, and Sam Park. Online health monitoring of a fuel cell using total harmonic distortion analysis. *International Journal of Hydrogen Energy*, 39(9):4558–4565, mar 2014. ISSN 03603199. doi: 10.1016/j.ijhydene.2013.12.180.

[138] Chris de Beer, Paul Barendse, Pragasen Pillay, Brian Bullecks, and Raghunathan Rengaswamy. Electrical circuit analysis of CO poisoning in high temperature PEM fuel cells for rapid fault diagnostics. *2013 IEEE Energy Conversion Congress and Exposition*, 51(1):4623–4630, 2013. ISSN 00939994. doi: 10.1109/ECCE.2013.6647320.

[139] Chris De Beer, Paul Barendse, Pragasen Pillay, Brian Pullecks, and Raghunathan Rengaswamy. Online fault diagnostics and impedance signature mapping of High Temperature PEM fuel cells using rapid small signal injection. *Electrochimica Acta*, 35(10):1798–1803, 2013. ISSN 1553-572X. doi: 10.1109/IECON.2013.6699404.

[140] Chris de Beer, Paul S. Barendse, Pragasen Pillay, Brian Bullecks, and Raghunathan Rengaswamy. Online Diagnostics of HTPEM Fuel Cells Using Small Amplitude Transient Analysis for CO Poisoning. *IEEE Transactions on Industrial Electronics*, PP(99):1–1, 2014. ISSN 0278-0046. doi: 10.1109/TIE.2014.2377131.

[141] Steven M. Kay. *Fundamentals of Statistical Signal Processing - Volume II Detection Theory*. Prentice Hall, 1st edition, 1998. ISBN 007-6092032243.

[142] Jakob Rabjerg Vang, Søren Juhl Andreasen, Samuel Simon Araya, and Søren Knudsen Kær. Comparative study of the break in process of post doped and sol-gel high temperature proton exchange membrane fuel cells. *International Journal of Hydrogen Energy*, 39(27):14959–14968, 2014. ISSN 03603199. doi: 10.1016/j.ijhydene.2014.07.017.

[143] Raffaele Petrone. *Electrochemical Impedance Spectroscopy for the onboard diagnosis of PEMFC via on-line identification of Equivalent Circuit Model parameters*. PhD thesis, University Of Salerno and University Of Franche-Comte, Femto-St Laboratory, 2014.

[144] RAINER STORN and KENNETH PRICE. Differential evolution – a simple and efficient heuristic for global optimization over continuous spaces. *Journal of global optimization*, pages 341–359, 1997. ISSN 0925-5001. doi: 10.1023/A:1008202821328.

[145] Rasmus K. Ursem. *Models for Evolutionary Algorithms and Their Applications in System Identification and Control Optimization*. PhD thesis, University of Aarhus, 2003.

[146] Ethem Alpaydin. *Introduction to Machine Learning*. The MIT Press, 2nd ed. edition, 2010.

[147] Daniel Hissel, Denis Candusso, and Fabien Harel. Fuzzy-clustering durability diagnosis of polymer electrolyte fuel cells dedicated to transportation applications. *IEEE Transactions on Vehicular Technology*, 56(5 I): 2414–2420, 2007. ISSN 00189545. doi: 10.1109/TVT.2007.898389.

[148] M. Chandesris, C. Robin, M. Gerard, and Y. Bultel. Investigation of the difference between the low frequency limit of the impedance spectrum and the slope of the polarization curve. *Electrochimica Acta*, 180:581–590, 2015. ISSN 00134686. doi: 10.1016/j.electacta.2015.08.089.

[149] I. a. Schneider, S. a. Freunberger, D. Kramer, A. Wokaun, and G. G. Scherer. Oscillations in Gas Channels - Part I. The Forgotten Player in Impedance Spectroscopy in PEFCs. *Journal of The Electrochemical Society*, 154(4):B383—-B388, 2007. ISSN 00134651. doi: 10.1149/1.2435706.

[150] I. a. Schneider, S. a. Freunberger, D. Kramer, A. Wokaun, and G. G. Scherer. Oscillations in Gas Channels - Part II. Unraveling the Characteristics of the Low Frequency Loop in Air-Fed PEFC Impedance Spectra. *Journal of The Electrochemical Society*, 154(4):B770—-B782, 2007. doi: 10.1149/1.2742291.

[151] Bin-Tsang Tsai, Chung-Jen Tseng, Zhong-Sheng Liu, Chih-Hao Wang, Chun-I Lee, Chang-Chung Yang, and Shih-Kun Lo. Effects of flow field design on the performance of a PEM fuel cell with metal foam as the flow distributor. *International Journal of Hydrogen Energy*, 37(17):13060–13066, 2012. ISSN 03603199. doi: 10.1016/j.ijhydene.2012.05.008.

[152] Steven M. Kay. *Fundamentals of Statistical Signal Processing - Volume I Estimation Theory*. Prentice Hall PTR, 1st edition, 1993. ISBN 0-13-345711-7.

[153] Mogens Blanke, Michel Kinnaert, Jan Lunze, and Marcel Staroswiecki. *Diagnosis and Fault-Tolerant Control*. Springer, 2nd edition, 2006. ISBN 978-3-540-35652-3.

Papers

Paper A

Impedance Characterization of High Temperature Proton Exchange Membrane Fuel Cell Stack under the Influence of Carbon Monoxide and Methanol Vapor

Christian Jeppesen, Pierpaolo Polverino, Søren Juhl Andreasen, Samuel Simon Araya, Simon Lennart Sahlin, Cesare Pianese, Søren Knudsen Kær

The paper has been submitted in the
International Journal of Hydrogen Energy

Impedance Characterization of High Temperature Proton Exchange Membrane Fuel Cell Stack under the Influence of Carbon Monoxide and Methanol Vapor

Christian Jeppesen[a,*], Pierpaolo Polverino[b], Søren Juhl Andreasen[c], Samuel Simon Araya[a], Simon Lennart Sahlin[a], Cesare Pianese[b], Søren Knudsen Kær[a]

[a] *Department of Energy Technology, Aalborg University, Pontoppidanstræde 101, 9220 Aalborg Ø, Denmark*
[b] *Department of Industrial Engineering, University of Salerno, via Giovanni Paolo II 132, 84084, Fisciano (SA), Italy*
[c] *Serenergy A/S, Lyngvej 8, 9000 Aalborg, Denmark*

Abstract

This work presents a comprehensive mapping of electrochemical impedance measurements under the influence of CO and methanol vapor contamination of the anode gas in a high temperature proton exchange membrane fuel cell, at varying load current. Electrical equivalent circuit model parameters based on experimental evaluation of electrochemical impedance spectroscopy measurements were used to quantify the changes caused by different contamination levels. The changes are generally in good agreement with what is found in the literature. It is shown that an increased level of CO contamination resulted in an increase in the high frequency and intermediate frequency impedances. When adding CO and methanol to the anode gas, the low frequency part of the impedance spectrum is especially affected at high load currents, which is clearly seen as a result of the high load current resolution used in this work. The negative effects of methanol vapor are found to be more pronounced on the series resistance. When CO and methanol vapor are both present in anode gas, the entire frequency spectrum and thereby all the equivalent circuit model parameters are affected. It is also shown that the trends of contamination effects are similar for all the test cases, namely, CO alone, methanol alone and a mix of the two, suggesting that effects of methanol may include oxidation into CO on the catalyst layer.

Keywords: Fuel Cell, PEM, PBI, Electrochemical impedance spectroscopy,

*Corresponding author
Email address: chj@et.aau.dk (Christian Jeppesen)
URL: http://et.aau.dk (Christian Jeppesen)

1. Introduction

Fuel cells are today considered as a promising alternative to internal combustion engines for applications such as automotive and backup power. Fuel cells are electrochemical devices that convert chemical energy of gases, typically hydrogen, into electricity and heat. They presents the advantage of have no particle emissions, silent operation, high efficiency and they can be deployed as green house gas neutral [1, 2]. Compared to batteries fuel cells can continuously produce electricity as long as reactants are supplied, and do therefore not require long down time during refuelling but can be refueled within minutes.

In the resent decades a large number of research projects have been conducted on fuel cells, and now the technology is maturing for commercial use, such as stationary power, portable power and automotive power. However durability and reliability need to be improved in order to justify a higher price tag compared to the alternatives or production and maintenance costs need to be reduced significantly [3].

The most common fuel cell type is by far the low temperature proton exchange membrane (LTPEM) fuel cell with Nafion® as proton conductor. It typically utilizes pure hydrogen and air as reactants, and for most applications the hydrogen is stored under high pressure. The compressed hydrogen vessel poses a potential safety risk and energy density is lower compared to gasoline and further the energy required for the compression is significant and the distribution is inefficient due to the low volumetric energy density compared to liquid fuels. An alternative to storing hydrogen under pressure is using e.g. liquid methanol in combination with a steam reformer, which converts methanol and water into a hydrogen rich gas mixture [4, 5, 6]. However the downside is that the output gas from steam reforming also contains CO_2, CO and vaporized methanol, and is therefore not suitable for LTPEM fuel cells since they require a 99.9 % purity of the hydrogen [7]. LTPEM fuel cell systems with a reformer requires a gas purification system, which is costly and lowers the system efficiency.

An alternative to LTPEM fuel cells are high temperature proton exchange membrane (HTPEM) fuel cells [8]. HTPEM fuel cells have the advantage of being more tolerant to impurities in the anode gas, and can operate with methanol vapor, CO and CO_2 at anode side [9, 10]. They can therefore be deployed together with a steam reformer without gas purification systems. However, performance of the fuel cell drops and the expected lifetime decrease, when

higher concentrations of CO and methanol vapor are present in the anode gas [11].

Several works have dealt with CO and methanol vapor contamination of the anode gas in a HTPEM fuel cell, but separately. Many works have treated the topic of performance loss during CO contamination. They have found that they can operate without major performance loss until a CO contamination level of up to 3 % by volume at temperatures above 160 ℃ [12, 13, 14]. These studies have investigated the CO effect on the steady state performance, while other studies have fitted electrical equivalent circuit (EEC) models to impedance measurements and compared the value of the EEC model parameters for different concentrations of CO [15, 9, 16]. All the studies which treat CO contamination of the anode gas all suggest that CO adsorbs on the platinum catalyst, and occupy otherwise active catalyst sites that could otherwise maintain the electrochemical fuel cell reactions.

In the literature there are not many works that deal with methanol vapor poisoning of the anode of a HTPEM fuel cell. Two works reported an increase in degradation when introducing methanol vapor in the anode gas of a HTPEM fuel cell by using the impedance and the direct fuel cell voltage, and confirming it by a membrane scanning in an electron microscope [17, 18]. In the work by Araya et al. [19], a methanol vapor concentration of 3 % in the anode gas corresponding to a methanol reformer conversion of less than 90 % was investigated at different fuel cell temperatures, with the conclusion that the effect of methanol is negligible for small concentrations in the anode gas. All the considered for the studies suggest that the performance drop is due to phosphoric acid leaching or DMFC phenomena, such as methanol crossover or the formation of formaldehyde or similar. Only one study investigates how both CO and methanol vapor in the anode gas affects the impedance of a HTPEM fuel cell [20]. In this study three concentrations of CO and three concentrations of methanol vapor where investigated, but not with realistic values of methanol slip for methanol reformers.

In the present work, a comprehensive study was carried out to investigate how the fuel cell impedance changes when CO and methanol vapor are introduced into the anode gas. An impedance mapping was done based on realistic reformer output gas compositions and the impedance change under different current loads was analyzed.

A mapping of the EEC model parameters could potentially be used for designing a model-based diagnostic algorithm, which relies on a suitable Fault Signature Matrix [21]. As proved in the literature [22], this latter could potentially be used for online diagnostic applications, as in this case, for detecting

CO and methanol vapor contamination in the anode gas. By detecting CO and methanol vapor contamination in the anode gas, a mitigation strategy could be deployed and thereby enhance the lifetime of fuel cell system [23].

This article is organized as follows: in section 2 the experimental setup and procedure will be described for the impedance mapping of the fuel cell stack. In section 3 the electrochemical impedance spectroscopy measurement method is introduced and how the impedance measurements can be quantified into equivalent electrical circuit model parameters. In section 4 the results are presented and discussed, and the conclusions drawn in section 5.

2. Experimental Setup

The experiments carried out in the current work have been conducted on a 10 cell short stack from SerEnergy A/S, which is made up of PBI-based SerEnergy MEAs, and flow plates from a SerEnergy S165L stack. The active area of the fuel cells is 165 cm^2. The short-stack is shown in Fig. 1. The short stack is mounted in a GreenLight G200 fuel cell test station, where anode gas composition such as H_2, CO_2 and CO can be controlled by mass flow controllers, and CH_3OH vapour can be controlled by a HPLC pump and a heat exchanger. The stack is liquid cooled by Paratherm oil, fed by an external Greenlight cooling cart.

Before starting the characterization experiments, the fuel cell stack was operated in a break-in procedure of 100 hr, at 0.194 A/cm^2 (32 A), as suggested in [24]. After end of break-in procedure the short-stack was operated for additional 40 hr to ensure steady voltage profile. The break-in procedure was conducted with an air stoichiometric ratio of $\lambda_{\text{air}} = 5$ and a hydrogen stoichiometric ratio of $\lambda_{H_2} = 2$.

During the experimental characterization of the fuel cell, the impedance is measured using a Gamry Reference 3000 instrument running in galvanostatic mode.

2.1. Fuel cell characterization procedures

The characterization of the short stack has been carried out at 21 different anode gas compositions, which are based on realistic gas outputs from a methanol steam reformer [25]. The H_2, CO, CO_2 and CH_3OH gas composition range used in this work, is based on experimental data from a SerEnergy H3-5000 reformer module. The CO content was varied from 0 % CO to 1.5 % CO by volume, in steps of 0.25 % Vol. These 7 CO set points were then repeated for 0 %, 0.25 % and 0.5 % by volume of vaporized CH_3OH in the anode gas.

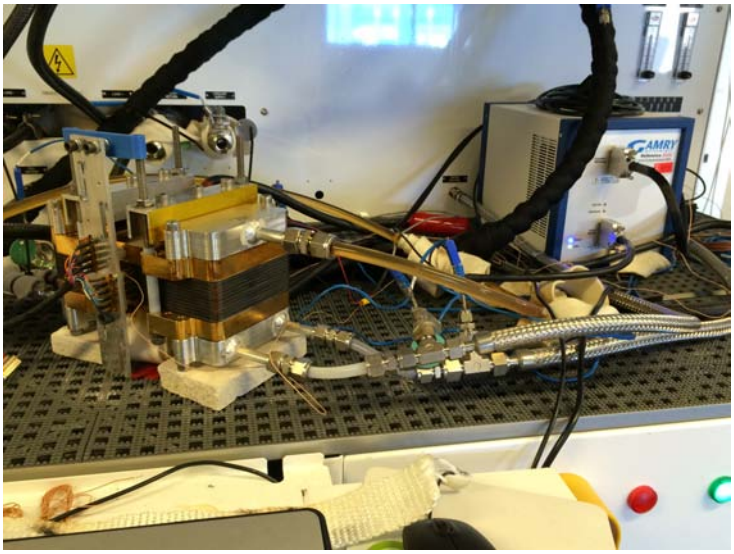

Figure 1: On the left the 10 cell short-stack used for the experimental work is shown. On the right the Gamry Reference 3000 instrument used for impedance measurements is shown. The stack is installed in a GreenLight G200 fuel cell test station, where operational conditions for the fuel cell stack can be controlled.

For all anode gas compositions, hydrogen content was set constant at 75 % by volume, and the remainder was filled by CO_2. The stoichiometric ratios were set to $\lambda_{H_2} = 1.5$ and $\lambda_{air} = 2.5$ throughout the entire experiment. The anode and cathode gases were preheated to 167 ℃. The cathode gas is atmospheric dry air. The anode gas is humidified by a bubbler at a dew point of 49 ℃, which corresponds to the normal level of water content in the anode gas when the fuel is reformed from methanol with a steam to carbon ratio of 1.5. The stack is heated and cooled by a inlet coolant temperature of 167 ℃.

An overview of the test set points is given in Table 1. A total of 441 unique current and gas composition set points were conducted, and for each of them three electrochemical impedance spectroscopy (EIS) measurements have been recorded with a 60 seconds interval between each of the 3 measurements. This yields a total of 1323 unique EIS measurements for the entire fuel cell characterization experiment.

The 21 current set points were varied from 5 A to 100 A as shown in Fig. 2, and the overall experiment is shown in Fig. 3. The vertical dashed black lines in Fig. 3 indicate a start/stop operation, where the start/stop at approximately 110 hr was an unscheduled emergency shutdown due to low gas supply.

Table 1: Overview of the set points during the fuel cell characterization experiment. All CO test points are repeated for current test points and all methanol test points are repeated for all CO and current set points. For each of the test points 3 EIS measurements are conducted.

Parameter	No. test points	Range
Current	21	5 - 100 A
CO	7	0 - 1.5 %
CH_3OH	3	0 - 0.5 %
total	441	

3. Impedance identification and model

For fuel cell characterization, several in-situ methods are available in the literature, where the most common are polarization curve, current interruption (CI), cyclic voltammetry (CV) and electrochemical impedance spectroscopy (EIS). The polarization curve method plots the stack voltage against the stack current for indicating the performance and indirectly the efficiency of the fuel cell stack [26]. The CV method sweeps the potential of the fuel cell stack while recording the current, which gives an indication of the electrochemical reactions of the cells [26, 27]. The CI method records the voltage while the current is interrupted, and the voltage response can be divided into an abrupt change and a transient voltage change [26, 28]. Based on the abrupt voltage change the ohmic resistance can be estimated, which is related to the membrane resistance. The EIS method is widely used in the electrochemical community for a broad range of applications, and yields high quality diagnostic abilities [26, 29, 30, 31]. In this work the EIS method has been used to characterize the fuel cell stack.

3.1. Electrochemical impedance spectroscopy

An EIS measurement is conducted by imposing a sinusoidal perturbation to the fuel cell and by analyzing the response from the fuel cell. Based on the sweep in frequency, the amplitude ratio and the phase shift between the input and output signals, the impedance can be calculated at each frequency. The measurement can be conducted in potentiostatic or galvanostatic mode, by perturbing a sinusoidal voltage or current, respectively. For this work all EIS measurements are conducted in galvanostatic mode. The number of frequency points differ from work to work, and must be balanced between high enough to ensure sufficient points for fitting equivalent electrical circuit (EEC) models and at the same time a higher number of frequencies increase the measurement duration. A long measurement time could yield non steady state operation, and

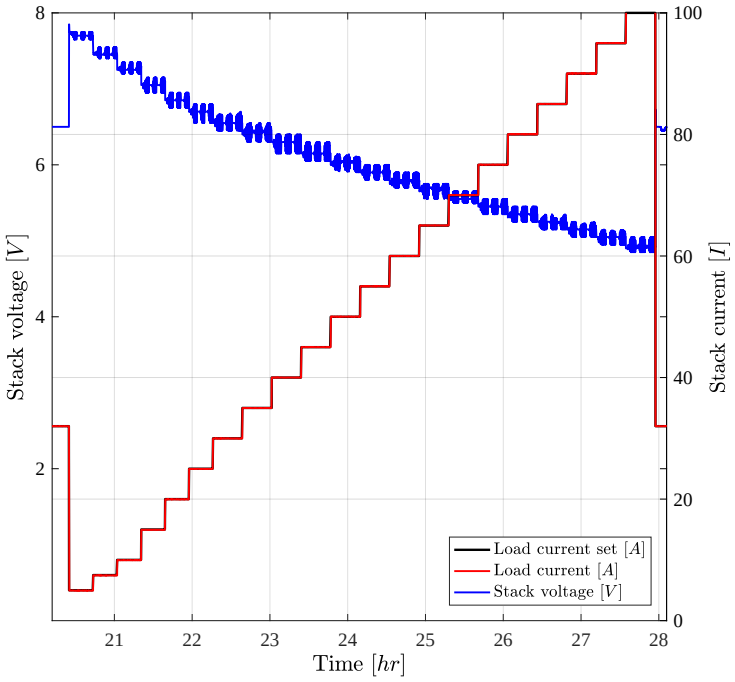

Figure 2: Stack voltage and current for a current sweep with 21 current set points. At each current set point are 3 EIS measurements are performed. This current sweep is repeated for 21 different anode gas compositions.

thereby results in a unusable measurement. The majority of papers dealing with EIS measurements of PEM fuel cells use between 10 to 20 points per decade [31]. In this work, the acquired frequency span is 10 kHz to 0.1 Hz, with 10 data points per decade, divided into logarithmic intervals.

During an EIS measurement it is assumed that the measured response is linear, meaning that the measured voltage is sinusoidal without any harmonics. This is not true for any electrochemical fuel cell reaction and the amplitude must therefore be minimized for the linearity assumption to be valid. However, if the perturbation amplitude is too small the impedance response will be scattered and the fitting of an EEC model can be difficult due to a higher level of noice [31]. The amplitude of the perturbation signal for this work was set to 7.5 % of the DC load current, which is a good trade-off between signal to noise ratio and being in the linear voltage region and is also recommended by Dale et al. [32]. The instrument limitation is ± 3 A of AC current perturbation.

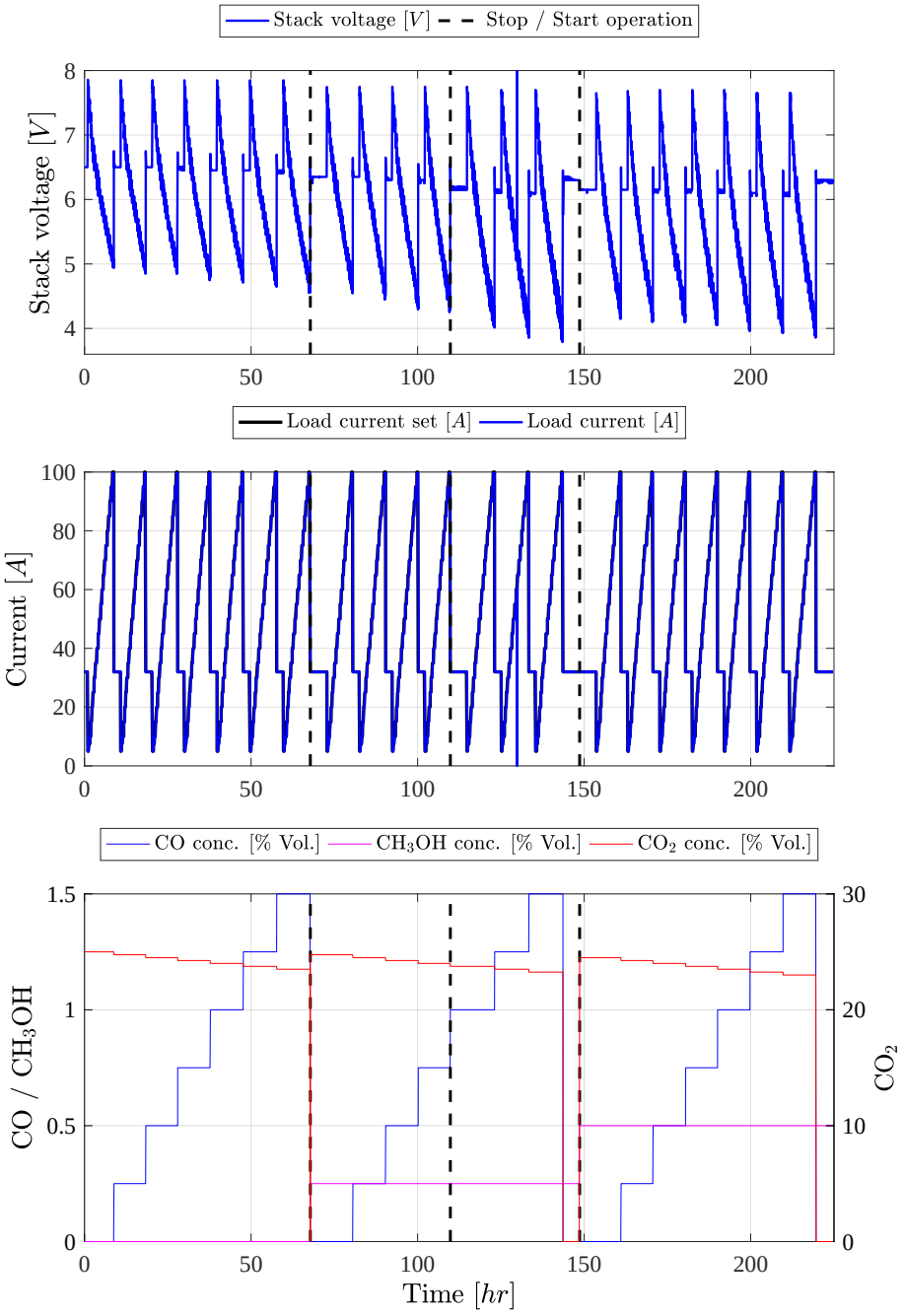

Figure 3: The total characterization experiment: 21 different gas composition set points all undergoing 21 current set points.

3.2. Equivalent electrical circuit model

The equivalent electrical circuit (EEC) models are often used for the transient behavior or often referred to as the impedance of fuel cells. The EEC models can be divided into two sub classes: a first principle class, where governing equations are used to model the impedance [33] and a second data-driven class, where an EEC model is used to describe the experimental impedance of a fuel cell. Common for both is that they quantify different operational conditions into a frequency dependent impedance spectrum. For multi-physics systems, such as fuel cells, the governing equations for the electrochemical process are complex and the EEC model becomes very comprehensive in terms of components [34]. For this reason, the experimental impedance is often fitted to a EEC model of simpler nature. The simplification of the EEC model comes with the consequence that the physical meaning of its parameters is questionable and are only valid in the neighborhood of the measured system's operational parameters [31]. For comparing the impact of different system operational parameters, the data driven approach is by far the most widely used method and therefore for this work this approach will be used.

The most common EEC model used in the literature is the Randles circuit [35] or variations of it. The original circuit was constructed with a resistor in series with a frequency dependent resistor and capacitor in parallel with a conventional capacitor. Later Grahame [36] proposed to replace the frequency dependent resistor and capacitor with a pseudocapacity element named the Warburg element. In Figure 4, the Randles EEC model used in this work is shown, where Z_W is the Warburg element and the capacitance element is replaced by a constant phase element (Z_{CPE}). This EEC model has not been derived based on fuel cell governing equations, but has been proven by Fouquet et al. [37] to capture most impedance measurements of PEM fuel cells.

The impedance of a constant phase element (Z_{CPE}) is defined as shown in equation 1.

$$Z_{CPE}(Q, \alpha, \omega) = \frac{1}{Q(\mathrm{j}\omega)^{\alpha}} \tag{1}$$

where ω is the angular frequency ($2\pi f$), Q is the pseudocapacitance and α is the CPE power coefficient, which can vary from 0.5 to 1, where 1 yields the same element properties as an ideal capacitor. Some papers suggest that α should be constant for the entire operation of a fuel cell [37], while others found that α should vary with the load current [38].

The bounded Warburg element (Z_W) used in this work, is defined as shown in equation 2 [37].

$$Z_W(R_W, T, \omega) = R_W \frac{\tanh(T_W\ (\mathrm{j}\omega)^{\frac{1}{2}})}{T_W\ (\mathrm{j}\omega)^{\frac{1}{2}}} \tag{2}$$

where ω is the angular frequency ($2\pi f$), T_W is the diffusion parameter and R_W is the Warburg coefficient.

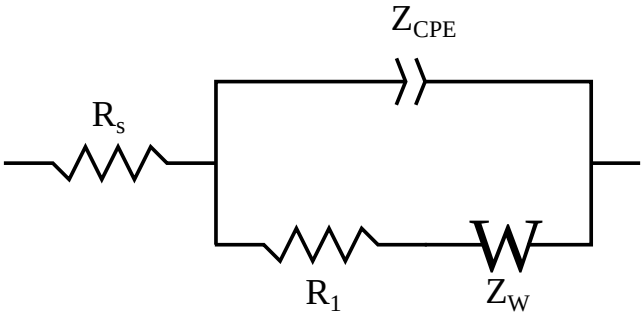

Figure 4: Equivalent electrical circuit model used in this work.

Previous studies have shown that the inductive part of the impedance is constant for different current loads and contamination and only slightly dependent on the temperature [9]. This is due to the fact that the inductive part is related to wiring and therefore constant for all measurements in this study. Furthermore, a low number of EEC model parameters will ease the fitting process which is important if the fitting process should be implemented in-situ at some point in the future. Therefore, all measurement points with a positive imaginary part have been deleted and excluded in the fitting process, and no inductive elements are included in the EEC model shown in Figure 4.

3.3. Parameter identification

For fitting the measured data to the EEC model presented in Figure 4, a fitting routine has been developed in Matlab. The routine is based on a differential evolution optimization algorithm [39] with a least squares objective function. The advantage of the optimization algorithm is that it is well suited for parameter estimation, it converges fast and yields a large chance for global minimum [39].

The cost function used for the parameter estimation is presented in equation 3, and is formulated as a least squares of the Euclidean norm of the complex impedance. The cost function is formulated with a penalty on the middle frequency region, to ensure a correct location of the transition between intermediate and low frequency semicircles. In this work, the middle frequency

region is defined from 20 to 0.5 Hz, and the size weighted penalty is 4. In order to avoid correlated solutions to the optimization problem, boundary values have been set for the parameters.

$$
\begin{aligned}
J(f,\underline{\hat{\theta}}) &= \sum_{f\in\{f_s\leq f<f_{m1}\}} \left\| z(f) - \hat{z}(f,\underline{\hat{\theta}}) \right\|^2 + \\
&= w_p \left(\sum_{f\in\{f_{m1}\leq f\leq f_{m2}\}} \left\| z(f) - \hat{z}(f,\underline{\hat{\theta}}) \right\|^2 \right) \\
&= \sum_{f\in\{f_{m2}<f\leq f_e\}} \left\| z(f) - \hat{z}(f,\underline{\hat{\theta}}) \right\|^2
\end{aligned} \tag{3}
$$

where f is the frequency of the perturbated signal, $\underline{\hat{\theta}}$ are the estimated parameters of the EEC model, $\hat{z}$ is the modelled impedance, w_p is the weight penalty coefficient, f_s is the start frequency, f_e is the end frequency, f_{m1} is the start of the mid frequency region and f_{m2} is the end of the mid frequency region.

4. EEC model parameter identification results

In the following, the identified EEC model parameters are analysed and discussed. After some general observations on the measurements, a detailed analysis of the effects of the different gas compositions in the anode feed are given based on the EEC model parameters.

Figures 5 and 6 show the initial EIS measurements without CO or CH_3OH at {5 , 7.5 , 10 , 15 , 30} A and at {30 , 50 , 75 , 100} A, respectively. In the figures, blue line indicates the EEC model fit of the measurements and the black markers indicates the frequency decades {1k, 100, 10, 1, 0.1} Hz of the sinusoidal current signal, with decreasing frequency to the right.

It can be seen that the impedance spectrum decreases with the increase in DC value of the current load. This is due to the nature of the polarization curve, where at higher currents the DC value of the fuel cell voltage is lower, which gives a lower amplitude of the sinusoidal AC voltage response and consequently a lower magnitude of the complex impedance.

Furthermore, the low frequency arc at 5 A in Figure 5 is almost negligible. It can also be seen that for an increasing current, the low frequency arc becomes relatively larger compared to the intermediate frequency arc, and for EIS measurements above 30 A the low frequency arc becomes larger than the intermediate frequency arc. This behavior manifest itself as a discontinuity for the Warburg element parameter R_W, which for the current sweeps, increases

until 10 A, and decreases for further increase in current. The low frequency arc is in some works related to diffusion limitations in the gas diffusion layer [34], in other studies it is suggested that it is related to the cathode supply [40], while Schneider et al. [41, 42] suggest it is due to oscillations in the gas along the gas channels. To collate the different explanations, mass transport issues are a common factor.

The intermediate frequency arc dependencies, are often explained by a relationship to the activations losses from the cathode [43], or as a combination of the anode and cathode activation losses [40]. In this work, the intermediate frequency arc is more dominant than the low frequency arc at low currents and contrary at higher currents.

As for the low and intermediate frequency arcs, the origin of the high frequency arc also has different point of views in the literature. Often the high frequency arc is correlated to the hydrogen oxidation reaction [44, 45], while others suggest that it is related to conduction in the catalyst layer [46]. As stated in section 3.2, a high frequency arc is not included in the EEC model. As seen on the extract in Figure 6, a very small high frequency arc is present between 1 kHz and 400 Hz, but its size makes it hard to obtain consistent model fits, since the high frequency arc merges with the intermediate frequency loop at lower currents. Furthermore, it can be seen that the high frequency arc does not depend on the current.

4.1. Measurements with CO

The advantage of HTPEM fuel cells is that they are tolerant toward contaminants, such as CO. Where LTPEM fuel cells require high quality of hydrogen, HTPEM can operate with up to 3 % of CO in the anode gas [12, 13, 14]. This is an advantage since many fuel cell applications have their hydrogen supply from reformers, which reform hydrocarbons to a hydrogen rich gas, where CO is typically also present. However, the presence of CO still affects the performance and durability of an HTPEM fuel cell.

It is well know that when CO is added to the anode gas it occupies platinum sites, and since platinum is the catalyst for adsorbing hydrogen molecules into hydrogen atoms and free electrons, this reduces the electrochemical process and thereby the fuel cell performance. At higher temperature the electrochemical kinetics increases and the adsorption of CO on platinum sites is disfavored [12], making HTPEM fuel cells more tolerant towards CO contamination than LTPEM fuel cells. However, when increasing the temperature, the degradation mechanisms also increase and the lifetime of the fuel cell is reduced. Therefore, when finding an optimum operating temperature it is important to consider

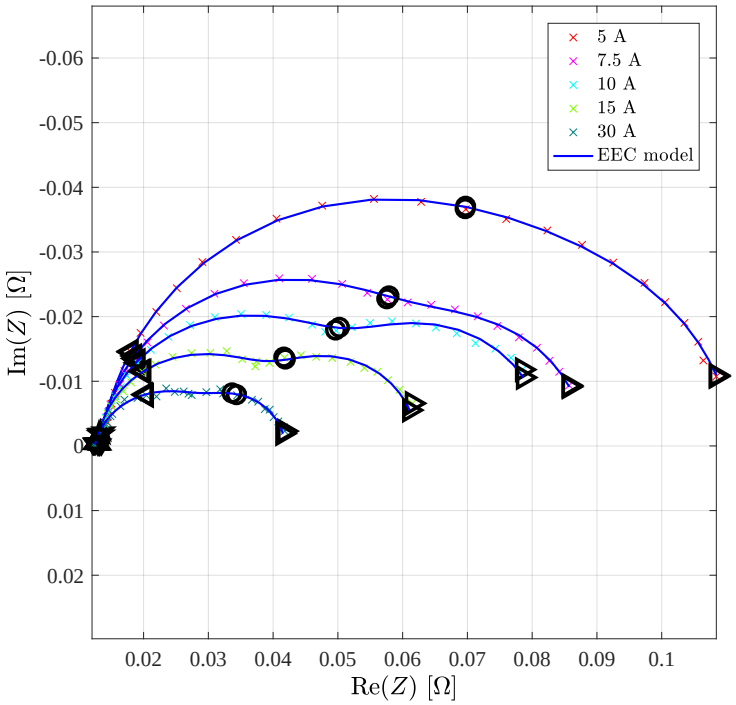

Figure 5: Nyquist impedance plot at {5A , 7.5A , 10A , 15A , 30A} current loads, without any contamination in the anode gas. The blue line indicates the EEC model fit for each EIS measurement. The black markers indicate the frequency decades {1k,100,10,1,0.1} Hz.

the tolerance towards contamination, performance, and lifetime of the fuel cell stack.

In Figure 7 the impedance spectra for EIS measurements at 30 A and at CO contamination levels of {0.25 , 0.5 , 0.75 , 1 , 1,25 , 1,5} % by volume in the anode gas are shown. As already stated, the high frequency arc is related to anode reactions. Therefore, a slight increase in the high frequency arc is observed, when CO contamination is increased. It is easily observed by the 100 Hz marker in Figure 7, in which both the real and imaginary part increase. Furthermore, the series resistance also increases as can be observed by the movement of the 1 kHz marker, for which there are no direct explanation in the literature, but has sometimes been ascribed to degradation effects [9]. Since no dedicated high frequency loop has been used in the EEC model illustrated in Figure 4, the increase in the real part seen at 100 Hz marker also results in an increase in the series resistance (R_S). It can also be seen in Figure 8 that the trend for the increase in the series resistance is independent of the

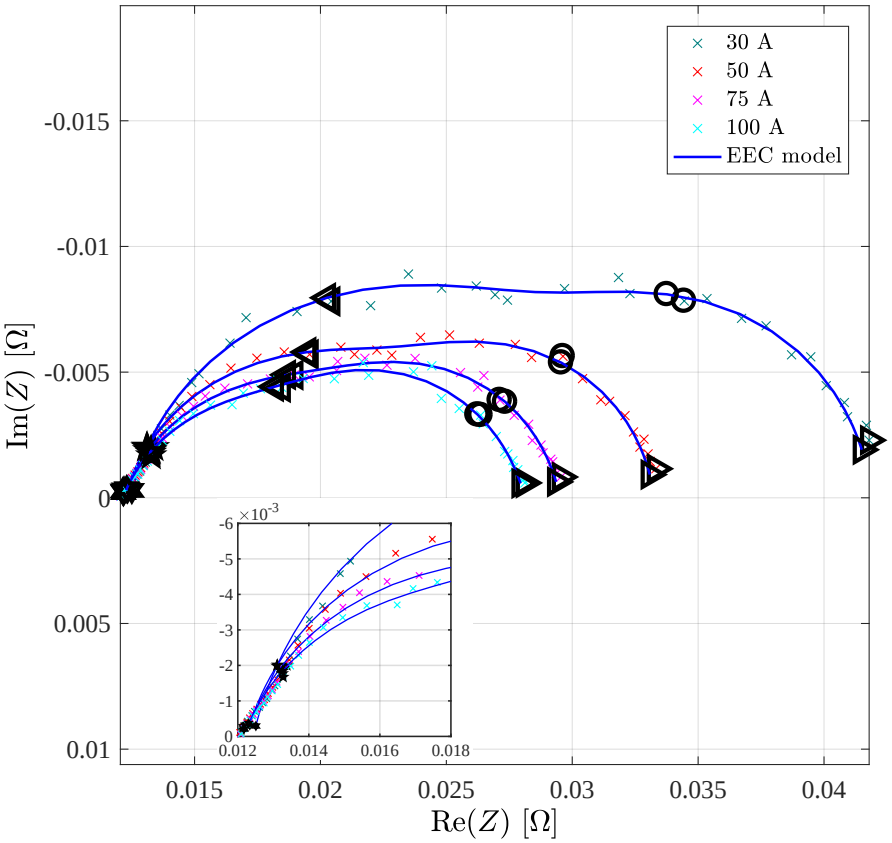

Figure 6: Nyquist impedance plot at {30A , 50A , 75A , 100A} current loads, without any contamination in the anode gas. The blue line indicates the EEC model fit for each EIS measurement. The black markers indicate the frequency decades {1k,100,10,1,0.1} Hz. On the extract a zoom-in on the high frequency part is shown.

load current. The EEC model parameters shown on Figure 8 are an average based on parameter estimation of the three EIS measurements taken at each gas composition and load current set point.

As it can be seen in Figure 7, the real part increases with increase in the level of CO contamination at the 10 Hz marker. This consolidates the argument that the intermediate frequency arc yields information on both the anode and the cathode reactions. By inspecting the second plot (R_1 in Figure 8), it can be seen that the change in the size of the intermediate frequency arc caused by the increase in CO contamination level is independent of the load current.

Similarly to the intermediate frequency arc, the low frequency arc also in-

creases with increasing CO contamination levels. The reason for this could be a dilution effect of the increased level of CO in the anode gas, which can hinder the diffusion of hydrogen into the gas diffusion layer, and thereby decrease the fuel cell performance. When investigating the size of the low frequency arc by the EEC model parameter R_W an increasing trend is observed for the EEC model parameter R_W at higher currents loads. This is in agreement with the work of Das et al. [14], who reported an increase in concentration losses on the polarization curve when adding CO, when compared to the polarization curve without any CO contamination. In Figure 8 the trend for R_W at low current loads is decreasing for increasing levels of CO contamination. There is no electrochemical explanation for this, but it could simply be a fitting phenomena when the impedance spectra changes from one arc to multiple arcs, as illustrated in Figure 5.

4.2. Measurements with methanol

When HTPEM fuel cells are deployed with a methanol reformer, often a small amount of unconverted methanol vapor is present in the anode gas. HTPEM fuel cells have the advantage of being able to operate with small amounts of methanol vapor in the anode gas, and therefore, do not require a gas purification system. However, if present at high concentrations, methanol vapor can affect the fuel cell performance negatively [47, 17, 18].

When methanol vapor is added to the anode gas a combination of phenomena occur in the fuel cell. It has been suggested by Boaventura et al. [17] that a formation of CO takes place inside the anode, via a reverse water-gas shift reaction on the catalyst layer. Additional CO in the anode affects the performance of the fuel cell as described in the previous section of this paper. Other works suggest that methanol undergoes electro-oxidation on the catalyst to forms non-CO species, such as formic acid or formaldehyde [48], which also cause a decrease in the fuel cell performance. Moreover, the presence of methanol and water vapor can dilute the phosphoric acid concentration [47]. However, this will mainly affect the long-term durability if the fuel cell, and not yield an instantaneous performance drop.

Figure 9 shows a Nyquist plot for data measured at 30 A, at different levels of methanol vapor in the anode gas. It can be seen that the 100 Hz marker increases with increasing level of methanol vapor contamination, similar to what is observed for CO contamination. This supports the assumption that the effect of methanol is through electro-oxidation into CO on the catalyst. Furthermore, it can be observed that the intermediate frequency arc and the low frequency arc slightly increase with the level of methanol vapor in the anode

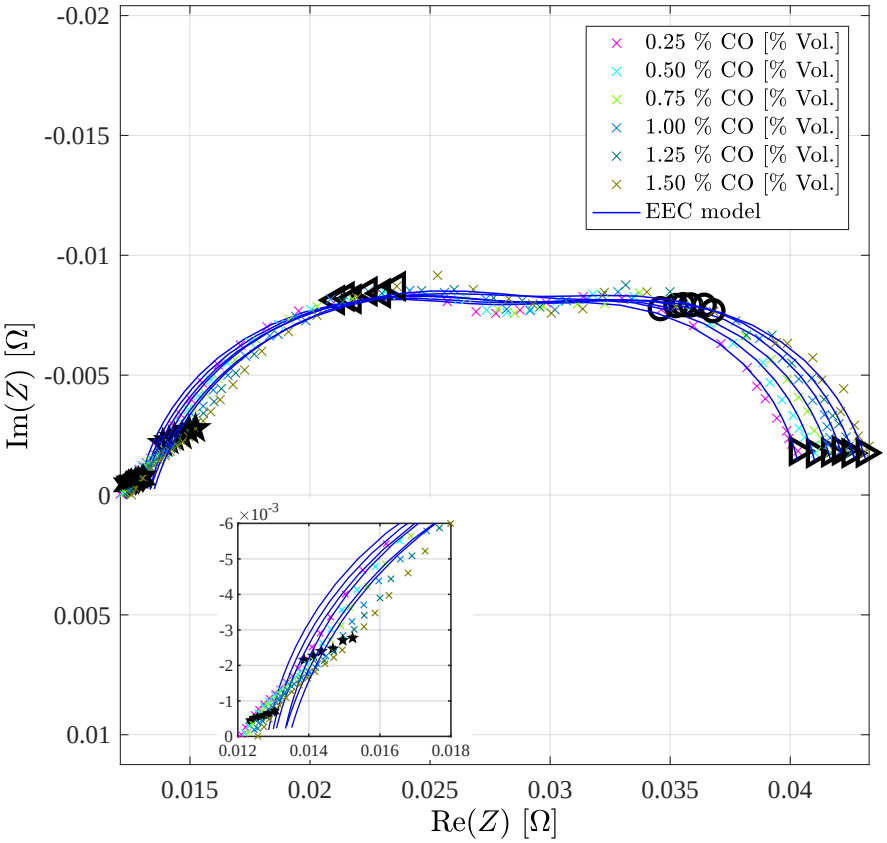

Figure 7: Nyquist impedance plot at 30 A current load, for different levels of CO contamination in the anode gas. The blue line indicates the EEC model fit for each EIS measurement. The black markers indicate the frequency decades {1k,100,10,1,0.1} Hz.

gas. This is also seen in Figure 10, where the middle plot show the EEC model parameter R_1, which is related to the intermediate frequency arc increases with level of methanol vapor in anode gas, independent of the load current. Moreover, it can be seen that the parameter R_1 increases for an increasing level of methanol vapor independent the load current. For the low frequency arc, it can be seen in Figure 10, that the resistances increase with load current.

It is clearly seen in Figures 9 and 10 that the parameter that is most sensitive to changes in the level of methanol vapor contamination is the series resistance (R_s), which increases with an increasing level of methanol vapor in the anode gas. Araya et al. [20] also support this finding, however not as distinct as found in this work. Some degradation mechanisms could play a role in this

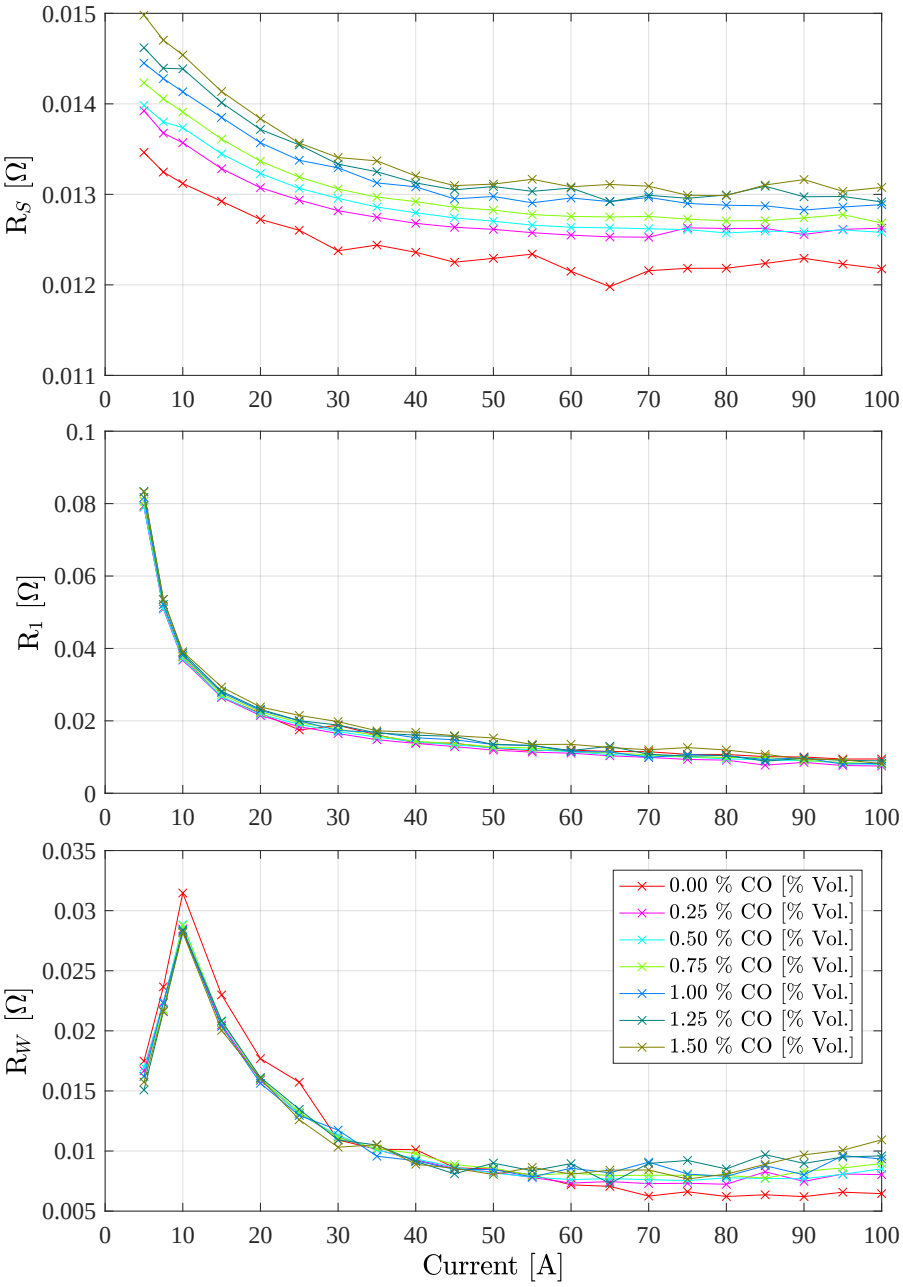

Figure 8: The EEC model parameters R_S, R_1 and R_W as a function of the fuel cell load current, for different levels of CO contamination.

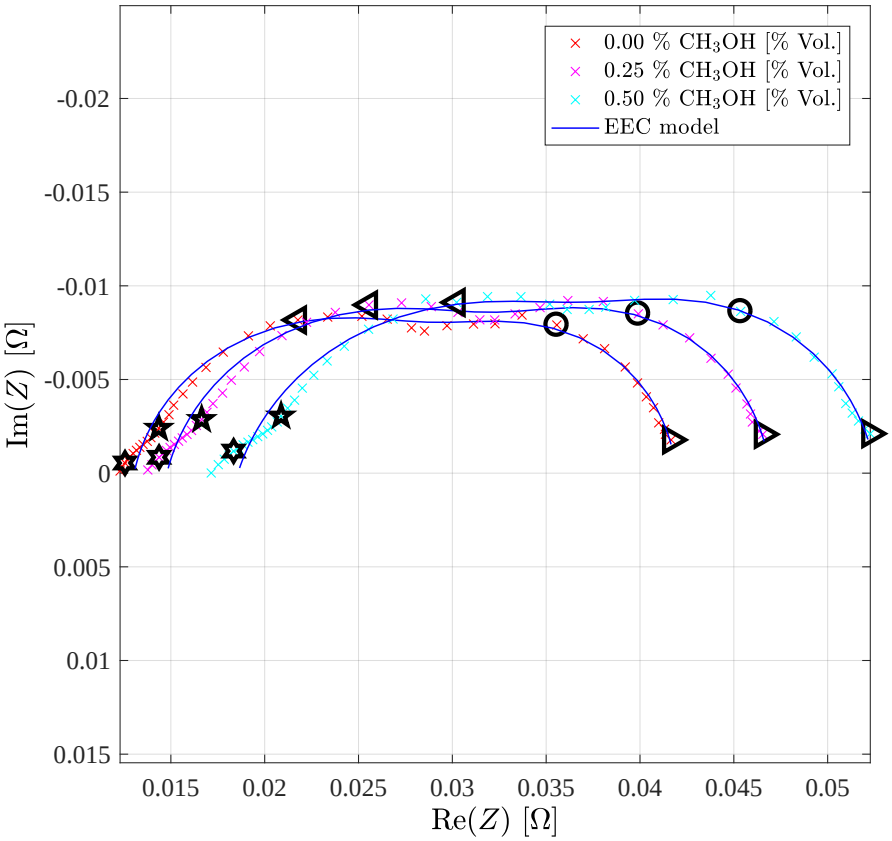

Figure 9: Nyquist impedance plot at 30 A current load, for different levels of methanol vapour contamination in the anode gas. The blue line indicates the EEC model fit for each EIS measurement. The black markers indicate the frequency decades {1k,100,10,1,0.1} Hz.

pronounced increase in series resistance, since there is approx. 75 hr of fuel cell operation between the EIS measurements, as illustrated in Figure 3.

4.3. CO and methanol EEC model parameter correlation

As mentioned in the introduction of the paper, a mapping of the EEC model parameters could potentially be used for designing a fault detection and isolation algorithm for on-line deployment in fuel cell systems. This requires a unique parameter signature of the faults (CO and CH_3OH in the current work) to isolate the faults [21]. However, when fuel cell stack is exposed to both CO and methanol vapor contamination the trend in EEC model parameters at different load currents are similar, as seen in Figure 11.

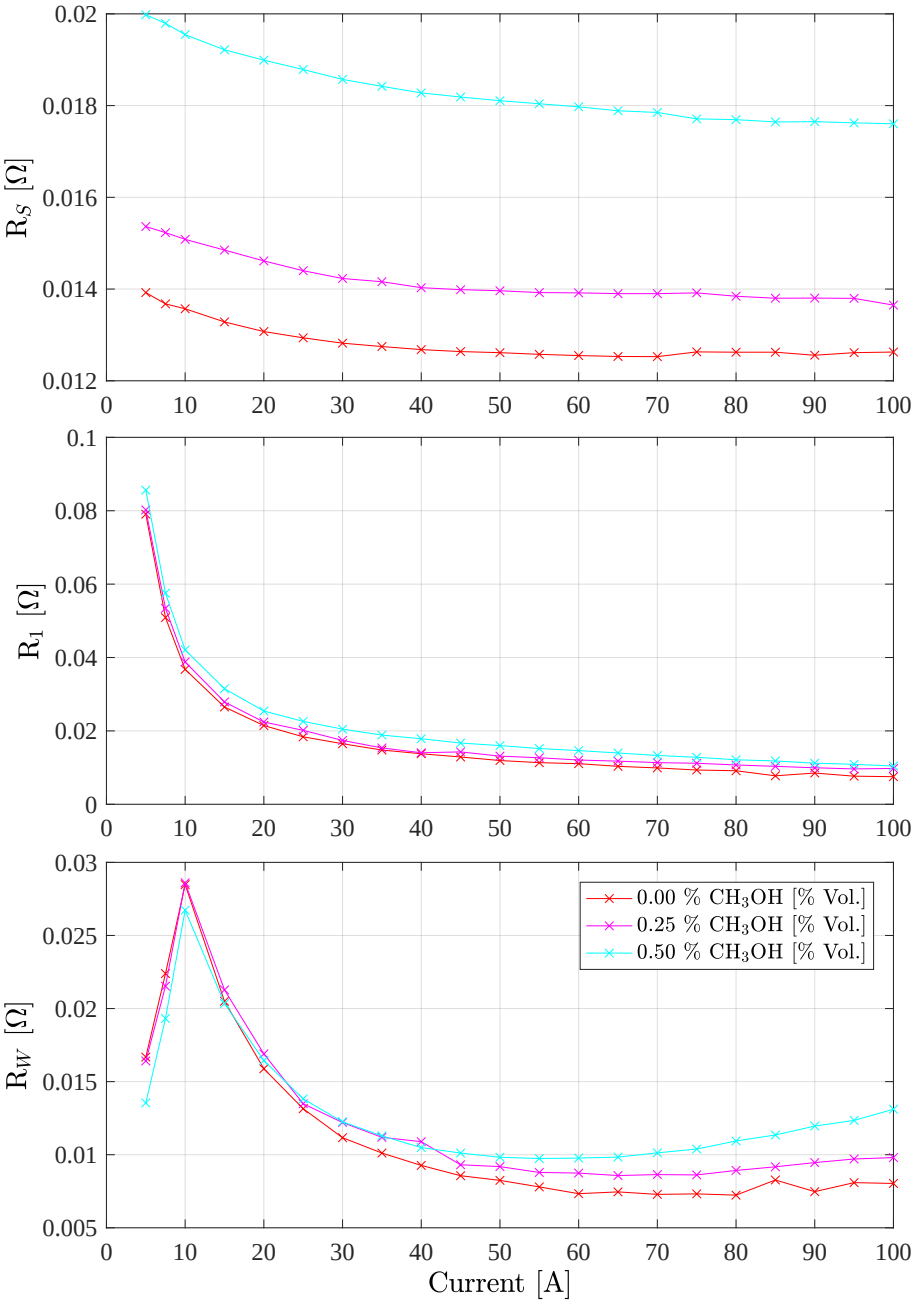

Figure 10: The EEC model parameters R_S, R_1 and R_W as a function of the fuel cell load current, for different levels of methanol vapor contamination.

For the EEC model parameter R_s, the trend across the entire span of contamination levels is illustrated in Figure 8 and 10, where it can be seen that R_s is increases with increasing levels of contamination of both CO and methanol vapor. Which is also shown on Figure 11, for different mixes of CO and methanol vapor contamination. The fit of the parameter is consistent, and could be used in a detection algorithm.

The EEC model parameter R_1 slightly with increasing levels of both CO and methanol vapor contamination in the anode gas. The R_1 parameters dependency on the change in contamination level is slightly higher at lower currents.

For the Warburg element, the parameter T_1 is close to be independent from the contamination level, but is highly dependent on the load current level. Contrary to the parameter T_1, the parameter R_W yields a clearer change at different levels of contamination. The value of the parameter R_W increases with with increasing level of contamination, especially at high load currents, and therefore would be the parameter that is best suited for fault detection. Further it can be seen on Figure 11 that adding the methanol vapor yields an influence, and that it e.g. is better to run with 1.5 % of CO and no methanol vapor, than running with 1 % of CO and 0.5 % of methanol vapor. However, as seen on Figure 3, there is approx. 100 hr of fuel cell operation between the two measurements and therefore the influence of degradations can also play a role.

Among the constant phase element parameters (α, Q_1), the value of the α element decreases with increasing level of CO and methanol vapor contamination. Furthermore, it is seen that the EEC model parameters α and Q_1 are correlated, i.e., when α decreases, Q_1 increases. It was difficult to get a consistent fit of the two parameters. The parameter α was kept constant, and it was observed that when fixing α to one value, the remaining five EEC model parameters fluctuate more. Therefore, it was decided that a more consistent fit of the remaining five parameters is a higher priority.

The correlation between EEC model parameters and increasing levels of CO and methanol vapor contamination is summarized in Table 2. It can be seen that all the EEC model parameters change in the same direction, for changes in both contamination of CO and methanol vapor. This means that based on the EEC model parameters, it is not possible to isolate whether CO or methanol vapor contaminates the anode gas. Moreover, when analyzing the data for realistic reformer gas outputs investigated based on the EEC model parameters in this work, it is not possible to design a robust fault detection algorithm with low probability of false alarm and a good probability of detection. In order to achieve data for detection of CO and methanol vapor in the anode gas using

Table 2: The correlation between increasing levels of CO and methanol vapor contamination of the anode gas and the EEC model parameters.

	R_1	R_2	α	Q_1	T_1	R_W
CO	↑	↑	↓	↑	-	↑
CH_3OH	↑	↑	↓	↑	-	↑

this method, the authors suggest that tests should be done on contamination levels above normal reformer gas composition outputs, where the differences between EIS spectra under faulty conditions and healthy conditions are more evident.

5. Conclusions

This work presents a comprehensive mapping of EEC model parameters to evaluate the influence of CO and methanol vapor contamination in the anode gas of a HTPEM fuel cell, at varying load values. The EEC model parameters are based on the evaluation of EIS measurements, where the data are fitted to an EEC model by a custom made fitting algorithm based on a differential evolution optimization algorithm.

The impedance results obtained using pure hydrogen are in good agreement with the literature. However, a change in the impedance spectra are observed at low current, where the impedance spectra shape yields one arc compared to higher currents, where the impedance spectra shape yields two to three arcs.

In this work, it is shown that when adding CO and methanol vapor to the anode gas, all the high, intermediate and low frequency parts of the spectrum are affected. This indicates that the two to three arcs in the spectrum are a combination of phenomena and cannot be ascribed to one reaction, an effect or a part of the fuel cell. However, there are strong indications that the low frequency part of the spectrum is related to mass transport effects.

When adding CO to the anode gas, the change in impedance was caused by CO adsorption on catalyst sites and thereby reduced active area of the fuel cell. It was found that an increased level of CO contamination in the anode gas resulted in an increase in the high and intermediate frequency arcs, which is in-line with what is described in the literature. When adding methanol to the anode gas, a pronounced increase in series resistance is observed in this work. This finding is supported in the literature, however, not to the same degree as reported in this work, and influence of degradation mechanisms cannot be ruled out. When adding methanol vapor to the anode gas, a slight increase in the high frequency impedance part is also observed, which supports the assumption

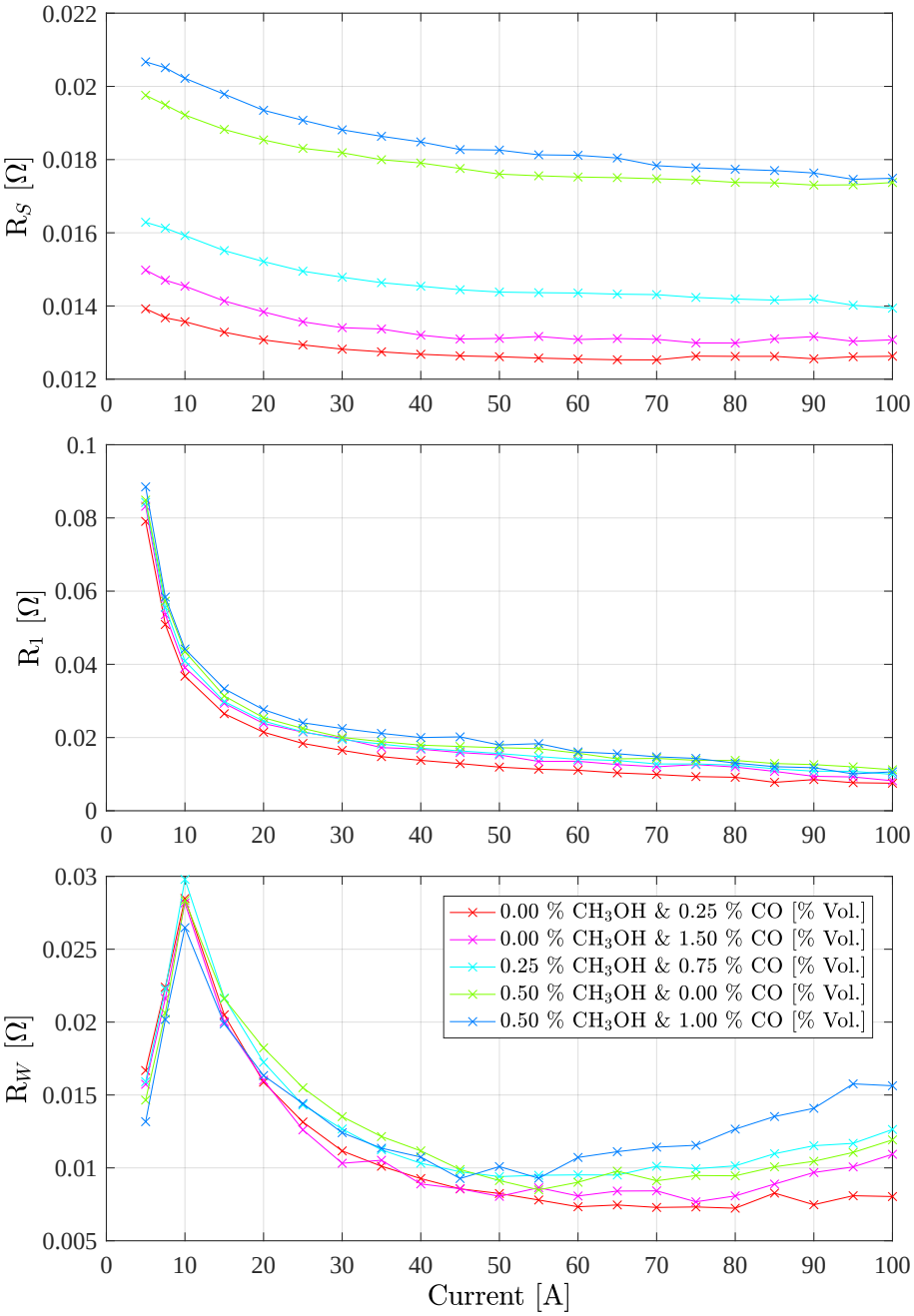

Figure 11: The EEC model parameters R_S, R_1 and R_W as a function of the fuel cell load current, for a mix of different levels of CO and methanol vapor contaminations.

that CO is formed, and thereby occupies catalyst sites. For higher currents, the low frequency part of the impedance spectrum distinctly increases with increasing level of CO and methanol vapor in the anode gas.

An experimental impedance mapping as the one presented in this work could be useful for determining design and control parameters for a methanol reformer, when deployed together with a HTPEM fuel cell, without installing any additional gas purification system. Moreover, an impedance mapping as presented in this work could be useful for designing diagnostic algorithms for detecting CO or methanol vapor in the anode gas. However, it can be concluded that it is not possible to isolate whether it is the CO or methanol vapor or both that are present in the anode gas based on the value of the EEC model parameters, since the same parameters change in the same direction when either or both levels are increased.

Acknowledgments

The work was supported by Innovation Fund Denmark in the frame of the 4M Centre. The data processing was conducted during Christian Jeppesen's research visit at University of Salerno and the experiments were conducted in the Fuel Cell Laboratory at Aalborg University. The authors would also like to acknowledge SerEnergy A/S for supplying the short-stack for testing.

References

References

[1] S. Pacala, R. Socolow, Stabilization Wedges: Solving the Climate Problem for the Next 50 Years with Current Technologies, Science 305 (5686) (2004) 968–972.
URL http://www.jstor.org/stable/3837555

[2] M. I. Hoffert, K. Caldeira, G. Benford, D. R. Criswell, C. Green, H. Herzog, A. K. Jain, H. S. Kheshgi, K. S. Lackner, J. S. Lewis, H. D. Lightfoot, W. Manheimer, J. C. Mankins, M. E.Mauel, L. J. Perkins, M. E. Schlesinger, T. Volk, T. M. L. Wigley, Advanced Technology Paths to Global Climate Stability: Energy for a Greenhouse Planet, Science 298 (5595) (2002) 981–987.
URL http://www.jstor.org/stable/3832889

[3] M. Becherif, H. S. Ramadan, K. Cabaret, F. Picard, N. Simoncini, O. Bethoux, Hydrogen Energy Storage: New Techno-Economic Emergence Solution Analysis, Energy Procedia 74 (0) (2015) 371–380. doi:10.1016/j.egypro.2015.07.629.

[4] J. M. Ogden, M. M. Steinbugler, T. G. Kreutz, Comparison of hydrogen, methanol and gasoline as fuels for fuel cell vehicles: implications for vehicle design and infrastructure development, Journal of Power Sources 79 (2) (1999) 143–168. doi:10.1016/S0378-7753(99)00057-9.

[5] C. Pan, R. He, Q. Li, J. O. Jensen, N. J. Bjerrum, H. A. Hjulmand, A. B. Jensen, Integration of high temperature PEM fuel cells with a methanol reformer, Journal of Power Sources 145 (2) (2005) 392–398. doi:10.1016/j.jpowsour.2005.02.056.

[6] D. E. Park, T. Kim, S. Kwon, C. K. Kim, E. Yoon, Micromachined methanol steam reforming system as a hydrogen supplier for portable proton exchange membrane fuel cells, Sensors and Actuators, A: Physical 135 (1) (2007) 58–66. doi:10.1016/j.sna.2006.07.008.

[7] X. Cheng, Z. Shi, N. Glass, L. Zhang, J. Zhang, D. Song, Z. S. Liu, H. Wang, J. Shen, A review of PEM hydrogen fuel cell contamination: Impacts, mechanisms, and mitigation, Journal of Power Sources 165 (2) (2007) 739–756. doi:10.1016/j.jpowsour.2006.12.012.

[8] J. Zhang, Z. Xie, J. Zhang, Y. Tang, C. Song, T. Navessin, Z. Shi, D. Song, H. Wang, D. P. Wilkinson, Z.-S. Liu, S. Holdcroft, High temperature PEM fuel cells, Journal of Power Sources 160 (2) (2006) 872–891. doi:10.1016/j.jpowsour.2006.05.034.

[9] S. J. Andreasen, J. R. Vang, S. K. Kær, High temperature PEM fuel cell performance characterisation with CO and CO2 using electrochemical impedance spectroscopy, International Journal of Hydrogen Energy 36 (16) (2011) 9815–9830. doi:10.1016/j.ijhydene.2011.04.076.

[10] F. Zhou, S. J. Andreasen, S. K. Kær, J. O. Park, Experimental investigation of carbon monoxide poisoning effect on a PBI/H3PO4 high temperature polymer electrolyte membrane fuel cell: Influence of anode humidification and carbon dioxide, International Journal of Hydrogen Energy 40 (43) (2015) 14932–14941. doi:10.1016/j.ijhydene.2015.09.056.

[11] A. Chandan, M. Hattenberger, A. El-kharouf, S. Du, A. Dhir, V. Self, B. G. Pollet, A. Ingram, W. Bujalski, High temperature (HT) polymer

electrolyte membrane fuel cells (PEMFC) – A review, Journal of Power Sources 231 (2013) 264–278. doi:10.1016/j.jpowsour.2012.11.126.

[12] Q. Li, R. He, J. Jensen, N. Bjerrum, Approaches and recent development of polymer electrolyte membranes for fuel cells operating above 100 C, Chemistry of materials (2003) 4896–4915doi:10.1021/cm0310519.

[13] G. Nguyen, S. Sahlin, S. J. Andreasen, B. Shaffer, J. Brouwer, Dynamic modeling and experimental investigation of a high temperature PEM fuel cell stack, International Journal of Hydrogen Energy 41 (8) (2016) 4729–4739. doi:10.1016/j.ijhydene.2016.01.045.

[14] S. K. Das, A. Reis, K. J. Berry, Experimental evaluation of CO poisoning on the performance of a high temperature proton exchange membrane fuel cell, Journal of Power Sources 193 (2) (2009) 691–698. doi:10.1016/j.jpowsour.2009.04.021.

[15] M. Boaventura, H. Sander, K. A. Friedrich, A. Mendes, The influence of CO on the current density distribution of high temperature polymer electrolyte membrane fuel cells, Electrochimica Acta 56 (25) (2011) 9467–9475. doi:10.1016/j.electacta.2011.08.039.

[16] O. Shamardina, M. S. Kondratenko, A. V. Chertovich, A. A. Kulikovsky, A simple transient model for a high temperature PEM fuel cell impedance, International Journal of Hydrogen Energy 39 (5) (2014) 2224–2235. doi:10.1016/j.ijhydene.2013.11.058.

[17] M. Boaventura, I. Alves, P. Ribeirinha, A. Mendes, The influence of impurities in high temperature polymer electrolyte membrane fuel cells performance, International Journal of Hydrogen Energy 1 (2016) 2–11. doi:10.1016/j.ijhydene.2016.06.201.

[18] S. S. Araya, S. J. Andreasen, H. V. Nielsen, S. K. Kær, Investigating the effects of methanol-water vapor mixture on a PBI-based high temperature PEM fuel cell, International Journal of Hydrogen Energy 37 (23) (2012) 18231–18242. doi:10.1016/j.ijhydene.2012.09.009.

[19] S. S. Araya, I. F. Grigoras, F. Zhou, S. J. Andreasen, S. K. Kær, Performance and endurance of a high temperature PEM fuel cell operated on methanol reformate, International Journal of Hydrogen Energy 39 (32) (2014) 18343–18350. doi:10.1016/j.ijhydene.2014.09.007.

[20] S. Araya, S. Andreasen, S. Kær, Experimental characterization of the poisoning effects of methanol-based reformate impurities on a PBI-based high temperature PEM fuel cell, Energies 5 (2012) 4251—-4267. doi:doi:10.3390/en5114251.

[21] P. Polverino, C. Pianese, M. Sorrentino, D. Marra, Model-based development of a fault signature matrix to improve solid oxide fuel cell systems on-site diagnosis, Journal of Power Sources 280 (2015) 320–338. doi:10.1016/j.jpowsour.2015.01.037.

[22] P. Polverino, A. Esposito, C. Pianese, B. Ludwig, B. Iwanschitz, A. Mai, On-line experimental validation of a model-based diagnostic algorithm dedicated to a solid oxide fuel cell system, Journal of Power Sources 306 (2016) 646–657. doi:10.1016/j.jpowsour.2015.12.046.

[23] P. Polverino, C. Pianese, Model-based prognostic algorithm for online rul estimation of pemfcs, in: 2016 3rd Conference on Control and Fault-Tolerant Systems (SysTol), 2016, pp. 599–604. doi:10.1109/SYSTOL.2016.7739814.

[24] J. R. Vang, S. J. Andreasen, S. S. Araya, S. K. Kær, Comparative study of the break in process of post doped and sol-gel high temperature proton exchange membrane fuel cells, International Journal of Hydrogen Energy 9 (2014) 2–11. doi:10.1016/j.ijhydene.2014.07.017.

[25] K. K. Justesen, S. J. Andreasen, H. R. Shaker, M. P. Ehmsen, J. Andersen, Gas composition modeling in a reformed methanol fuel cell system using adaptive neuro-fuzzy inference systems, International Journal of Hydrogen Energy 38 (25) (2013) 10577–10584. doi:10.1016/j.ijhydene.2013.06.013.

[26] J. Wu, X. Z. Yuan, H. Wang, M. Blanco, J. J. Martin, J. Zhang, Diagnostic tools in PEM fuel cell research: Part I Electrochemical techniques, International Journal of Hydrogen Energy 33 (6) (2008) 1735–1746. doi:10.1016/j.ijhydene.2008.01.013.

[27] R. E. Rosli, A. B. Sulong, W. R. W. Daud, M. A. Zulkifley, A review of high-temperature proton exchange membrane fuel cell (HT-PEMFC) system, International Journal of Hydrogen Energy (2016) 1–22doi:10.1016/j.ijhydene.2016.06.211.

[28] M. A. Rubio, A. Urquia, S. Dormido, Diagnosis of PEM fuel cells through current interruption, Journal of Power Sources 171 (2) (2007) 670–677. doi:10.1016/j.jpowsour.2007.06.072.

[29] X. Yuan, J. C. Sun, H. Wang, J. Zhang, AC impedance diagnosis of a 500W PEM fuel cell stack, Journal of Power Sources 161 (2) (2006) 929–937. doi:10.1016/j.jpowsour.2006.07.020.

[30] C. Brunetto, A. Moschetto, G. Tina, PEM fuel cell testing by electrochemical impedance spectroscopy, Electric Power Systems Research 79 (1) (2009) 17–26. doi:10.1016/j.epsr.2008.05.012.

[31] S. M. Rezaei Niya, M. Hoorfar, Study of proton exchange membrane fuel cells using electrochemical impedance spectroscopy technique - A review, Journal of Power Sources 240 (2013) 281–293. doi:10.1016/j.jpowsour.2013.04.011.

[32] N. V. Dale, M. D. Mann, A. M. Dhirde, T. Han, ac Impedance Study of a Proton Exchange Membrane Fuel Cell Stack Under Various Loading, Journal of Fuel Cell Science and Technology 7 (June 2010) (2010) 1–10. doi:10.1115/1.3207871.

[33] J. R. Vang, S. J. Andreasen, S. K. Kær, A Transient Fuel Cell Model to Simulate HTPEM Fuel Cell Impedance Spectra, Journal of Fuel Cell Science and Technology 9 (2) (2012) 021005. doi:10.1115/1.4005609.

[34] T. E. Springer, T. A. Zawodzinski, M. S. Wilson, S. Gottesfeld, Characterization of Polymer Electrolyte Fuel Cells Using AC Impedance Spectroscopy, Journal of the Electrochemical Society 143 (2) (1996) 587–599. doi:10.1149/1.1836485.

[35] J. E. B. Randles, Kinetics of Rapid Electrode Reactions, Discussions of the Faraday Society 1 (1947) 11–19. doi:10.1039/DF9470100011.

[36] D. C. Grahame, Mathematical Theory of the Faradaic Admittance - Pseudocapacity and Polarization Resistance, Journal of the Electrochemical Society 99 (12) (1952) 370–385. doi:10.1149/1.2779638.

[37] N. Fouquet, C. Doulet, C. Nouillant, G. Dauphin-Tanguy, B. Ould-Bouamama, Model based PEM fuel cell state-of-health monitoring via ac impedance measurements, Journal of Power Sources 159 (2) (2006) 905–913. doi:10.1016/j.jpowsour.2005.11.035.

[38] C. Jeppesen, M. Blanke, F. Zhou, S. J. Andreasen, Diagnosis of CO Pollution in HTPEM Fuel Cell using Statistical Change Detection, IFAC-PapersOnLine 48 (2015) 547–553. doi:10.1016/j.ifacol.2015.09.583.

[39] R. Storn, K. Price, Differential evolution – a simple and efficient heuristic for global optimization over continuous spaces, Journal of global optimization (1997) 341–359doi:10.1023/A:1008202821328.

[40] J. L. Jespersen, E. Schaltz, S. K. Kær, Electrochemical characterization of a polybenzimidazole-based high temperature proton exchange membrane unit cell, Journal of Power Sources 191 (2) (2009) 289–296. doi:10.1016/j.jpowsour.2009.02.025.

[41] I. a. Schneider, S. a. Freunberger, D. Kramer, A. Wokaun, G. G. Scherer, Oscillations in Gas Channels - Part I. The Forgotten Player in Impedance Spectroscopy in PEFCs, Journal of The Electrochemical Society 154 (4) (2007) B383—-B388. doi:10.1149/1.2435706.

[42] I. a. Schneider, S. a. Freunberger, D. Kramer, A. Wokaun, G. G. Scherer, Oscillations in Gas Channels - Part II. Unraveling the Characteristics of the Low Frequency Loop in Air-Fed PEFC Impedance Spectra, Journal of The Electrochemical Society 154 (4) (2007) B770—-B782. doi:10.1149/1.2742291.

[43] C. Y. Chen, W. H. Lai, Effects of temperature and humidity on the cell performance and resistance of a phosphoric acid doped polybenzimidazole fuel cell, Journal of Power Sources 195 (21) (2010) 7152–7159. doi:10.1016/j.jpowsour.2010.05.057.

[44] S. J. Andreasen, J. L. Jespersen, E. Schaltz, S. K. Kær, Characterisation and modelling of a high temperature PEM fuel cell stack using electrochemical impedance spectroscopy, Fuel Cells 9 (4) (2009) 463–473. doi:10.1002/fuce.200800137.

[45] W. H. Zhu, R. U. Payne, B. J. Tatarchuk, PEM stack test and analysis in a power system at operational load via ac impedance, Journal of Power Sources 168 (1 SPEC. ISS.) (2007) 211–217. doi:10.1016/j.jpowsour.2007.02.071.

[46] X. Yuan, H. Wang, J. C. Sun, J. Zhang, AC impedance technique in PEM fuel cell diagnosis–A review, International Journal of Hydrogen Energy 32 (17) (2007) 4365 – 4380. doi:DOI: 10.1016/j.ijhydene.2007.05.036.

[47] S. S. Araya, F. Zhou, V. Liso, S. L. Sahlin, J. R. Vang, S. Thomas, X. Gao, C. Jeppesen, S. K. Kœr, A comprehensive review of PBI-based high temperature PEM fuel cells, International Journal of Hydrogen Energy 41 (46) (2016) 21310–21344. doi:10.1016/j.ijhydene.2016.09.024.

[48] D. Cao, G. Q. Lu, A. Wieckowski, S. A. Wasileski, M. Neurock, Mechanisms of methanol decomposition on platinum: A combined experimental and ab initio approach, Journal of Physical Chemistry B 109 (23) (2005) 11622–11633. doi:10.1021/jp0501188.

Paper B

Investigation of Current Pulse Injection as an On-line Characterization Method for PEM fuel cell stack

Christian Jeppesen, Samuel Simon Araya, Simon Lennart Sahlin, Søren Juhl Andreasen, Søren Knudsen Kær

The paper has been submitted to the
International Journal of Hydrogen Energy

Investigation of Current Pulse Injection as an On-line Characterization Method for Proton Exchange Membrane Fuel Cell Stack

Christian Jeppesen[a,*], Samuel Simon Araya[a], Simon Lennart Sahlin[a], Søren Juhl Andreasen[b], Søren Knudsen Kær[a]

[a]*Department of Energy Technology, Aalborg University, Pontoppidanstræde 111, 9220 Aalborg Ø, Denmark*
[b]*Serenergy A/S, Lyngvej 8, 9000 Aalborg, Denmark*

Abstract

In this paper a method for estimating the fuel cell impedance is presented, namely the current pulse injection (CPI) method, which is well suited for on-line implementation. This method estimates the fuel cell impedance and unlike electrochemical impedance spectroscopy (EIS), it is simple to implement at a low cost. This makes it appealing as a characterization method for on-line diagnostic algorithms. In this work a parameter estimation method for estimation of equivalent electrical circuit (EEC) parameters, which is suited for on-line use is proposed. Tests on a 10 cell high temperature PEM fuel cell show that the method yields consistent results in estimating EEC parameters for different current pulse at different current loads, with a low variance. A comparison with EIS shows that despite its simplicity the response of CPI can reproduce well the impedance response of the high and intermediate frequencies.

Keywords: Fuel Cell, PEM, characterization, EIS, CPI, Current Pulse Injection

1. Introduction

In recent years, the environmental effect of the rising temperatures around the world, has been gaining attention from politicians. The consequences of climate change are being more widely accepted in the general public, and the approval of renewable energy sources is increasing. With more fluctuating

*Corresponding author
Email address: chj@et.aau.dk (Christian Jeppesen)
URL: http://et.aau.dk (Christian Jeppesen)

renewable energy sources providing power for the electrical grid, new storage solutions that can balance the grid are necessary [1]. Hydrogen produced from water electrolysis using renewable electricity can be a viable option as an energy carrier, which among other things can be used in fuel cells both for stationary and mobile power generation.

The Department of Energy (DoE) in USA, has set a target for fuel cell price and durability for stationary and transport applications. For fuel cells to be competitive the lifetime of a fuel cell must exceed 5000 hours for transport applications and 40000 for stationary applications [2]. During the last decade the durability of fuel cells has improved significantly, due to extensive research in the field and experiences from the industry. However, the lifetime span is still has not reached the targets yet.

For improving the durability of advanced systems such as fuel cells, it is crucial that a proper online diagnostic system is deployed [3]. Such a system could detect faults early, and through a mitigation strategy change the system settings and prevent rapid degradation of the fuel cell stack. Furthermore, a well-designed diagnostic system, could be a part of a prognostics system, which could predict component failure to manage service of the fuel cell system, thus reducing the down time of the systems.

When dealing with diagnostics of fuel cells, the majority of methods available in the literature treats the topic of fault detection in three parts, as shown in Figure 1 [4, 5]. In many studies the fuel cell fault detection is done by detecting a change in the parameters of an equivalent electrical circuit (EEC) model of the fuel cell's dynamic voltage behavior. The most used technique for obtaining EECs model is electrochemical impedance spectroscopy (EIS) [6, 7], with current interruption (CI) method also used to some extent [8, 9]. The former yields the full impedance response and the latter primarily yields a simpler response and often only the ohmic resistance is extracted.

An alternative method for estimating the impedance of an electrochemical device is the Current Pulse Injection (CPI) method. This method is widely used in the battery community, for estimating the state of charge and the state of health [10, 11, 12, 13]. The CPI characterization method works by drawing a small current pulse from the electrochemical device, and then measuring the corresponding transient voltage. By using the current as input and the fuel cell stack voltage as output, an input/output parameter estimation methods can be utilized for estimate the parameters of a EEC model.

In the fuel cell community, different papers have focused on the transient voltage during current steps as a method for fuel cell characterization [14, 15, 16, 17, 18], but not as a diagnostics tool for fuel cells. In [19], small

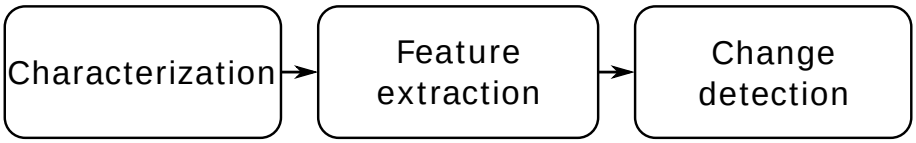

Figure 1: Flow chart of most available model based methods for fuel cell fault detection.

current pulses have been used for estimating EEC model parameters. In another paper, the CPI method was treated in relation to diagnostics of PEM fuel cells, however with a limited access to experimental data and a parameter estimation method not suited for online fuel cell diagnostics [20].

In this work, the CPI method will be used for characterization of a fuel cell short stack, and EEC model parameter estimation method suited for online deployment are suggested. Furthermore, the CPI method performance is compared to the electrochemical impedance spectroscopy characterization method.

The paper is structured as follows:

In section 2 the current pulse characterization method is presented and discussed, and the applied parameter estimation method is presented. In section 3 the experimental setup is presented and the experimental procedure is explained. In section 4 the results of the characterization of the fuel cell stack are presented and in section 5 the current pulse injection characterization method is compared with the electrochemical impedance spectroscopy method.

2. Current Pulse Injection method

Current Pulse Injection (CPI) method is an alternative fuel cell characterization method that utilizes small current pulses in the form of an extra drawn current step in a small period of time. Based on the corresponding transient voltage time signals, the fuel cell impedance can be estimated, by standard available system identification methods. A conceptual voltage profile of a fuel cell voltage is shown in Figure 2, during a small current step. The EEC model estimated based on the CPI method is in general simpler than what can be observed by EIS measurements, but for some diagnostic purposes this technique could be proven sufficient.

The EIS and CPI characterization methods can be conducted in-situ contrary to the CI method, as for the CI method the load must completely be discontinued.

The EIS method is very expensive on lab scale, and even though there are European projects, such as the D-code project (FCH JU, grant No 256673),

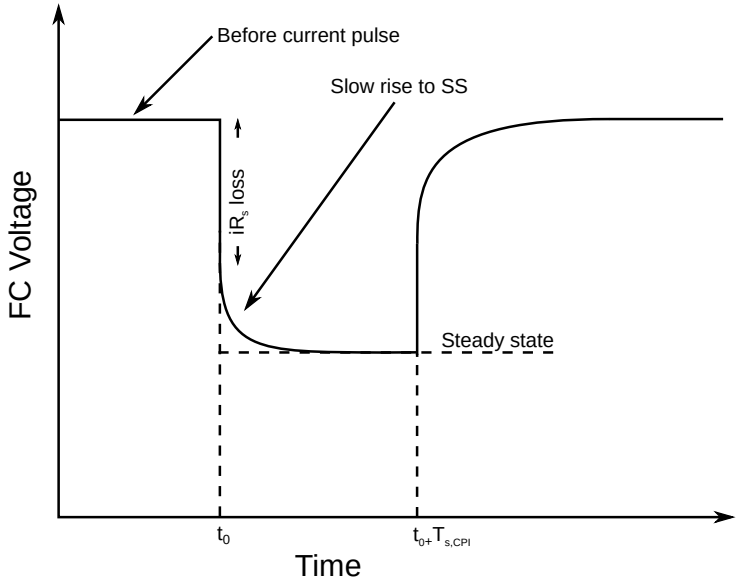

Figure 2: Conceptual drawing of transient voltage durring a small current step.

working on implementing the EIS measurement on an onboard DC-DC converter for fuel cell systems, it still has strict requirements to the bandwidth of the DC-DC converter. The idea behind EIS measurements is simple but will still require a great deal of engineering before it can run on real life fuel cell systems.

The main advantage of the CPI method is that it can be implemented at relatively low cost. As shown in Figure 3, the current pulses used for the CPI method can be implemented by a series resistor and transistor in parallel with the fuel cell terminals. By controlling the transistor with a PWM signal the small electrical circuit will then draw small current pulses from the fuel cell, depending on the size of the resistor.

In order to use CPI method for estimating the impedance of a fuel cell, a common approach is to use a parameter estimation method to fit the voltage response to an EEC model. Most fuel cell EEC models utilize a form of the Randles circuit, with 1-3 parallel RC loops. For this work a Randles circuit with one parallel RC loop is used, giving one semicircle in the complex plane, as shown in Figure 4. This is a quite simple circuit, giving a simple response, and yielding a similar transient response as shown in Figure 2. The advantage of such a simple model is that it has lower fitting times and a more consistent parameter fitting algorithm performance and parameter space. Furthermore,

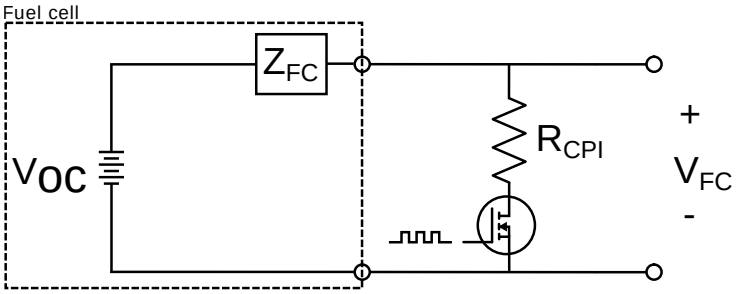

Figure 3: Electrical implementation of the current pulse injection characterization method.

as reported in [21], a more complex model might yield a better fit to the data, but at the same time becomes more sensitive to small variations such as measurement noise, and it is therefore the recommendation by Vang et al. [21] to use the less complex EEC models if their accuracy is sufficient for the application.

2.1. Parameter estimation

There are many different methods available for parameter estimation of fuel cell systems, such as EEC models. An extensive review and collection of these methods are available in Ljung's work on system identification [22].

The most common methods available utilize a model prediction error (ϵ), which is the difference between the measured value and the output of a model. The parameter estimation method then aims to minimize the prediction error, and is thereby treated as an optimization problem. For this work a non-recursive least squares method is applied for estimating the parameters of the EEC model, shown in Figure 4. The optimization problem is solved as a linear regression problem, where the prediction error is defined as shown in equation 1, where $\underline{V}_{FC}$ is a column vector of the measured voltage of N length of dataset used for the parameter estimation, and $\underline{\hat{V}}_{FC}$ is a column vector of the model output also of length N.

$$\underline{\epsilon} = \underline{V}_{FC} - \underline{\hat{V}}_{FC} \tag{1}$$

The model output $\hat{V}_{FC}$, which is a mathematical representation of V_{FC}, can be described as the open circuit voltage (V_{OC}) minus the voltage drop across the EEC model (where s is the Laplace operator), where I_{FC} is the fuel cell current:

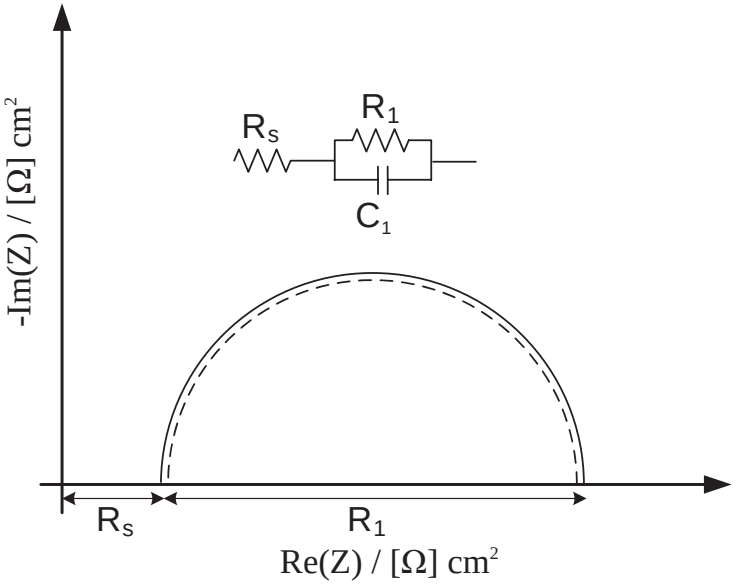

Figure 4: Conceptual Nyquist plot of the EEC model used for the CPI method.

$$V_{FC} = V_{OC} - R_s I_{FC} - \frac{R_1}{R_1 C_1 s + 1} I_{FC} \tag{2}$$

The model given in equation 2 is not linear due to the V_{OC} term. Equation 2 is therefore linearized, and the terms are collected as one fraction. The linear input / output dynamics for V_{FC} can thereby be described as the transfer function, where I_{CPI} is the pulse current:

$$\frac{V_{FC}}{I_{CPI}} = \frac{R_s R_1 C_1 \cdot s + (R_s + R_1)}{R_1 C_1 \cdot s + 1} \tag{3}$$

The transfer function given in equation 3, must be converted to the discrete time domain in order to apply the parameter estimation method to the model, where lower-case z is the z-domain operator and T_s is period of time between the samples. The transfer function in equation 3, will be mapped into the discrete domain using the bilinear transform (Tustin):

$$s \leftarrow \frac{2}{T_s} \frac{z-1}{z+1} \tag{4}$$

The transfer function given in equation 3, is converted to the discrete time domain using equation 4:

$$\frac{V_{FC}}{I_{CPI}} = \frac{b_1 \cdot z^{-1} + b_2}{a_1 \cdot z^{-1} + 1} \tag{5}$$

where:

$$b_1 = \frac{T_s(R_1 + R_s) - 2R_S R_1 C_1}{2R_1 C_1 + T_s} \tag{6}$$

$$b_2 = \frac{2R_s R_1 C_1 + T_s(R_1 + R_s)}{2R_1 C_1 + T_s} \tag{7}$$

$$a_1 = \frac{T_s - 2R_1 C_1}{2R_1 C_1 + T_s} \tag{8}$$

The input / output dynamics for equation 5 can be described as a difference equation, where k indicates the k^{th} sample ($k \in \{1, 2, ..., N\}$):

$$V_{FC,k} = -a_1 V_{FC,(k-1)} + b_1 I_{FC,(k-1)} + b_2 I_{FC,k} \tag{9}$$

Based on the above an unknown parameter vector ($\hat{\theta}$) can be defined:

$$\underline{\hat{\theta}} = \begin{bmatrix} a_1 \\ b_1 \\ b_2 \end{bmatrix} \tag{10}$$

and a data row vector:

$$\underline{\phi}_k = \begin{bmatrix} -V_{FC,(k-1)} & I_{FC,(k-1)} & I_{FC,k} \end{bmatrix} \tag{11}$$

The difference equation (9) can then be expressed as:

$$V_{FC,k} = \underline{\phi}_k \, \underline{\hat{\theta}} \tag{12}$$

The entire fuel cell voltage model output ($\underline{V}_{FC}$) with length N, can be described by replacing the data row vector with the entire dataset matrix $\left(\underline{\underline{\phi}}\right)$ in equation 12, where $\underline{\underline{\phi}}$ has the dimension of $N \times 3$).

In order to formulated the residual prediction error, described in equation 1, the formulation from above can now be inserted:

$$\underline{\epsilon} = \underline{V}_{FC} - \underline{\underline{\phi}} \, \underline{\hat{\theta}} \tag{13}$$

The residual prediction error vector given in 13 can now be squared, and minimized as a convex optimization problem, where the cost function ($J(\hat{\theta})$) is given as:

$$J(\hat{\theta}) = \underline{\epsilon}^T \underline{\epsilon} \tag{14}$$

$$= \left(\underline{V_{FC}}^T - \underline{\underline{\phi}}^T \hat{\underline{\theta}}^T\right)\left(\underline{V_{FC}} - \underline{\underline{\phi}}\,\hat{\underline{\theta}}\right) \tag{15}$$

It can be shown that the solution to the convex optimization problem given in eq. 15 is given by [23]:

$$\hat{\underline{\theta}} = \left(\underline{\underline{\phi}}^T \underline{\underline{\phi}}\right)^{-1} \underline{V_{FC}} \tag{16}$$

The estimated parameter vector ($\hat{\underline{\theta}}$) can now be converted back to the continuous EEC model parameters, by solving equations 6-8 for the parameters R_1, C_1 and R_s:

$$R_1 = \frac{2a_1b_2 - 2b_1}{a_1^2 - 1} \tag{17}$$

$$C_1 = \frac{T_s a_1^2 - 2T_s a_1 + T_s}{4b_1 - 4a_1b_2} \tag{18}$$

$$R_s = \frac{b_1 - b_2}{a_1 - 1} \tag{19}$$

3. Experimental setup

To verify the CPI method, experiments have been conducted on a 10 cell SerEnergy high temperature PEM fuel cell short stack. The method can also be used for other types of fuel cells, however this stack was available at the start of the experiment. The stack was operated in a GreenLight Innovation test stand, with an external cooling cart for oil circulation. The stack consisted of 10 cells based on BASF MEAs with an active area of 165 cm^2 and standard flow plates form a S165L SerEnergy stack.

The short stack is shown in Figure 5. It is heated and cooled by an external oil circuit at a forward temperature set point of 169 °C. The anode gas consists of dry hydrogen with a stoichiometric of λ_{H2}= 2, and the cathode gas consists of non-humidified atmospheric air from an air compressor, where the volume flow is controlled at stoichiometric ratio of λ_{air}=4. During the current pulses, the H_2 and air flows are not changed. This is done due to the fact that the bandwidth

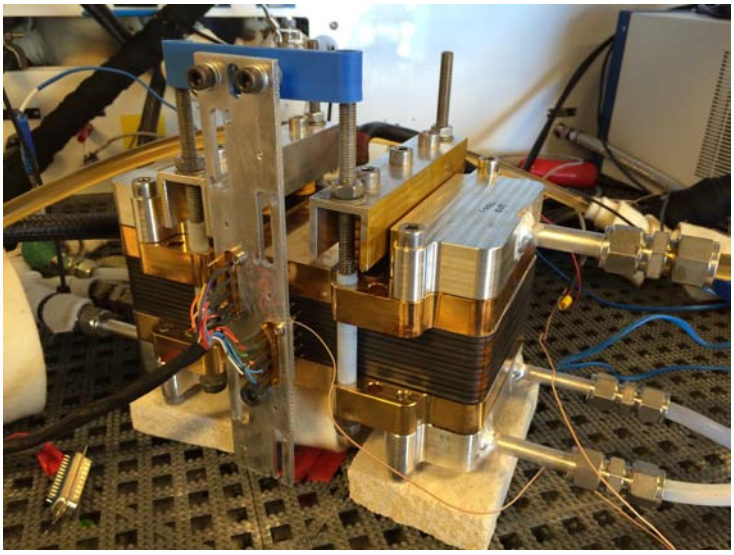

Figure 5: The 10 cell HT-PEM fuel cell stack, used for the experimental work.

of the mass flow controllers are too slow compared to the frequency of the current pulses. Furthermore, the anode and cathode stoichiometric ratios are high enough to accommodate the extra current load. The anode and cathode gases are not preheated or pre-humidified.

The current is drawn from an external TDi RBL-488 electronic load with a 20 kHz bandwidth, which is controlled by a NI cRIO-9033 with a NI-9263 voltage output module. The internal data logging system in the GreenLight Innovation test stand is too slow for the purpose of this work, and therefore, cRIO is also utilized for data logging of the current and voltage. For voltage input a NI-9223 module was used for simultaneous measurements, with a sampling frequency of V_{FC} and I_{FC} of F_s=100 kHz.

In order to compare the CPI method to the full impedance spectrum, EIS measurements were conducted in a galvanostatic mode using a Gamry reference 3000 potentiostat. The EIS measurements are performed at a starting frequency of 10 kHz and a final frequency of 0.1 Hz, with 10 points per decade. The AC perturbation current was fixed to 7.5 % of the DC value of the load current.

4. Results

The CPI characterization method is demonstrated below based on the experimental data, and EEC model parameters were fitted using the method

described in section 2.1.

4.1. Experimental data

During the test of the CPI method, the fuel cell stack was tested at the following DC levels:

$$i_{FC} = \{0.2, 0.3, 0.4\} \quad \text{Acm}^{-2}$$

which correspond to 32 A, 48 A and 64 A, respectively, for this size of fuel cell stack.

For testing the CPI characterization method, different amplitudes are tested to identify the effect of different current pulse amplitudes on the transient behavior. The amplitudes of the injected current pulses are:

$$I_{CPI} = \{1, 2, 3, 4, 5\} \quad \text{A}$$

As an initial experiment the CPI method was tested at different pulse frequencies. Figure 6 shows the data from an initial experiment, where the CPI method was tested at the following frequencies:

$$f_{CPI} = \{100, 10, 1, 0.1\} \quad \text{Hz}$$

It can be seen that at 100 and 10 Hz, the transient over potential is not fully developed. These frequencies are therefore not suited for this method, since the parameter estimation method descried in section 2 of this paper yields the best and most accurate performance if the transient voltage is fully developed. The time series data shown in Figure 6 are conducted with current pulses of 1 A, and the transient voltage behavior at different frequencies is representative for the remaining current pulse amplitudes.

For the frequencies 1 and 0.1 Hz, it can be seen that the transient voltage response is fully developed, as can be illustrated from the example of two pulses at 1 Hz with a duty cycle of 0.5 shown in Figure 7. These two frequencies can therefore be used for the parameter estimation of the electrical equivalent circuit. It can also be seen that in Figure 7 that the frequency could not e.g. be 2 Hz, since the period of steady state voltage level after the transient period would be cut off. It can also be seen in Figure 7 that the time the voltage is steady state is as long as the transient period during the pulses.

When inspecting the 0.1 Hz data in Figure 6, it can be seen that the transient voltage is fully developed to a steady state level. At this frequency, the voltage is at steady state for the majority of the pulse time. This data could also be used for the parameter estimation, but the time required for one characterization experiment is 10 times longer than the 1 Hz data set. This is not a

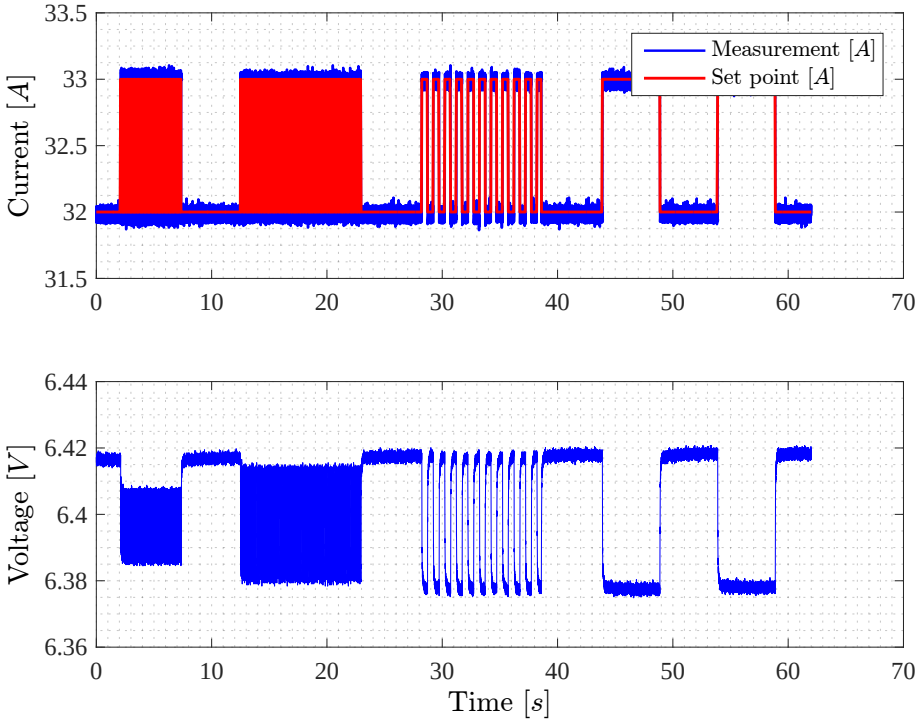

Figure 6: Time series of small current steps for the 1 A amplitude experiment, at different frequencies ($f_{CPI} = \{100, 10, 1, 0.1\}$ Hz).

problem, when temperatures and operational parameters are constant during the characterization experiment, but by choosing the 1 Hz current pulses this uncertainty is eliminated. The 1 Hz current pulses seems to be a good trade-off, and are chosen for the parameter estimation.

4.2. CPI EEC model parameter estimation at different current pulse amplitudes

The CPI characterization method was tested based on the experimental data, at the two different DC current loads and at five different current pulse amplitudes.

In Figure 8 a typical dataset of two 1 A pulses, at a DC current density of 0.2 Acm^{-2} can be seen. The red dots are measured voltage data, and the blue line is the EEC model fit, where the EEC model parameters are estimated using the parameter estimation method described in section 2.1. The voltage response has been superpositioned by subtracting the DC value of the fuel cell voltage and by projecting the voltage signal into the positive plane. This is

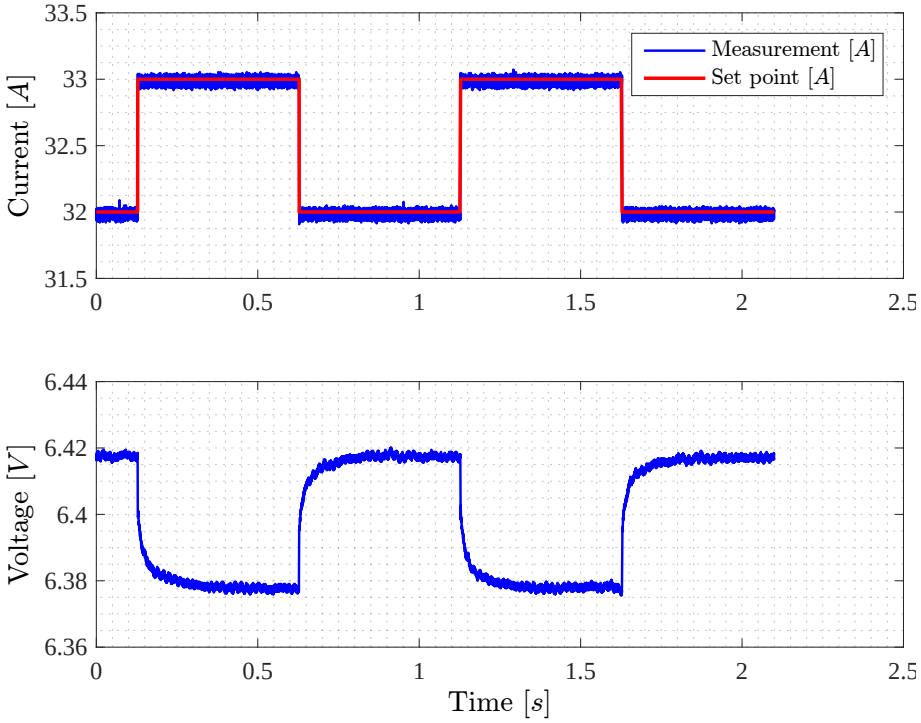

Figure 7: Selected time series data of two current pulses at 1 Hz (duty cycle=0.5), with 1 A current amplitude.

done in order to have a linear response, as described in section 2.1 and shown in Figure 8.

The time series window, where the parameters estimation was conducted is 2.1 s. It was kept constant for all the CPI tests to ensure comparability between them, meaning that two pulses at 1 Hz and a duty cycle of 0.5 are used for all CPI tests. The EEC model parameter estimation could also be done with different number of pulses, however two pulses were chosen as a trade-off between sufficient data and low enough time span of the experiment.

In Figure 8, it can be seen that some noise is present. However, this noise is Gaussian, and can be considered as normal measurement noise, with a low amplitude of approximately 2 mV. The noise could be filtered, but this would change the amplitude of the abrupt voltage jump caused by the fuel cell stack series resistance. Furthermore, the signal to noise ratio is sufficiently low for the EEC model parameter estimation.

The blue model fit shown in Figure 8 is representative of the abrupt change of 17.5 mV, in the fuel cell stack voltage caused by the fuel cell stack series

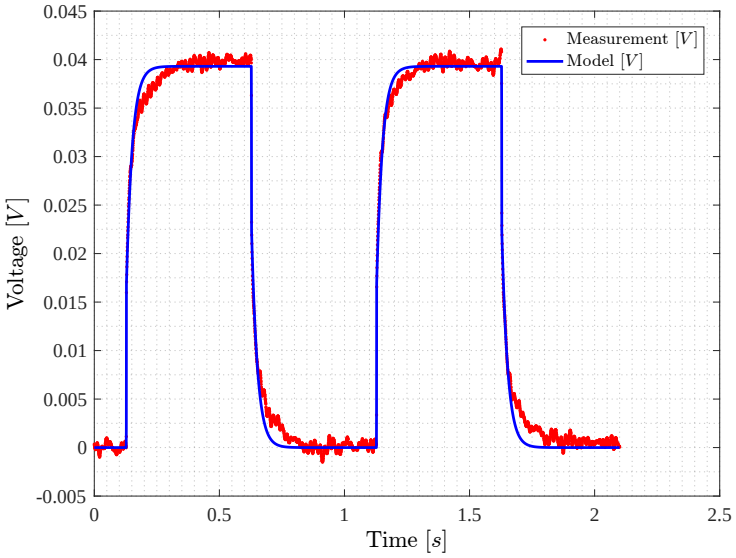

Figure 8: Selected time series data of 1 Hz (duty cycle=0.5) pulses, including the simple R-RC EEC model, at a 1 A current pulse amplitude.

resistance. The first half of the transient voltage period shows a good fit to the model, but the second half of the transient period is slightly off. However, this EEC model fit is, as stated in section 2.1, the optimal solution to the parameter estimation problem. A more complex EEC model could yield a better model fit for the second half of the transient period, but this would require more fitting time and the authors found the solution to the parameter estimation problem of more complex EEC models to be unstable in some cases. Moreover, the sum of the resistances of the EEC model would be constant, independent of the EEC model structure.

In Tables 1, 2 and 3 are shown the results of the EEC model parameter estimation of the CPI characterization experiments at 0.2 Acm^{-2}, 0.3 Acm^{-2} and 0.4 Acm^{-2}, respectively.

Throughout all the three DC current loads, all the EEC model parameters are consistent with low variance (σ^2). The variance of the parameters can be seen in the right column of the Tables 1, 2 and 3. The variance is especially important when the measurement method is being used for fault detection, since a low variance can withhold a more aggressive threshold between faulty and non-faulty operation with relatively low probability of false alarm. As expected, the R_1 resistance of the RC loop decreases with increase in current density, which is also reported in previous works [24, 25].

Table 1: Estimated EEC parameters for using the current pulse injection method at 0.2 Acm^{-2} DC fuel cell output current for 5 current pulse amplitudes.

	1 A	**2** A	**3** A	**4** A	**5** A	σ^2
$\mathbf{R}_s$ $[m\Omega]$	16.5	16.6	16.6	16.0	16.3	0.06
$\mathbf{R}_1$ $[m\Omega]$	22.8	22.6	22.5	22.9	22.4	0.04
$\mathbf{C}_1$ $[F]$	1.05	1.06	1.1	1.01	1.06	0.001

Table 2: Estimated EEC parameters for using the current pulse injection method at 0.3 Acm^{-2} DC fuel cell output current for 5 current pulse amplitudes.

	1 A	**2** A	**3** A	**4** A	**5** A	σ^2
$\mathbf{R}_s$ $[m\Omega]$	15.4	15.2	15.7	15.4	15.8	0.06
$\mathbf{R}_1$ $[m\Omega]$	17.9	17.6	17.4	17.4	17.5	0.04
$\mathbf{C}_1$ $[F]$	1.08	1.11	1.13	1.12	1.13	0.0004

The value of the EEC model parameters are independent of the current pulse amplitude, between 1 – 5 A, which is the range of testing in this work. This is an advantage when the characterization method is physically implemented as suggested in Figure 3. The amplitude of the pulse will depend on the fuel cell voltage, which changes according to the polarization curve, which at its time changes with degradation. The amplitude of the current pulse will therefore be smaller at higher fuel cell stack load currents compared to the current pulse amplitude at lower load. It is important that the size of the resistor R_{CPI} is chosen small enough to accommodate sufficient signal to noise ratio. However, smaller current pulse amplitude also means a larger energy usage and the size of the current pulse should be limited in such a way that the anode and cathode stoichiometric ratios do not change, since these will affect the transient behavior of the fuel cell voltage, and thereby change the EEC model parameters. A constant flow of the anode and cathode gasses, will also ease the implementation of the method.

Table 3: Estimated EEC parameters for using the current pulse injection method at 0.4 Acm^{-2} DC fuel cell output current for 5 current pulse amplitudes.

	1 A	**2** A	**3** A	**4** A	**5** A	σ^2
$\mathbf{R}_s$ $[m\Omega]$	15.2	15.0	15.1	15.1	14.9	0.01
$\mathbf{R}_1$ $[m\Omega]$	15.6	16.3	15.6	15.7	15.8	0.08
$\mathbf{C}_1$ $[F]$	1.16	1.21	1.17	1.19	1.15	0.0006

4.3. Comparison between CPI and EIS EEC model parameters

To validate the EEC model parameters identified using the CPI fuel cell characterization method, EIS measurements are conducted at each current load set point.

As it is known the low frequency part of the impedance spectra is related to the mass transport and the gas channel geometry [25]. Unlike during EIS measurements, CPI do not cause oscillation of gas flows due to low frequency current [26, 27, 28, 29]. The low frequency part of the measured impedance spectrum is therefore not represented in the impedance spectrum reassembled by the CPI EEC model parameters. When fitting EEC model parameters to the EIS data set, only the high and intermediate frequency points were considered. The experimental fuel cell EIS data in Figure 9 shows a clear boundary between the intermediate and low frequency data points in the range between the 10 and 1 Hz frequency markers, at around 2 Hz. Therefore, the fitting of the EIS EEC model parameters includes only data points above 2 Hz.

The fitting algorithm used for fitting the EIS EEC model parameters is a home made algorithm that utilizes a least square objective function and a Differential evolution optimization algorithm. The EIS fitted EEC model has been plotted using the entire frequency span (from 10k – 0.1 Hz) in order to show the low frequency intersection with the real axis on the Nyquist plot, as can be seen in Figure 9.

In Figure 9 an example of a model fit of the EIS data set can be seen. A more accurate model fit could have been accomplished using a constant phase element instead of the capacitor in the RC loop. However, since the EIS fitted EEC model parameters are to be compared to the CPI EEC model parameters, a capacitor has been used.

The result of the EIS fitted EEC model parameters and the CPI fitted EEC model parameters for 1 A current pulse amplitude are given in Tables 4, 5 and 6 for fuel cell current densities of 0.2, 0.3 and 0.4 Acm^{-2}, respectively. At 0.2 and 0.3 Acm^{-2} the difference between the CPI and the EIS fitted EEC model resistances are low, with 2.3 % difference for R_s at 0.2 Acm^{-2} compared to the EIS fitted R_s parameter. The differences between the two are more pronounced at 0.4 Acm^{-2}, as can be seen in Table 6. However, they are within the same order of magnitude, and it can be concluded that the CPI characterization method can reproduce the EIS measurements for high and intermediate frequencies.

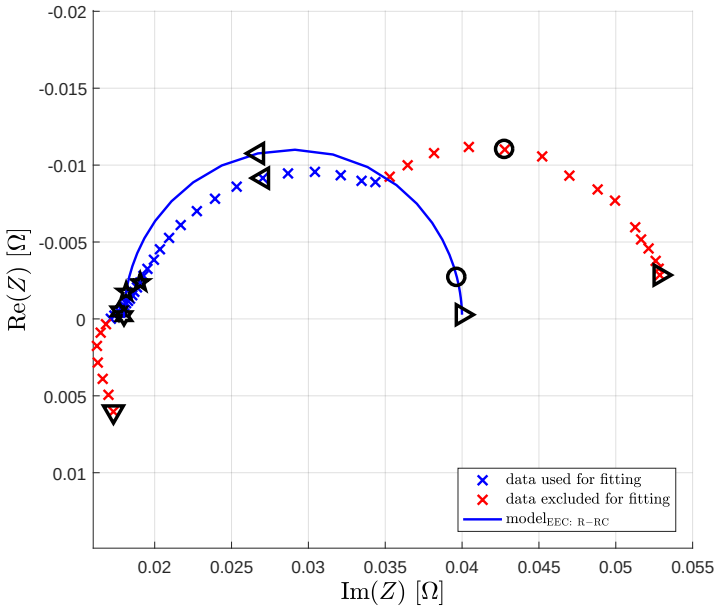

Figure 9: Simple R-RC EEC model fitted to high and intermediate frequencies. EIS data collected at 0.2 Acm^{-2} load current density. The black markers indicate the frequency decades $\{10k, 1k, 100, 10, 1, 0.1\}$ Hz.

5. Conclusion

In this work an EIS alternative to fuel cell characterization method has been investigated, namely the current pulse injection (CPI) characterization method. The proposed technique is a parameter estimation method for the electrical equivalent circuit (EEC) model parameters, based on the transient voltage response during current pulses, and can be said suitable for online use.

The method yields consistent EEC model parameter sets at different current pulse amplitudes, with low variance. The low variance makes the method attractive in fault detection systems, as it can minimize the probability of false alarm.

It can be concluded that the CPI fitted EEC model parameters can predict the impedance measurements similarly to the EIS fitted EEC model parameters, for the high and intermediate frequencies impedance loops. The EEC model estimated using CPI is generally simpler than what can be observed by EIS measurements, but could be sufficient for many diagnostics systems, such as the detection of drying or flooding of a low temperature PEM fuel cell stack, or it could be used for poisoning detection of CO contamination in the anode

Table 4: Comparing the estimated EEC parameters using the CPI method and the EIS method at 0.2 Acm^{-2} DC fuel cell output current.

	1 A CPI	**EIS**	
$\mathbf{R}_s$	16.5 $m\Omega$	16.9 $m\Omega$	2.3 %
$\mathbf{R}_1$	22.8 $m\Omega$	23.6 $m\Omega$	3.4 %
$\mathbf{C}_1$	1.05 F	0.99 F	6 %

Table 5: Comparing the estimated EEC parameters using the CPI method and the EIS method at 0.3 Acm^{-2} DC fuel cell output current.

	1 A CPI	**EIS**	
$\mathbf{R}_s$	15.4 $m\Omega$	16.5 $m\Omega$	6.6 %
$\mathbf{R}_1$	17.9 $m\Omega$	18.2 $m\Omega$	1.6 %
$\mathbf{C}_1$	1.08 F	0.89 F	19 %

Table 6: Comparing the estimated EEC parameters using the CPI method and the EIS method at 0.4 Acm^{-2} DC fuel cell output current.

	1 A CPI	**EIS**	
$\mathbf{R}_s$	15.2 $m\Omega$	16.7 $m\Omega$	9 %
$\mathbf{R}_1$	15.6 $m\Omega$	16.9 $m\Omega$	7.7 %
$\mathbf{C}_1$	1.16 F	1.03 F	12.6 %

gas of a high temperature PEM fuel cell stack.

The characterization method can be implemented physically using a single resistor and transistor. This makes the solution attractive for mass deployment in fuel cell system diagnosis.

6. Acknowledgment

This work was funded by Innovation Fund Denmark in the framework of the 4M Centre.

7. References

References

[1] M. Becherif, H. S. Ramadan, K. Cabaret, F. Picard, N. Simoncini, O. Bethoux, Energy Procedia 74 (2015) 371–380. URL: `http://dx.doi.org/10.1016/j.egypro.2015.07.629`. doi:`10.1016/j.egypro.2015.07.629`.

[2] The Department of Energy, USA, Fuel cell technologies office multi-year research, Technical Report, 1, 2012. http://www1.eere.energy.gov/hydrogenandfuelcells/mypp/.

[3] P. Pei, H. Chen, Applied Energy 125 (2014) 60–75. URL: http://dx.doi.org/10.1016/j.apenergy.2014.03.048. doi:10.1016/j.apenergy.2014.03.048.

[4] R. Petrone, Z. Zheng, D. Hissel, M. C. Péra, C. Pianese, M. Sorrentino, M. Becherif, N. Yousfi-Steiner, International Journal of Hydrogen Energy 38 (2013) 7077–7091. URL: http://www.sciencedirect.com/science/article/pii/S0360319913007465. doi:10.1016/j.ijhydene.2013.03.106.

[5] C. Jeppesen, M. Blanke, F. Zhou, S. J. Andreasen, in: IFAC-PapersOnLine, volume 48, Elsevier Ltd., 2015, pp. 547–553. doi:10.1016/j.ifacol.2015.09.583.

[6] N. Fouquet, C. Doulet, C. Nouillant, G. Dauphin-Tanguy, B. Ould-Bouamama, Journal of Power Sources 159 (2006) 905–913. URL: http://www.sciencedirect.com/science/article/pii/S0378775305015946. doi:10.1016/j.jpowsour.2005.11.035.

[7] Z. Zheng, M. C. Péra, D. Hissel, M. Becherif, K. S. Agbli, Y. Li, Journal of Power Sources 271 (2014) 570–581. doi:10.1016/j.jpowsour.2014.07.157.

[8] M. A. Rubio, A. Urquia, S. Dormido, Journal of Power Sources 171 (2007) 670–677. doi:10.1016/j.jpowsour.2007.06.072.

[9] T. Mennola, M. Mikkola, M. Noponen, T. Hottinen, P. Lund, Journal of Power Sources 112 (2002) 261–272. doi:10.1016/S0378-7753(02)00391-9.

[10] G. H. Boyle, F. Goebel (1995).

[11] Y. Zou, X. Hu, H. Ma, S. E. Li, Journal of Power Sources 273 (2015) 793–803. URL: http://dx.doi.org/10.1016/j.jpowsour.2014.09.146. doi:10.1016/j.jpowsour.2014.09.146.

[12] K. Propp, M. Marinescu, D. J. Auger, L. O'Neill, A. Fotouhi, V. Knap, G. J. Offer, G. Minton, S. Longo, M. Wild, V. Knap, Journal of Power Sources 328 (2016) 289–299. doi:10.1016/j.jpowsour.2016.07.090.

[13] C. E. Holland, J. W. Weidner, R. A. Dougal, R. E. White, Journal of Power Sources 109 (2002) 32–37. doi:10.1016/S0378-7753(02)00044-7.

[14] K. P. Adzakpa, K. Agbossou, Y. Dubé, M. Dostie, M. Fournier, A. Poulin, Ieee Transactions on Energy Conversion 23 (2008) 581–591. doi:10.1109/TEC.2007.914170.

[15] J. Cho, H. S. Kim, K. Min, Journal of Power Sources 185 (2008) 118–128. doi:10.1016/j.jpowsour.2008.06.073.

[16] F. Marignetti, M. Minutillo, A. Perna, E. Jannelli, IEEE Transactions on Industrial Electronics 58 (2011) 2420–2426. doi:10.1109/TIE.2010.2069073.

[17] S. Didierjean, O. Lottin, G. Maranzana, T. Geneston, Electrochimica Acta 53 (2008) 7313–7320. doi:10.1016/j.electacta.2008.03.079.

[18] H. Yu, C. Ziegler, Journal of The Electrochemical Society 153 (2006) A570–A575. doi:10.1149/1.2162450.

[19] P. T. Ha, H. Moon, B. H. Kim, H. Y. Ng, I. S. Chang, Biosensors and Bioelectronics 25 (2010) 1629–1634. URL: http://dx.doi.org/10.1016/j.bios.2009.11.023. doi:10.1016/j.bios.2009.11.023.

[20] C. de Beer, P. S. Barendse, P. Pillay, B. Bullecks, R. Rengaswamy, IEEE Transactions on Industrial Electronics PP (2014) 1–1. URL: http://ieeexplore.ieee.org/articleDetails.jsp?arnumber=6975174{\%}5Cnhttp://ieeexplore.ieee.org/lpdocs/epic03/wrapper.htm?arnumber=6975174. doi:10.1109/TIE.2014.2377131.

[21] J. R. Vang, S. J. Andreasen, S. S. Araya, S. K. Kær, International Journal of Hydrogen Energy 39 (2014) 14959–14968. doi:10.1016/j.ijhydene.2014.07.017.

[22] L. Ljung, System Identification: Theory for the User, 2nd ed., Prentice Hall, 1999.

[23] S. Shanmugan, A. M. Breipohl, Random Signals - Detection, Estimation and Data Analysis, Wiley Sons, Inc., 1988.

[24] J. L. Jespersen, E. Schaltz, S. K. Kær, Journal of Power Sources 191 (2009) 289–296. URL: http://www.sciencedirect.com/science/article/pii/S0378775309002742. doi:10.1016/j.jpowsour.2009.02.025.

[25] S. J. Andreasen, J. R. Vang, S. K. Kær, International Journal of Hydrogen Energy 36 (2011) 9815–9830. URL: http://dx.doi.org/10.1016/j.ijhydene.2011.04.076. doi:10.1016/j.ijhydene.2011.04.076.

[26] M. Chandesris, C. Robin, M. Gerard, Y. Bultel, Electrochimica Acta 180 (2015) 581–590. URL: http://dx.doi.org/10.1016/j.electacta.2015.08.089. doi:10.1016/j.electacta.2015.08.089.

[27] I. a. Schneider, S. a. Freunberger, D. Kramer, A. Wokaun, G. G. Scherer, Journal of The Electrochemical Society 154 (2007) B383–B388. doi:10.1149/1.2435706.

[28] I. a. Schneider, S. a. Freunberger, D. Kramer, A. Wokaun, G. G. Scherer, Journal of The Electrochemical Society 154 (2007) B770. doi:10.1149/1.2435706.

[29] B.-T. Tsai, C.-J. Tseng, Z.-S. Liu, C.-H. Wang, C.-I. Lee, C.-C. Yang, S.-K. Lo, International Journal of Hydrogen Energy 37 (2012) 13060–13066. URL: http://www.sciencedirect.com/science/article/pii/S0360319912011160. doi:10.1016/j.ijhydene.2012.05.008.

Paper C

Diagnosis of CO Pollution in HTPEM Fuel Cell using Statistical Change Detection

Christian Jeppesen, Mogens Blanke, Fan Zhou, Søren Juhl Andreasen

The paper has been published in the
IFAC-PapersOnLine Vol. 48-21, pp. 547–553, 2015.
http://dx.doi.org/10.1016/j.ifacol.2015.09.583

Diagnosis of CO Pollution in HTPEM Fuel Cell using Statistical Change Detection

Christian Jeppesen[a], Mogens Blanke[b,c], Fan Zhou[a], Søren Juhl Andreasen[a]

[a] *Department of Energy Technology, Aalborg University, 9220 Aalborg, Denmark (e-mail: chj@et.aau.dk)*
[b] *Department of Electrical Engineering, Technical University of Denmark, 2800 Kgs. Lyngby, Denmark, (e-mail: mb@elektro.dtu.dk)*
[c] *AMOS CoE, Institute of Technical Cybernetics, Norwegian University of Science and Technology, Trondheim, Norway*

Abstract

The fuel cell technologies are advancing and maturing for commercial markets. However proper diagnostic tools needs to be developed in order to insure reliability and durability of fuel cell systems. This paper presents a design of a data driven method to detect CO content in the anode gas of a high temperature fuel cell. In this work the fuel cell characterization is based on an experimental equivalent electrical circuit, where model parameters are mapped as a function of the load current. The designed general likelihood ratio test detection scheme detects whether a equivalent electrical circuit parameter differ from the non-faulty operation. It is proven that the general likelihood ratio test detection scheme, with a very low probability of false alarm, can detect CO content in the anode gas of the fuel cell.

Keywords: Change detection, GLRT, Fault Diagnosis, PEM Fuel Cell, HTPEM, EIS

1. Introduction

Proton exchange membrane (PEM) fuel cells have been predicted to have a promising future in applications such as auxiliary power, backup power, etc. where gasoline or diesel generators used to be the preferred electricity generator. Fuel cells are appealing in areas with high air pollution, since fuel cells can be operated without particle emissions in the exhaust gas. This is an important property since in many major cities around the world, are introducing regulations on particle emissions, such as NO_x and SO_2 etc. Fuel cells could be a solution to designing an energy system without particle emissions. [1]

The majority of commercial fuel cell applications use low temperature PEM fuel cells, which is one of the most advanced fuel cell technologies, however it often requires an advanced humidity control system for the membrane. If the membrane is too humidified the membrane will flood, and thereby reduce the gas flow. If the humidity gets too low, the membrane will dry out, and this will also reduce the performance of the fuel cell. [2]

To overcome this problem, the temperature of the fuel cell can be raised to above 100 °C. Thereby the water evaporate, and the water management is not an issue any more. To achieve this, the membrane material is changed to for example a polybenzimidazole (PBI) based polymer doped with phosphoric acid. The increase in temperature also yields a raise in electrochemical kinetic rates. This has the benefit that the fuel cell becomes more tolerant to impurities in the gas composition.
High temperature PEM (HTPEM) fuel cells are therefore often used in combination with a natural gas or methanol reformer. Reformed gas often contains CO, [3] which at too high concentrations damage the fuel cell, but can maintain normal operation at low concentrations of CO in the anode gas. It is therefore desirable to detect small concentration variations in the CO anode gas concentration.

Very little in the literature have done in the area of detecting CO in the anode gas of HTPEM fuel cells. In [4] and others the effect on the fuel cell impedance when introducing CO an CO_2 in the anode gas was investigated. In [5] the author investigates the effect of CO in the anode gas on an extended equivalent electrical circuit, where an dedicated fault element is introduced. In [6] the amount of CO was estimated by examining the fuel cell impedance at 100 Hz.

The purpose of this paper is to develop a methodology for indirect detection of CO in the anode gas, of a high temperature fuel cell. The paper first characterize normal fuel cell behavior, mainly seen through the electrical impedance of the fuel cell under non-faulty conditions and under variations in load current, and based on this, developing a equivalent electrical circuit parameter estimation as a function of the load current. Statistical properties are investigated for the non-faulty state, and based on that a generalized likelihood ratio test (GLRT) is implemented, and proven suitable for this diagnostic problem. A change detection scheme that can detect when a CO concentration in anode gas begins to reach a level, where the cell could develop non-reversible degradation

which will lead to a lifetime reduction which will require timely demanding maintenance of the fuel cell system. A detection scheme that detects a high level of CO in the anode gas could therefore shutdown the fuel cell system before it gets damaged, or change operating conditions in the hydrogen supplying reformer in order to reduce the CO contamination.

2. Fuel cell characterization and Equivalent model

For characterization of fuel cells the most popular method by far, based on the number of publications, is electrochemical impedance spectroscopy (EIS). In galvanostatic EIS a small AC current signal, of known frequency and amplitude, is applied to the fuel cell. The resulting amplitude and phase of the voltage is measured, and the experiment is repeated for a wide sweep of frequencies. From the frequency data, the impedance can be calculated, and plotted in a Bode plot or Nyquist plot. In Fig. 1 is an example of a Nyquist plot shown, where the impedance spectra for a typical PEM fuel cell with one arc, where the frequencies decrease from left to right.
Based on the impedance data, the parameters of an equivalent electric circuit (EEC) network can be fitted, and thereby the impedance data can be quantified into electric component parameters. Many different EEC have been proposed, for PEM fuel cells, and some of the have been adopted for HTPEM fuel cells as in [7]. In this paper, a simplified Randle's EEC is utilized, where only one arc is included. This is done since the impedance response of the fuel cell used in this work is rather simple. A simpler EEC also reduces the fitting time, which is convenient for online diagnostic purpose.
The EEC used in this work is shown in Fig. 1, where the impedance response for a small L_1 is shown in same figure. In order to incorporate mass transport phenomenons and the adsorption of CO in the electrochemical reaction, the capacitor in the Randle's EEC is modeled as a constant phase element (CPE). Furthermore it has been found necessary to get a suitable fit. The impedance response for a CPE, is represented as follows:

$$z_{CPE}(\omega, C_1, \alpha) = \frac{1}{C_1(j\omega)^{\alpha}} \tag{1}$$

It was proven in [8] that EEC parameter estimation can be done effectively by evolutionary optimization algorithms such as Differential evolution [9]. The Differential evolution optimization algorithm is adapted, to fit the acquired impedance data to the EEC shown in Fig 1.

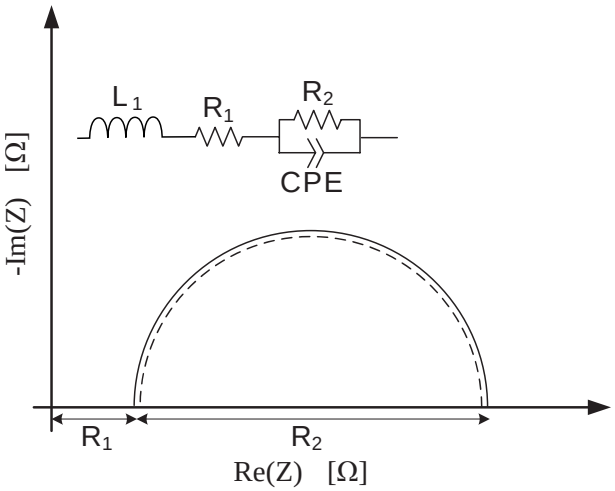

Figure 1: Nyquist plot for a HTPEM fuel cell, with corresponding equivalent model.

3. Experimental setup

The tests were conducted using a single BASF prototype Celtec P2100 HT-PEM fuel cell, designed for reformate gas. The active fuel cell area is 45 cm^2, and was operated at 160 $°C$ by electric heaters and waste heat from the fuel cell. The fuel cell was installed in a G60 800 W Greenlight fuel cell test station, where the concentration of CO in the anode gas can be controlled. The experiment set-up is shown in Fig. 2.

Before the experiment, the fuel cell was operated in a break-in procedure for 100 hr at 0.2 A/cm^2, as an activation procedure in order to achieve a state of equilibrium between the phosphorus acid and the platinum in the membrane. The break-in and the experiment was conducted by an air stoichiometry of $\lambda_{\text{air}} = 4$ and a hydrogen stoichiometry of $\lambda_{\text{H}_2} = 2.5$. The experiment was preformed at a load current of 10A.

The EIS measurements are preformed using a Gamry Reference 3000 instrument running in galvanostatic mode, in a frequency range from 10 kHz to 0.1 Hz, with 20 data points per decade. During the entire CO experiment an EIS measurement is conducted every 20 min. This is also shown in Fig. 5, where it is clearly seen that a change in voltage amplitude occurs every 20 min. This change in voltage amplitude occurs due to the overlaid small amplitude AC current. The duration of one EIS measurement is approximately 4,5 min.

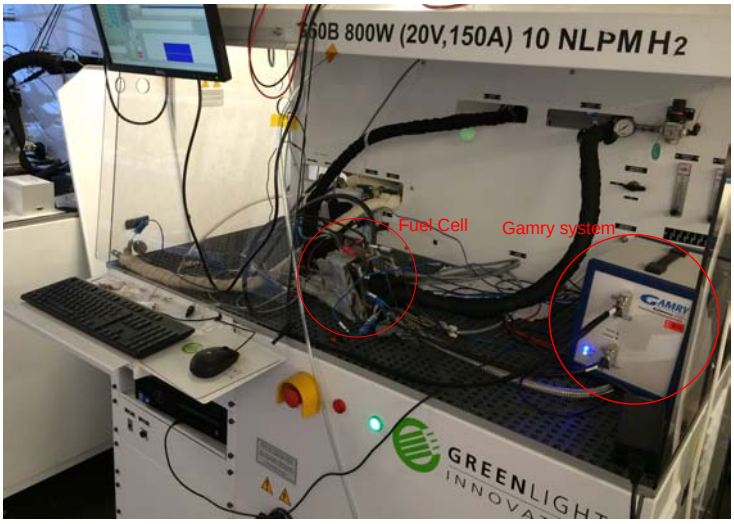

Figure 2: Test setup used for the experiment. In the left and right circle, the fuel cell assembly and the Gamry system are shown, respectively.

4. System analysis

Since the impedance is used as a model for the fuel cell, it is necessary to know how the EEC parameters vary, at different operating conditions. Their value depends on different parameters such as the current, temperature, contamination of the anode and cathode gas, etc. as shown in [7]. This is also why the EEC parameters can be used for change detection.

4.1. Experiment to characterize $\mathcal{H}_0$ conditions

This therefore requires some pre knowledge on how the EEC parameters vary, as a function on the current and temperature. However, the temperature is kept constant at all time during operation, and therefore the change in EEC parameters as a function of the temperature is neglected.
In order to map the EEC parameters as a function of the current, an experiment is conducted in order to identify this mapping. The fuel cell impedance is measured from 1 A to 4 A for 6 hours, and from 5 A to 25 A for 12 hours, with an impedance measurement every 10 minutes. This results in an 11.5 days experiment. The experiment is conducted without any CO contamination in the anode gas. The current and voltage profile is shown in Fig. 3. For every individual impedance measurement, the EEC parameters are estimated using a Differential evolution optimization algorithm. For every current set point, all the EEC parameters are averaged, giving values for each current set point.

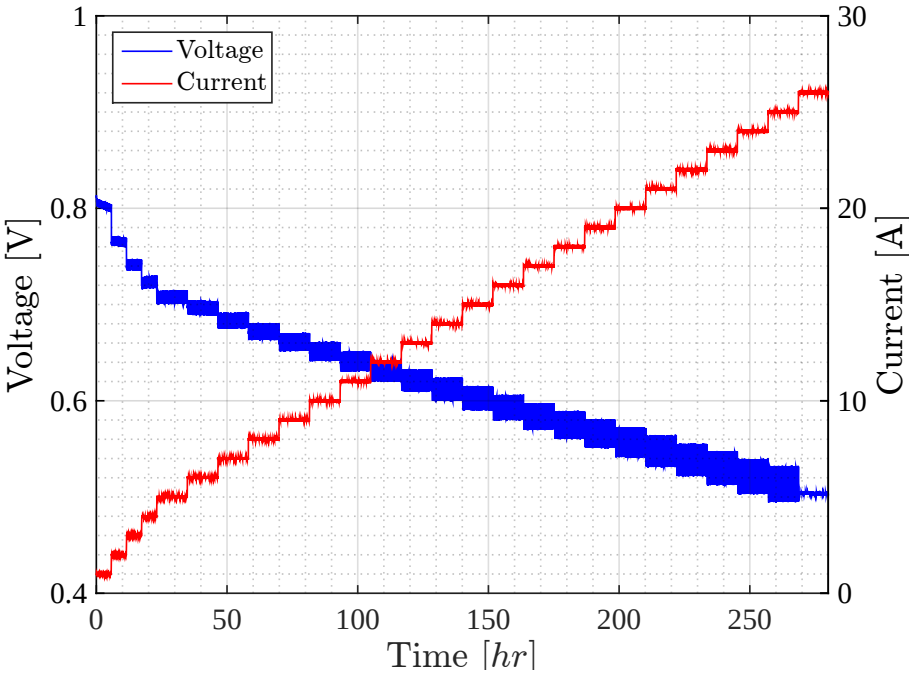

Figure 3: The voltage polarization profile from the EEC parameters mapping experiment.

The average EEC parameters is shown in Fig. 4.
The EEC parameters have a uniform variance at all set points. The mean the variance at each setpoint for R_1 is $\sigma^2_{R_1} = 1.6 \cdot 10^{-8}$, for R_2 is $\sigma^2_{R_2} = 3.5 \cdot 10^{-6}$, for C_1 is $\sigma^2_{C_1} = 2.4 \cdot 10^{-2}$, for α_1 is $\sigma^2_{\alpha_1} = 1.8 \cdot 10^{-8}$. It is therefore seen that the dispersion of R_1, R_2 and α_1 is very low, which is convenient for the application of fault detection.

The average EEC parameters in normal operation (no CO contamination in anode gas) is shown in Fig. 4, are fitted using a power function, as shown in eq. 2.

$$\{R_1, R_2, C_1, \alpha\} = a \cdot \bar{I}^{\,b} + c \tag{2}$$

The power function parameters giving the mapping between the steady state current and the EEC parameters, are listed in Table 1. For this mapping to be accurate, it is important that the current used in Eq. 2 is the steady state current. It is therefore suggested that $\bar{I}$ the average current during the

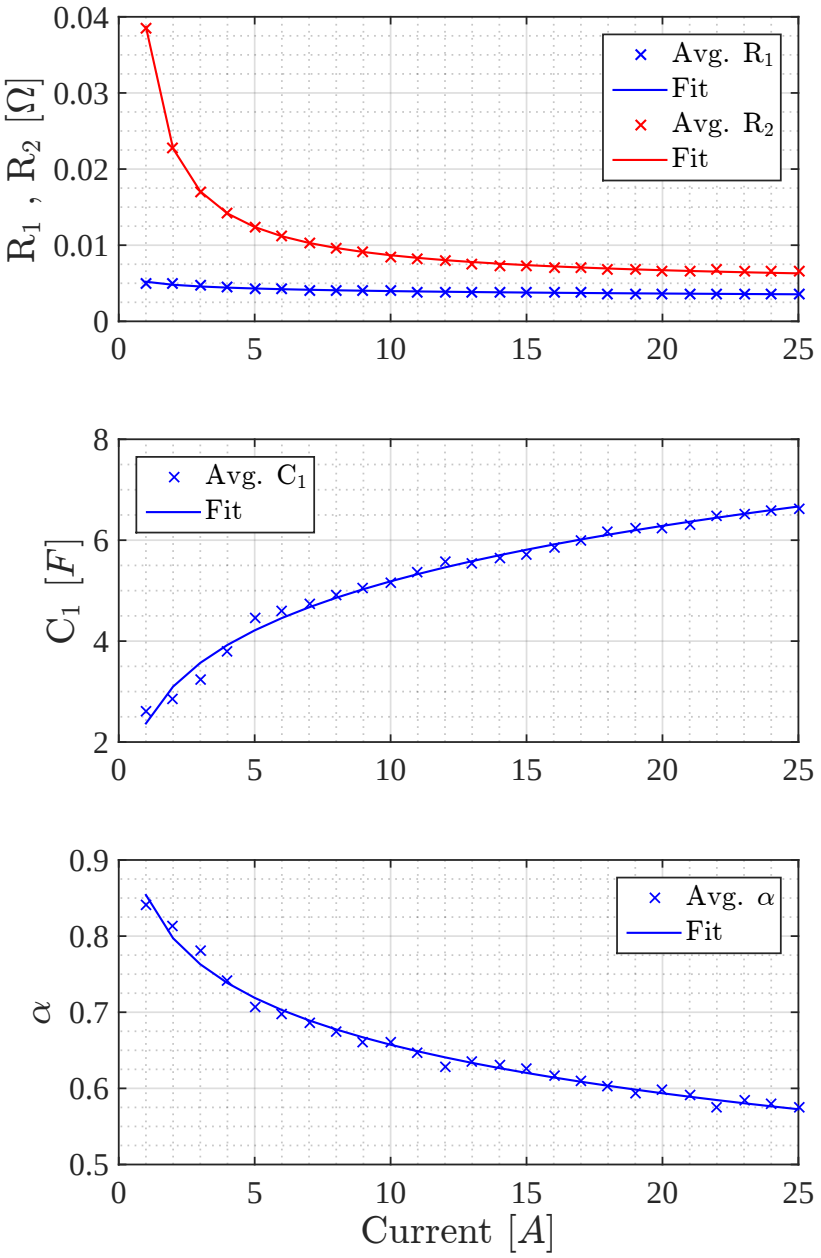

Figure 4: The EEC parameters as function of the current. The experiment is conducted at 160 °C with pure hydrogen as anode gas. $\lambda_{H_2} = 2.5$ and $\lambda_{air} = 4$.

Table 1: Parameters for the EEC model mapping as a function of the current.

	a	b	c
R_1	0.006204	-0.09585	-0.001004
R_2	0.03421	-0.9097	0.004472
C_1	5.583	0.1774	-3.215
α	-1.631	0.04947	2.485

time span of an impedance measurement, or a longer period.

4.2. Experiment to characterize $\mathcal{H}_1$ conditions

In order to obtain the statistical basis for the change detection scheme of the CO content in the anode gas, an experiment has been conducted. The fuel cell is operated 24 hours in normal operation with no CO present in the anode gas with a load of 10 A. This base test will form the basis of a statistical analysis of the non-faulty operation. In the first 24 hours, an EIS measurement will be conducted every 20 minutes, giving a total of 72 unique model parameter sets. Based on this data an estimation of a probability density function (PDF) for the non-faulty operation will be estimated.
After the first period at normal operation, a concentration of 0.5% CO will be mixed into the anode gas, and the system will operate at 10 hours, with an EIS measurement every 20 minutes. After the first period with CO mixed into the anode gas, a small period of 2 hours without CO mixed into the gas followed by a 10 hours period with 1% of CO mixed into the anode gas. In Fig. 5 the actual volume flow of CO is illustrated by the green line.
As shown in Fig. 5 the CO flow for 0.5% contamination corresponds to less that 1 $\frac{mL}{min}$ at 10 A and $\lambda_{\mathrm{H}_2} = 2.5$, which is the lower limit of the CO mass flow controller. The fuel cell can therefore not be tested at lower contamination rates.

In Fig. 5 it can clearly be seen that when CO is introduced, the fuel cell is rapidly losing performance, by means of a reduction in the cell voltage.
The change in performance can also clearly be seen in Fig. 6. The red data shows the fuel cell impedance without CO mixed into the anode gas, and the blue data shows the impedance with 0.5% CO mixed into the anode gas. It is clearly seen that by introducing CO in the anode gas, the impedance is spread. This corresponds with previously published work. [10]

The changes in EEC parameters over time are given in given in Fig. 7. The first step in CO concentration is introduced at sample nr. 74. As seen in Fig.

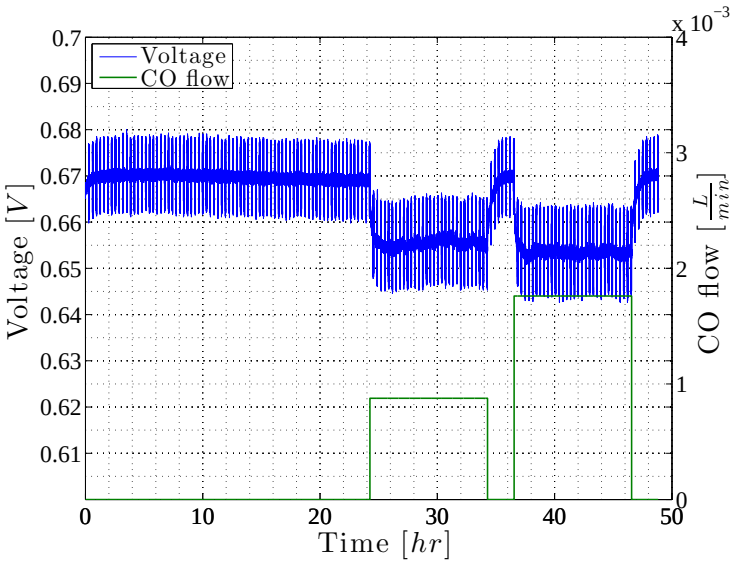

Figure 5: Fuel cell voltage during the experiment. After 24 hours 0.5% of CO in introduced in the gas, and after 36 hours 1% of CO is introduced in the gas.

7 the parameters R_2 and α indicates evident detectability, when the fault is introduced. The parameter R_1 remains constant when CO is introduced and the C_1 parameter changes when CO is introduced but with slower dynamics.
In Fig. 7 it is seen that the amplitude change for R_2 and α not is the same, for the two different CO concentrations. It can therefore be concluded, that when designing a detection scheme, for an arbitrary change in CO concentration, it have to detect a change with unknown amplitude.
Examining Fig. 7 it is seen that a detection scheme designed to detect on parameter R_2 or α will yield strong detectability of a steady injection of CO in the anode gas. The parameter R_2 is chosen to be the driving parameter in the design of the detection scheme.

The best distribution that fits the data of the parameter R_2, before the CO is introduced, is a Gaussian distribution which is shown in Fig. 8 with a red color. The Gaussian distribution is fitted to the data with a mean of $\mu_0 = 7.459 \cdot 10^{-3}$ and a variance of $\sigma^2 = 2.179 \cdot 10^{-9}$.

The best distribution that fits the data of the parameter R_2, after there is mixed 0.5 % CO into the anode gas, is a Gaussian distribution which is shown in Fig. 8 with blue color. The Gaussian distribution is fitted to the data with a mean of $\mu_0 = 9.45 \cdot 10^{-3}$ and a variance of $\sigma^2 = 0.188 \cdot 10^{-3}$. On the basis of this prior knowledge, the change detection scheme can aim to detect a change

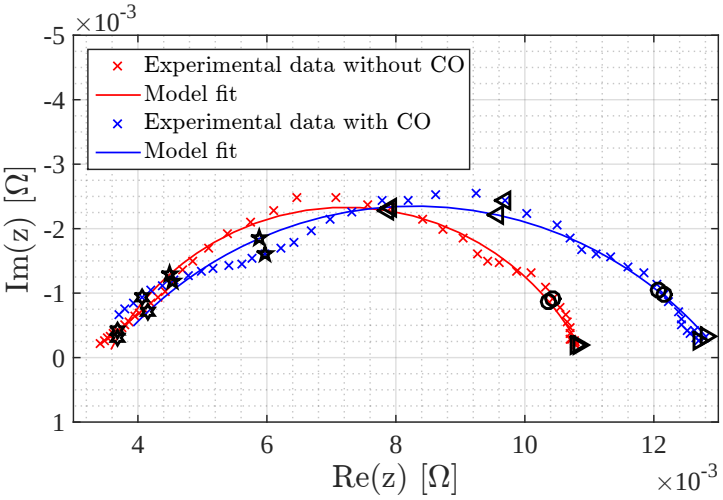

Figure 6: Impedance data and EEC model fit for operation without CO (red) and with 0.5% CO in the anode gas (blue). The markers indicate the frequency decades.

in mean with unknown amplitude.

5. Detection scheme

The statistical change detector will be designed to detect a deviation in the R_2 parameter amplitude, indicating a rise in CO concentration in the anode gas. The detector will be designed based on the experimental data. The problem can therefore be formulated as a one-sided hypothesis test, to detect a change of R_2 with an unknown amplitude, with the null hypothesis ($\mathcal{H}_0$) as the no-faulty state and the alternative hypothesis ($\mathcal{H}_1$) as the faulty state.

$$\mathcal{H}_0 : R_2 = \mu_0(\bar{I})$$
$$\mathcal{H}_1 : R_2 > \mu_0(\bar{I})$$

Since the test aims to detect a change in mean value of R_2, but with an unknown amplitude, for an unknown CO concentration, the detector will be a Composite hypothesis testing. Composite hypothesis testing without prior knowledge of the likelihood of whether or not CO pollution is present, is based on the Neumann-Pearson approach and the Generalized Likelihood Ratio Test (GLRT)is employed. [11]. When the change has unknown magnitude, the

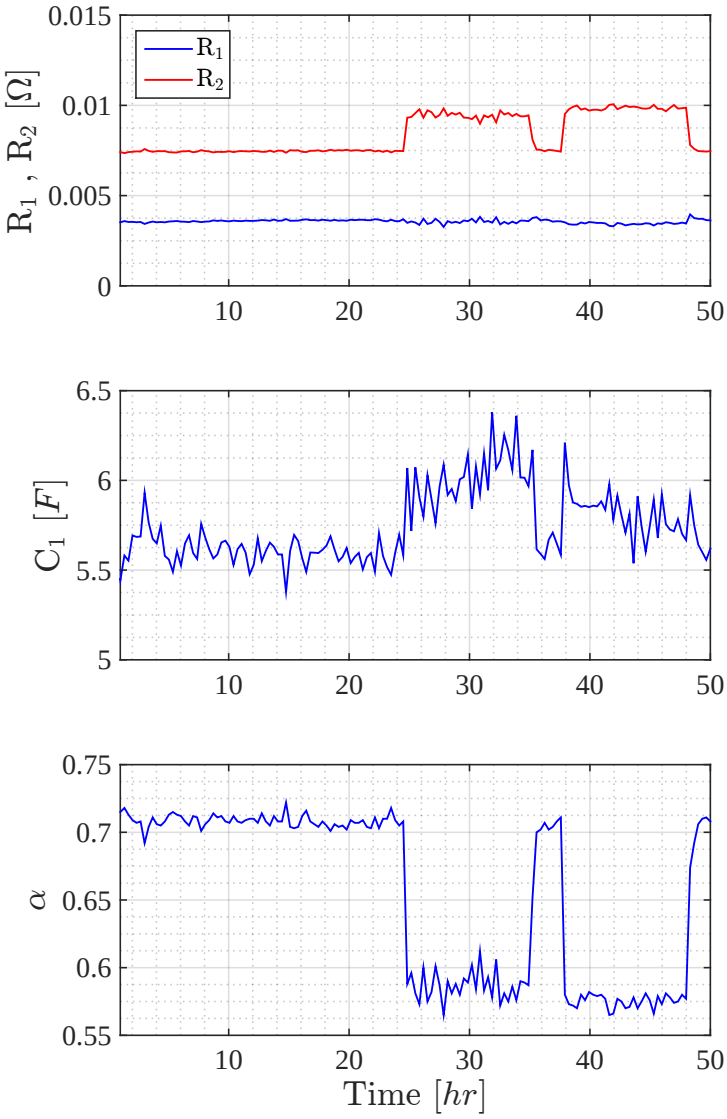

Figure 7: The EEC parameters as function of time. The experiment is conducted at 160 °C and 10 A with different CO consentrations mixed into the hydrogen. $\lambda_{H_2} = 2.5$ and $\lambda_{air} = 4$.

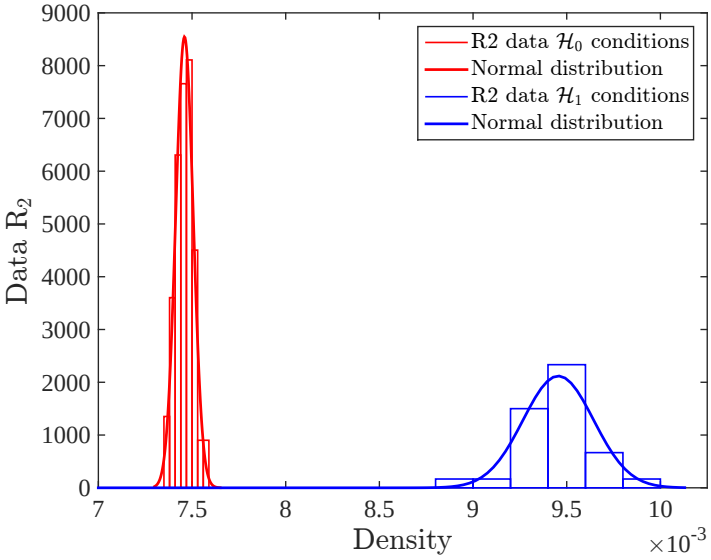

Figure 8: Histogram of the R_2 EEC parameter in non-faulty and faulty operation. The non-faulty operation R_2 data follows a normal distribution with mean of $\mu_0 = 7.459 \cdot 10^{-3}$ and a variance of $\sigma^2 = 2.179 \cdot 10^{-9}$. The faulty operation R_2 data follows a normal distribution with mean of $\mu_0 = 9.45 \cdot 10^{-3}$ and a variance of $\sigma^2 = 0.188 \cdot 10^{-3}$.

change is estimated by the GLRT using a maximum likelihood estimation (MLE) approach. Based on previous experience, it appears to preform extremely well in technical applications, even though optimality is not guaranteed for the GLRT.

The first step in the GLRT is to determine the unknown parameter, in this case the amplitude of change of resistance from $\mathcal{H}_0$ to $\mathcal{H}_1$ conditions. MLE of the amplitude in a Gaussian signal, is in [12] determined to be the mean of the signal.

The GLRT decision algorithm $g(k)$ detects a rise in the CO concentration, through monitoring of the resistance changes in the fuel cell and decides $\mathcal{H}_1$ when the $g(k)$ function becomes larger than a threshold γ. Two versions of the GLRT algorithm are tested, one is implemented as shown in Eq. 4 [13] where both change magnitude and instant of change are estimated, the other is Eq. 3, which does not estimate the most likely instant of change. In Eqs. 3 and 4 σ^2 is the variance of R_2 in the non-faulty operation, $\mu_0(\bar{I})$ is the mean value of R_2 in non-faulty operation and obtained as given in Eq. 2, where $\bar{I}$ denotes the steady state current.

The GLR test statistic for detection of a change in mean with unchanged

variance before and after the change, and a window size M, reads

$$g(k) = \frac{1}{2\sigma^2 M}\left[\sum_{i=k-M+1}^{k}\left(R_2(i) - \mu_0(\bar{I})\right)\right]^2 \tag{3}$$

A slight variation, which estimates the instant of change, and is more computation heavy, is also tested. The $g_{\mathrm{m}}(k)$ GLRT from [13] is shown in Eq. 4.

$$g_{\mathrm{m}}(k) = \frac{1}{2\sigma^2}\max_{k-M+1\leq j\leq k}\frac{1}{k-j+1}\left[\sum_{i=j}^{k}\left(R_2(i) - \mu_0(\bar{I})\right)\right]^2 \tag{4}$$

The maximization of $g(k)$ is implemented with a window of size M, as shown in Eq. 3. The window size is chosen as a balance between probability P_D to detect a change of a desired magnitude, and the delay of detection. As seen in Fig. 5, the voltage changes during 2 hours, when a CO contamination is introduced. The window size is therefore chosen to $M = 6$ corresponding to 2 hours.

The test statistic $g(k)$ is shown for the time series of the EEC parameter $\mathrm{R}_2(k)$, in Fig. 9. The red line shows the threshold (γ).

It is seen in Fig. 9 that $g_{\mathrm{m}}(k)$ given in Eq. 4 has a slightly faster detection compared with $g_(k)$, the two tests are alike outside this transient region. In praxis, therefore, since CO contamination could be imagined to be incipient, the computationally cheaper $g(k)$ could be used.

A probability plot of $g(k)$ is shown in Fig. 11 for the non-faulty $\mathcal{H}_0$ case. According to [11], the test statistics the square sum of normal distributed random variables that are independent and identically distributed (IID), should follow a χ^2_ν distribution where ν is the number of parameters being estimated. In our case, $\nu = 1$

The autocorrelation of R_2 is plotted in Fig. 10, which shows samples to be reasonably uncorrelated. However, as seen in Fig. 11 the $g(k)$ data do not follow the theoretical χ^2_1 distribution. The low number of samples in R_2 under $\mathcal{H}_0$ conditions results in a relatively high whiteness level, and the identical distribution of samples has not been experimentally verified. If more samples were available, the whiteness level would be lower, and the indication of independence would change. The test statistics $g(k)$ is therefore fitted to a exponential distribution which provides the best fit of the data, as shown in Fig. 11. The estimated parameters are shown in Table 2.

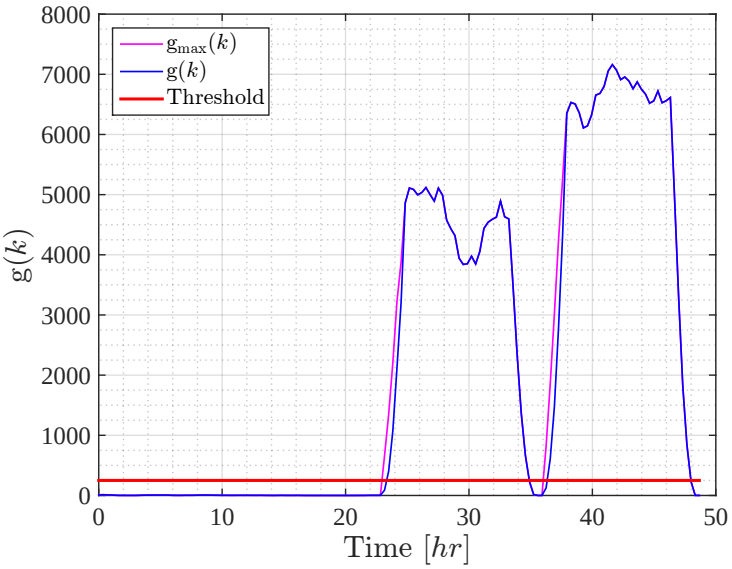

Figure 9: The GLRT decision algorithm $g(k)$ detecting a change in the mean value of R_2.

Table 2: Parameters for the probability distributions fitted to the $\mathcal{H}_0$ data in Fig. 11.

	μ_{g0}	a	b
Exponential	2.7820		
Gamma		0.7022	3.962

Table 3: Parameters for the probability distributions fitted to the $\mathcal{H}_1$ data in Fig. 12.

	a	b
Gamma	108.169	42.4392

The threshold (γ) needs to be determined to give an good balance between P_{FA} and P_{D}. The P_{FA} can be determined from the test statistics for $g(k)$ given in Fig. 11, as $P\{g > \gamma|\mathcal{H}_0\}$. The threshold ($\gamma$) is determined by the right tail area of the exponential density function, see [11] for theoretical results and [14] for discussion of various real-life issues.

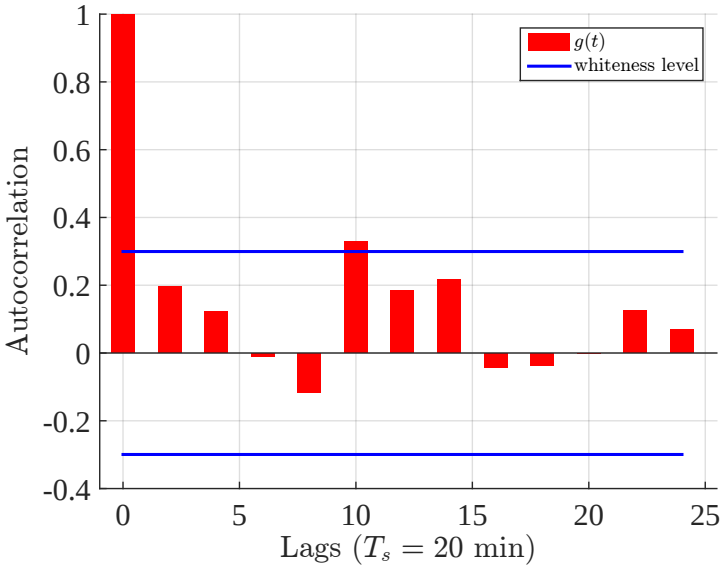

Figure 10: Autocorrelation for the EEC parameter R_2 under $\mathcal{H}_0$ conditions.

$$P_{\text{FA}} = P\{g > \gamma|\mathcal{H}_0\} \tag{5}$$

$$= \int_{\gamma}^{\infty} P\{g > \gamma|\mathcal{H}_0\}\mathrm{d}g \tag{6}$$

$$= \int_{\gamma}^{\infty} \frac{1}{\mu_{g0}} \exp\left(-\frac{1}{\mu_{g0}} \cdot g\right) \mathrm{d}g \tag{7}$$

$$= \exp\left(-\frac{\gamma}{\mu_{g0}}\right) \Leftrightarrow \tag{8}$$

$$\ln\left(P_{\text{FA}}\right) = \frac{-\gamma}{\mu_{g0}} \Leftrightarrow \tag{9}$$

$$\gamma = -\mu_{g0} \ln\left(P_{\text{FA}}\right) \tag{10}$$

Designing for an extremely low $P_{FA} = 10^{-39}$, gives $\gamma = 250$. This results in a good detection probability but at the same time a negligible probability of false detection. This is due to a very strong sensitivity of the R_2 parameter to CO contamination and due to low variance on .

A probability plot of $g(k)$ for the faulty $\mathcal{H}_1$ conditions is shown in Fig. 12 with a Gamma distribution fittet to the data. Furthermore the threshold (γ) is shown in Fig. 12 by a red line. It is clearly seen that the probability of detection is very high, and in practice the probability of detection will be

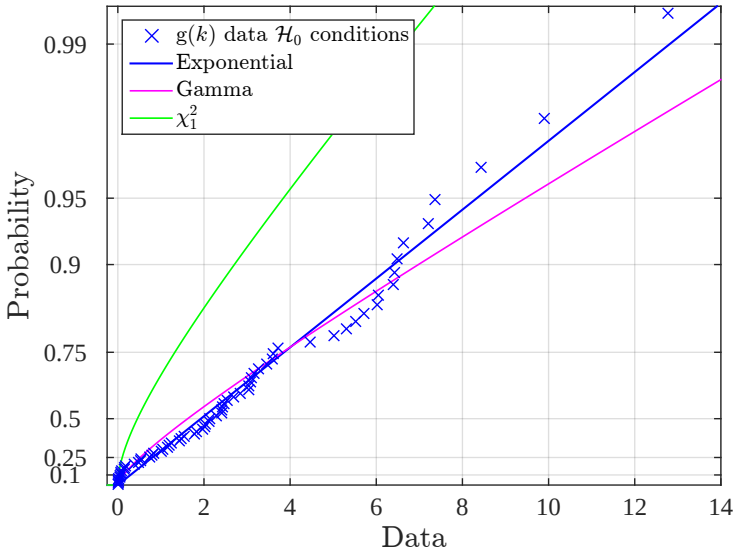

Figure 11: Probability plot of the data for $g(k)$ compared to different distributions, for $\mathcal{H}_0$ conditions.

$P_D \approx 1$. A probability of detection of $P_D \approx 1$ indicates that lower rates of CO contamination can be detected.

6. Discussion

This method indicates a strong detectability for CO contamination in the anode gas of a HTPEM fuel cell. The method does not take into account that the fuel cell impedance is changing with catalyst degradation and other degradation mechanisms. Furthermore the fuel cell impedance is dependent on different operating conditions such as the current, temperature, contamination of the anode and cathode gas, etc. as shown in [4]. This method takes the change in current into account and is neglecting other operating conditions. As stated in this paper the temperature is kept constant during all operation, however in practice this is hard to accomplish. Small temperature variations of the fuel cell will the detection scheme be robust toward, since around the temperature set point is the cell impedance only varying within small limits. [7] It is suggested to be investigated further what effect the degradation and change in other operating conditions will have on the EEC parameters, so the mapping of the EEC parameters done in Fig. 4, can be expanded if necessary to take these phenomena into account.
The fault is introduced as step in the CO gas flow. In real life the introduction

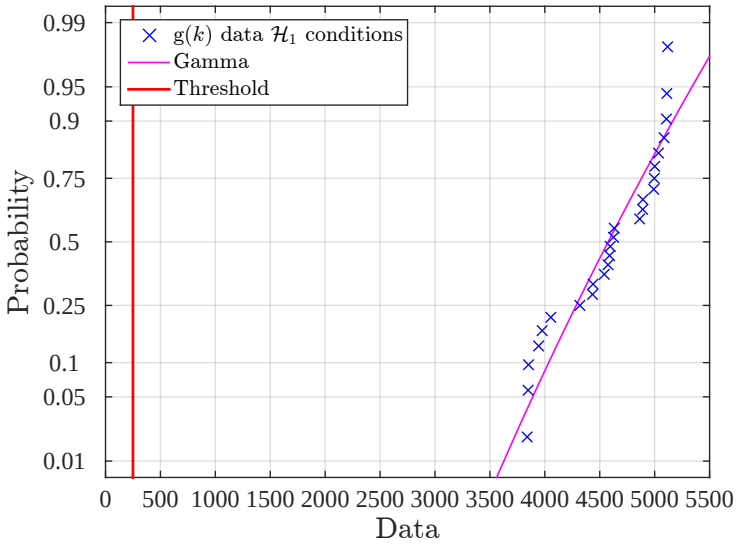

Figure 12: Probability plot of the $g(k)$ data for $\mathcal{H}_1$ conditions of 1% CO contamination fitted to a Gamma distribution. The red line shows the threshold ($\gamma = 250$).

of CO will happen with some dynamic and therefore not as a step. However the GLRT detection scheme detects a change in the amplitude of the R_2 parameter and can therefore also detect incipient faults.

7. Conclusion

This paper has shown design and empirical verification of a detection scheme to diagnose CO contamination in the anode gas of a high temperature PEM fuel cell. The data was experimentally determined impedance that was used to estimate parameters in an electrical equivalence model. The equivalence circuit was a simplified Randle's circuit, which was found sufficient for the purpose. A differential evolution optimization method was used to fit impedance data to the electrical equivalent circuit model. The method that uses the change in impedance as a function of varying load current was found effective for the purpose. A generalized likelihood ratio change detection test was designed to detect possible CO contamination. The method showed very high detectability for the 0.5% CO concentration used in experiments, with a negligible probability of false alarms. The detection method promise very high sensitivity of contamination. Further investigation of the change in impedance as function of fuel cell degradation and other impedance dependencies, and also effects of

contamination with other than CO need be investigated before the method could be implemented in full scale applications.

References

[1] M. W. Ellis, M. R. V. Spakovsky, D. J. Nelson, Fuel cell systems: Efficient, flexible energy conversion for the 21st century, Proc. of the IEEE 89 (12) (2001) 1808–1818.

[2] O. Lottin, B. Antoine, T. Colinart, S. Didierjean, G. Maranzana, C. Moyne, J. Ramousse, Modelling of the operation of polymer exchange membrane fuel cells in the presence of electrodes flooding, International Journal of Thermal Sciences 48 (2009) 133–145.

[3] K. K. Justesen, S. J. Andreasen, H. R. Shaker, M. P. Ehmsen, J. Andersen, Gas composition modeling in a reformed methanol fuel cell system using adaptive neuro-fuzzy inference systems, International Journal of Hydrogen Energy 38 (2013) 10577–10584.

[4] S. J. Andreasen, J. R. Vang, S. K. Kær, High temperature pem fuel cell performance with co and co2 using electrochemical impedance spectroscopy, International journal of hydrogen energy 36 (2011) 9815–9830.

[5] C. Beer, P. Barendse, P. Pillay, B. Bullecks, R. Rengaswamy, Electrical circuit analysis of co poisoning in high temperature pem fuel cells for rapid fault diagnostics, in: Energy Conversion Congress and Exposition (ECCE), 2013 IEEE, 2013, pp. 4623–4630.

[6] H.-C. B. Jensen, S. J. Andreasen, S. K. Kær, E. Schaltz, Estimation of co concentration in high temperature pem fuel cells using electrochemical impedance, Proceedings of the 5th International Conference on Fundamentals and Development of Fuel Cells.

[7] S. J. Andreasen, J. L. Jespersen, E. Schaltz, S. K. Kær, Characterisation and modelling of a high temperature pem fuel cell stack using electrochemical impedance spectroscopy, Fuel Cells (2009) 463–473.

[8] G. Yang, Battery parameteriastion based on differential evolution via boundary evolution strategy, International Journal Power Sources 245 (2014) 583–593.

[9] R. Storn, K. Price, Differential evolution - a simple and efficient heuristic for global optimization over continuous spaces, Journal of Global Optimization 11 (1997) 341–359.

[10] S. S. Araya, S. J. Andreasen, S. K. Kær, Experimental characterization of the poisoning effects of methanol-based reformate impurities on a pbi-based high temperature pem fuel cell, Energies 5 (2012) 4251–4267.

[11] S. M. Kay, Fundamentals of Statistical Signal Processing - Volume II Detection Theory, Prentice Hall, 1998.

[12] S. M. Kay, Fundamentals of Statistical Signal Processing - Volume I Estimation Theory, Prentice Hall PTR, 1993.

[13] M. Blanke, M. Kinnaert, J. Lunze, M. Staroswiecki, Diagnosis and Fault-Tolerant Control, 2^{nd} Edition, Springer, 2006.

[14] M. Blanke, S. Fang, R. Galeazzi, B. J. Leira, Statistical change detection for diagnosis of buoyancy element defects on moored floating vessels, in: Proc. IFAC Safeprocess 2012, Mexico, 2012, pp. 462–467.

Paper D

Fault Detection and Isolation of High Temperature Proton Exchange Membrane Fuel Cell Stack under the Influence of Degradation

Christian Jeppesen, Samuel Simon Araya, Simon Lennart Sahlin, Sobi Thomas, Søren Juhl Andreasen, Søren Knudsen Kær

The paper has been submitted to the
Journal Power Sources

Fault Detection and Isolation of High Temperature Proton Exchange Membrane Fuel Cell Stack under the Influence of Degradation

Christian Jeppesen[a,*], Samuel Simon Araya[a], Simon Lennart Sahlin[a], Sobi Thomas[a], Søren Juhl Andreasen[b], Søren Knudsen Kær[a]

[a]*Department of Energy Technology, Aalborg University, Pontoppidanstræde 101, 9220 Aalborg Ø, Denmark*
[b]*Serenergy A/S, Lyngvej 8, 9000 Aalborg, Denmark*

Abstract

This study proposes a data-drive impedance-based methodology for fault detection and isolation of low and high cathode stoichiometry, high CO concentration in the anode gas, high methanol vapour concentrations in the anode gas and low anode stoichiometry. The fault detection and isolation algorithm is based on an artificial neural network classifier, which uses three extracted features as input. Two of the proposed features are based on angles in the impedance spectrum, and are therefore relative to specific points, and independent of degradation. The experimental data is based on a 35 day experiment, where 2010 unique electrochemical impedance spectroscopy measurements were recorded. The test of the algorithm resulted in a good detectability of the faults, except for high methanol vapour concentration in the anode gas fault, which was found to be difficult to distinguish from a normal operational data. The achieved accuracy for faults related to CO pollution, anode- and cathode stoichiometry is 100 % success rate. Overall global accuracy on the test data is 94.6 %.

Keywords: Fault diagnosis, Classification, Pattern recognition, Fuel Cell, PEM, Electrochemical impedance spectroscopy (EIS)

1. Introduction

In the transition from fossil fuel powered electrical grid to a renewable energy supplied electrical grid, many fluctuating energy sources such as solar

*Corresponding author
Email address: chj@et.aau.dk (Christian Jeppesen)
URL: http://et.aau.dk (Christian Jeppesen)

and wind has been adapted. Since the renewable energy sources are fluctuating, energy storage technologies are needed, and here hydrogen could play a role, both for transport and stationary applications [1, 2, 3, 4, 5].

Hydrogen storage uses electrolyzers to produces hydrogen from the excess energy in the electrical grid, and when electrical production from renewable energy sources are low the hydrogen is feed into fuel cells, which produce electrical energy. The most common type of fuel cells are proton exchange membrane (PEM) fuel cells, which operate between 60-100 °C with Nafion® as membrane conductor. These fuel cells require high purity of the hydrogen supplied to the fuel cell. An alternative to PEM fuel cells are high temperature proton exchange membrane (HTPEM) fuel cells, which operate between 150-200 °C with phosphoric acid-doped polybenzimidazole (PBI) as membrane conductor [6]. The advantage of HTPEM fuel cells is that they are more tolerant towards impurities in the anode gas, without a gas purification system [7]. The HTPEM fuel cells can thereby be deployed with a methanol reformer system, which is an environmental friendly technology, given the methanol is produced based on renewable hydrogen [8].

Hydrogen storage technologies are expensive and some of the most important factors for commercial success are reliability, cost and durability. The American Department of Energy (DoE) has set ambitious minimum targets for the lifetime of fuel cell applications, meaning 40,000 h for stationary and 5,000 h for automotive, before degrading to 80 % of rated power [9].

One of the ways to improve fuel cell reliability and durability is a well-designed on-line diagnostics scheme, which can detect faults on the fuel cell and with a mitigation strategy impede fault factors before the fuel cell degradation is accelerated [10, 11].

On-line diagnostic algorithms are usually divided into model based [12] and non-model based [13] methods. Common for these are that they are divided into fuel cell characterization, feature extraction and change detection. For the non-model based methods, the change detection part is often conducted by a machine learning method. Common for many of these diagnostics methods are that the fuel cell characterization often is done by electrochemical impedance spectroscopy (EIS) [12, 13], which has the main advantage that it can be done in-situ at low energy cost [10]. When using EIS as fuel cell characterization technique, the model based methods utilize the parameters of an electrical equivalent circuit (EEC) as features [14, 15, 16]. For the non-model based methods, using EIS as fuel cell characterization method, often uses parts of the impedance spectrum as features for fault detection [17, 18, 19].

The above methods are manly applied on PEM fuel cells and most of them focus on detecting flooding and drying. When moving to HTPEM fuel cells the water management issue are no longer present since they are operated above 100 °C, but alternative faults arises when deployed with a hydrocarbon or alcohol-based fuel reformer, such as detecting impurities in the anode gas. Such faults have been addressed in the literature by model based methods using EIS as fuel cell characterization method, and EEC model parameters as features [20, 21]. However, non-model based fault diagnostics method for HTPEM fuel cells have not been investigated yet.

It is a well-established fact in the literature, that the impedance spectrum spread during normal degradation which applies to both the high- and the low-frequency intersect with the real axis. This complies for both PEM fuel cells [22, 23] and HTPEM fuel cells [24]. In the work by Hissel et al. [25] life time EIS data from two different fuel cell stacks, were used to design a fuzzy-clustering algorithm to determine the type of ageing. However, to date there are no fault detecting algorithms for fuel cells, which is robust towards the change in the impedance spectrum due to degradation.

In this work, an impedance data driven non-model based fault detection and isolation (FDI) method has been described. The method is used for the detection of five different faults, which commonly occur on a HTPEM fuel cell methanol reformer system. Furthermore, the described method is independent of the fuel cell degradation.

The paper is structured as follows:
In section 2 the experimental setup and the experimental procedure will be presented. In section 3, the feature extraction and the diagnostic algorithm will be explained. The results will be presented and discussed in section 4. Finally the concluding remarks will be made in section 5.

2. Experimental data foundation

Since the FDI method presented in this work is data-driven, a fuel cell database both in healthy and faulty conditions is necessary. Therefore, tests have been conducted on a short HTPEM fuel cell stack, where real life situations were emulated using a GreenLight Innovation fuel cell test station. The test matrix was based on the operating parameters and conditions of a methanol reformer-HTPEM fuel cell systems, such as the SerEnergy H3-5000 fuel cell

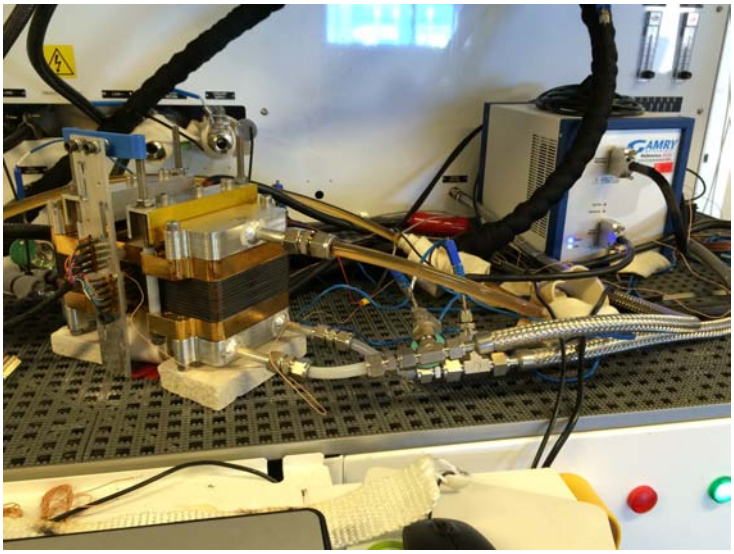

Figure 1: On the right the Gamry Reference 3000 instrument used for impedance measurements is shown. On the left the 10 cell short-stack used for the experimental work is shown. The stack is installed in a GreenLight G200 fuel cell test station, fuel cell faults can be emulated.

system, for healthy and non-healthy operations. The fuel cell stack used for this work is a 10 cell SerEnergy short stack, shown in Figure 1.

As stated in the introduction, EIS will be utilized as fuel cell characterization technique, which is well described in the literature, and is a powerfull characterization technique for fault detection of fuel cells [10, 26]. An electrochemical device such as a fuel cell is a highly non-linear system, and a full mechanistic impedance model based on first principles are very complex. EIS is therefore often used as an empirical linearization of the fuel cell, where a sinusoidal signal is superimposed to the DC value, and by measuring the responding signal, the amplitude ratio and the phase shift can be determined and on that basis the impedance can be calculated. This is typically done in galvanostatic mode in fuel cells, where a small AC current perturbation is induced on the DC current load and the voltage response is measured. By sweeping over the desired frequency range, the full impedance spectrum can be determined. The drawback of this method is that the impedance is only valid at one operating point, and therefore, EIS measurements at all the operational points of interest are needed.

Since one of the scopes of this work is designing a FDI algorithm, which is robust toward degradation, the experimental work needs to ensure a large

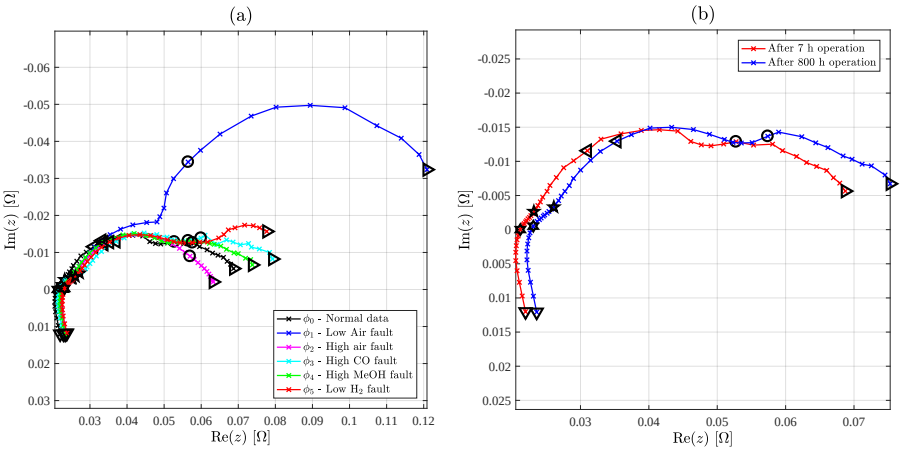

Figure 2: **(a)** Impedance spectra for the 5 different faults considered in this work and normal operation impedance spectra for reference. Impedance spectra measured at 16.5 A. **(b)** Impedance spectra at normal operation conditions, from beginning of experiment and end of experiment. Impedance spectra measured at 16.5 A.

amount of healthy data for determining how the impedance changes during degradation.

2.1. Considered faults

In this work five different conditions identified as abnormal fuel cell operation, are considered as faults (ϕ_1-ϕ_5) and listed in Table 1.

When fuel cell systems are deployed in the field, the cathode oxygen is normally supplied by a fan or a compressor, from the surrounding air. It is desired to be able to detect and isolate faults related to the air delivery system, which can be divided into two different cases:

ϕ_1 A decrease in cathode stoichiometry (λ_{Air}). This could be due to a faulty fan/compressor or that the deployed systems is at high altitude.

ϕ_2 An increase in cathode stoichiometry (λ_{Air}). This could be due to a change in fan/compressor characteristics or a software error.

The advantage of HTPEM fuel cells is that they are more tolerant toward impurities in the anode gas, due to the faster kinetics at higher temperatures. HTPEM fuel cells can therefore be deployed in combination with a reformer, such as a methanol reformer, without a gas purification system. However, this requires that the reformer is in nominal operation. If the reformer differs from normal operation or the reformer goes into faulty operation, three different effects can occur:

Table 1: Overview of the faults considered. The faults are investigated for the fuel cell current set points 16.5, 24.75, 33, 41.25, 49.5 A with 6 EIS measurements for each fault at each current set point.

Nr.	**Fault**	**Normal**	**Abnormal**
ϕ_1	Low λ_{Air}	2.5 [-]	1.5 [-]
ϕ_2	High λ_{Air}	2.5 [-]	4 [-]
ϕ_3	High CO	0.5 % Vol.	2.5 % Vol.
ϕ_4	High MeOH vapor	0 % Vol.	5 % Vol.
ϕ_5	Low λ_{H_2}	1.4 [-]	1.15 [-]

ϕ_3 The anode gas content of carbon monoxide increases from the normal level. This could be due to a change in the temperature profile of the reformer, or a fault on the reformer catalyst.

ϕ_4 Methanol vapour content in the anode gas appears, which could be due to a change in the temperature profile of the reformer, or a fault on the reformer catalyst. Alternatively, it could be due to more methanol delivered by the methanol pump than expected or a fault on the methanol evaporation system.

ϕ_5 A decrease in the anode stoichiometry (λ_{H_2}). This could be due to a decrease in methanol delivered by the methanol pump or due to a fault on the reformer catalyst.

The impedance spectrum for each of the five faults and the normal operation impedance (black), is shown on Figure 2.a. The data shown is from the experiment described in the next section. It can be seen, that the low air fault (ϕ_1), yields the most significant change in the impedance spectrum, and that during the high air fault (ϕ_2), the low frequency arch disappears. Additionally, it can be seen that the high CO content fault (ϕ_3) and the low hydrogen stoichiometry fault (ϕ_5) increases the low frequency arch. Further, it can be observed that the high content of methanol fault (ϕ_4) is quite close to the normal operational data (ϕ_0).

2.2. Experimental procedure

The experiments for this work is conducted on a 10-cell short stack, based on standard flow plates and MEA's from a SerEnergy S165L stack, with a cell active area of 165 cm^2. The stack is installed in a GreenLight fuel cell test station, and shown on Figure 1, where the Air, H_2, CO and CO_2 gas flows can

be controlled by mass flow controllers. The methanol vapour delivery systems is based on a liquid HPLC pump and a heat exchanger.

Before the experiment, the fuel cell short stack was operated in a break-in procedure as suggested by Vang et al. [27]. The short stack break-in duration was 100 h at 33 A (0.2 A cm^{-2}), with λ_{Air}=4 and λ_{H_2}=2.

The experiment duration is 35 days, where each day is structured as shown on Figure 3.a. During the first 6 h and aprox. the last 8 h of each day, the stack is operated at 82.5 A, which corresponds to 0.5 Acm^{-2}. After the first 6 h of operation the fuel cell characterization is scheduled at 16.5 A (0.1 Acm^{-2}), 24.75 A (0.15 Acm^{-2}), 33 A (0.2 Acm^{-2}), 41.25 A (0.25 Acm^{-2}) and 49.5 A (0.3 Acm^{-2}). 12 EIS measurements were conducted at each current set point. This procedure is repeated every day, except for day 14, 21, 28 and 35, where a faulty condition is introduced. The same current set points are repeated for each faulty operation, with 6 EIS measurements at each current set point. An overview of the number of EIS measurements is given in Table 2.

On day 14 the low air stoichiometry, fault (ϕ_1) and high air stoichiometry, fault (ϕ_2) were induced; on day 21 high content of CO was introduced in the anode gas, fault (ϕ_3); on day 28 high content of MeOH vapour was introduced in the anode gas, fault (ϕ_4) and on day 35 the low anode stoichiometry, fault (ϕ_5) is induced.

The overview of the fuel cell stack voltage and current for the entire experiment is given in Figure 3.b.

2.2.1. Gas composition

The anode gas composition is based on experience with a H3-5000 SerEnergy methanol reformer. Hydrogen fraction is kept constant at 75 % by volume, and for normal days the CO content is kept at 0.5 % by volume. CO_2 is used as a fill gas, meaning that at normal days the CO_2 fraction is kept at 24.5 % by volume of the total anode gas flow, and at abnormal days the CO_2 fraction is kept lower. The stoichiometric ratios are kept at λ_{Air}=2.5 and λ_{H_2}=1.4 during the experiment, except for day 14 and day 35, where they are changed accordingly to Table 1.

2.2.2. Gas humidification

The anode gas is humidified by mean of a bubbler, with a dew point temperature of 49 °C. This corresponds the anode gas water content, for the output gas of a methanol steam reformer operating with a fuel steam to carbon ration of 1.5. A mass flow controller supplies the cathode gas, from oil free air compressor.

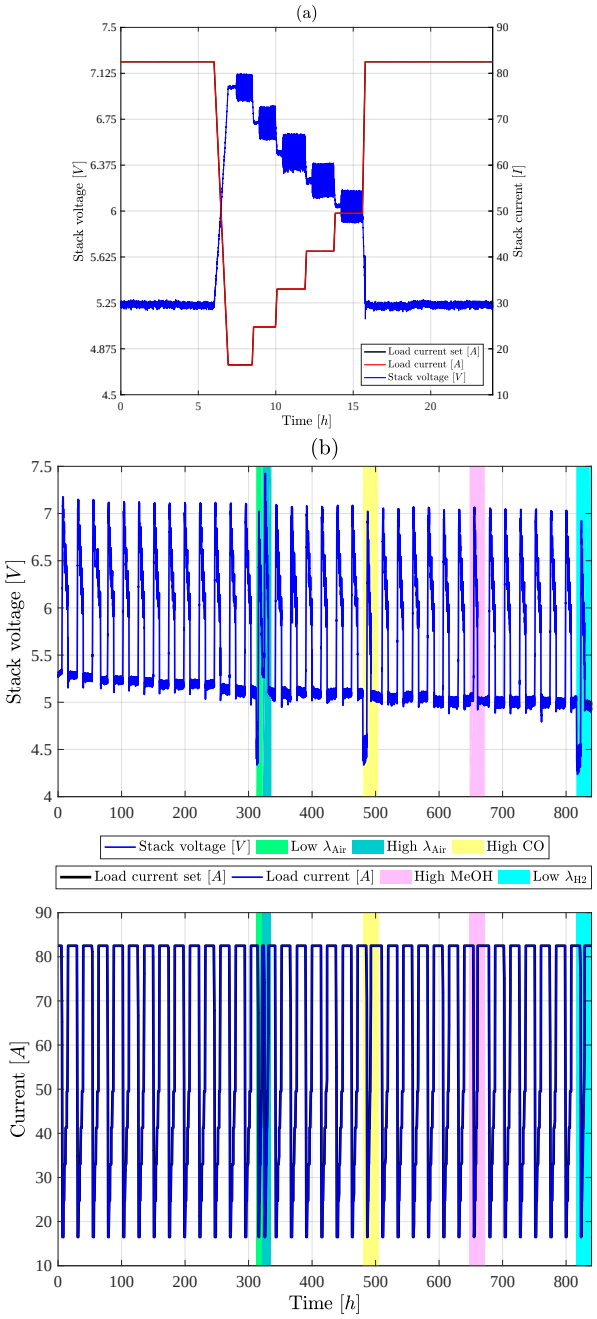

Figure 3: **(a)** Stack voltage and current during a day with normal operating conditions. During the characterization 12 EIS measurements is acquired at each current set point. **(b)** Fuel cell stack voltage and current during the entire 810 h experiment, corresponding to 35 days of operation.

Table 2: Overview of the set points during the fuel cell characterization experiment.

	No. of EIS
Nr. at each normal current set point	12
Nr. at each abnormal current set point	6
Total at Normal day	60
Total at Abnormal day	30
Total experiment	2010

2.2.3. Temperature

The short stack of subject in this work is oil heated and cooled by an external cooling cart using Paratherm oil, in a closed circuit. The temperature controller is set to keep a fuel cell output temperature of 167 °C throughout the entire experiment. When changing current set point, a current ramp of 0.05 As^{-1} is applied to ensure minimum temperature variation. Furthermore, a 20 min delay without any temperature deviations of more than 0.5 °C is performed, before any EIS measurement is conducted.

2.2.4. EIS measurements

For EIS measurements a Gamry Reference 3000, running in galvanostatic mode is utilized. The AC current amplitude is set to 7.5 % of current DC value, as recommended by Dale et al. [28], however, with a maximum of ±3 A due to instrumental limitation. The starting frequency is 10 kHz and the end frequency is 0.1 Hz with 10 points pr. decade, divided into logarithmic intervals. In Table 2 the number of EIS measurements at each current set point and at each day are listed.

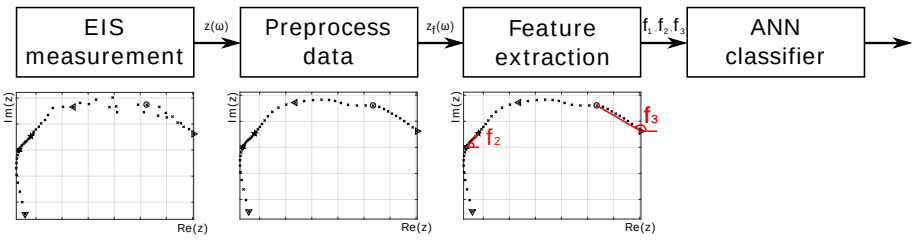

Figure 4: Flow chart of the proposed artificial neural network fault detection and isolation methodology.

3. FDI Algorithm

As seen in Figure 2.b, the impedance spectrum changes due to degradation. The impedance spectrum spreads and moves to the right during degradation, which manifest itself by an increase in the series resistance (the first intersect with the real axis), and more significantly expressed by an increasing real part of the low frequency part of the spectrum. Thus, it is evident that an impedance based FDI algorithm for fuel cell applications needs to be robust towards degradation.

In this work, a feedforward artificial neural network (ANN) classifier fault detection and isolation (FDI) methodology is proposed, for detecting the faults listed in Table 1. The principle of the methodology is illustrated in Figure 4, where the four different steps are listed. This is a supervised machine learning approach, and therefore the 2010 EIS measurements, from the experiment described in section 2.2, needs to be labeled with the 6 different cases (ϕ_0-ϕ_5), prior to the training, validation and testing of the ANN classifier.

The proposed FDI methodology initially takes a real time EIS measurement from a deployed fuel cell system, runs the acquired impedance spectrum through a pre-processing layer, which will be described in section 3.1. Hereafter three selected features will be calculated based on section 3.2, which are used as input to the ANN classifier algorithm. The ANN classifier algorithm which is trained is explained in section 3.3.

3.1. Data pre-processing

After the EIS measurement is acquired, a pre-processing step of the methodology is applied. The purpose of this step is to prepare the impedance spectrum for the feature calculation. Some of the EIS measurements, especially at higher currents are slightly noisy, for the low frequencies. The primarily reason for this, is the ± 3 A current limit of the Gamry galvanostat used for the experimental characterization. This makes the relative AC current amplitude smaller compared to the DC component of the fuel cell current, and thereby decreasing the signal to noise ratio. The impedance spectrum is therefore filtered, for noise rejection.

The filter used in the pre-processing step is a zero phase butterworth filter, by filtering the impedance spectrum in both forward and reverse direction [29], going from high to low and again back to high frequency. Two examples can be seen in Figure 5.a, where a low noise spectrum can be seen (red) and a high

noise spectrum (magenta). For the low noise spectrum it can be observed that the phase between the unfiltered and the filtered data is low, and for the high noise spectrum it can be noted that the filter rejects the noisy measurement points.

3.2. Feature extraction/selection

For dimensional reduction of the measurements space, for FDI algorithms for fuel cell applications using EIS as characterization, there are in general two different approaches, feature extraction or feature selection.

Feature selection is preformed, by directly choosing k of the d dimensions which yield the most information needed for the fault classification, where d is the dimension of the measurements space [18, 30]. Alternatively, k features can be calculated based on the measurement space, as a feature extraction. Some of the most common dimensional reduction methods described in machine learning literature are statistically based methods such as principal component analysis and linear discriminant analysis [13, 30]. Alternatively, feature extraction can be performed by fitting an electrical equivalent circuit to the impedance spectrum, and using the parameters as features [20, 31], mathematically representing the impedance spectrum by more generic model, or extracting features which are based on knowledge of the fault nature.

This work will be based on simple knowledge based feature extraction. In Figure 5.b, a typically impedance spectrum is illustrated, with the four (a-d) typically knowledge based features found in the literature. The four features are listed here:

(a) The internal series resistance, often extracted as the value of the first intersect with the real axis [17]

(b) The difference between the internal resistance and the real part of the second intersect with the real axis, or put differently, the span of the impedance spectrum [19, 25].

(c) The second intersect with the real axis, sometimes denoted as the polarizing resistance or just the maximum amplitude of the impedance spectrum [19, 32].

(d) The maximum angle of the impedance spectrum [17, 32] or the frequency at the maximum angle [19].

The features (a-d), which are shown in Figure 5 and listed above, are often used for detecting flooding and drying of low temperature PEM fuel cells. The

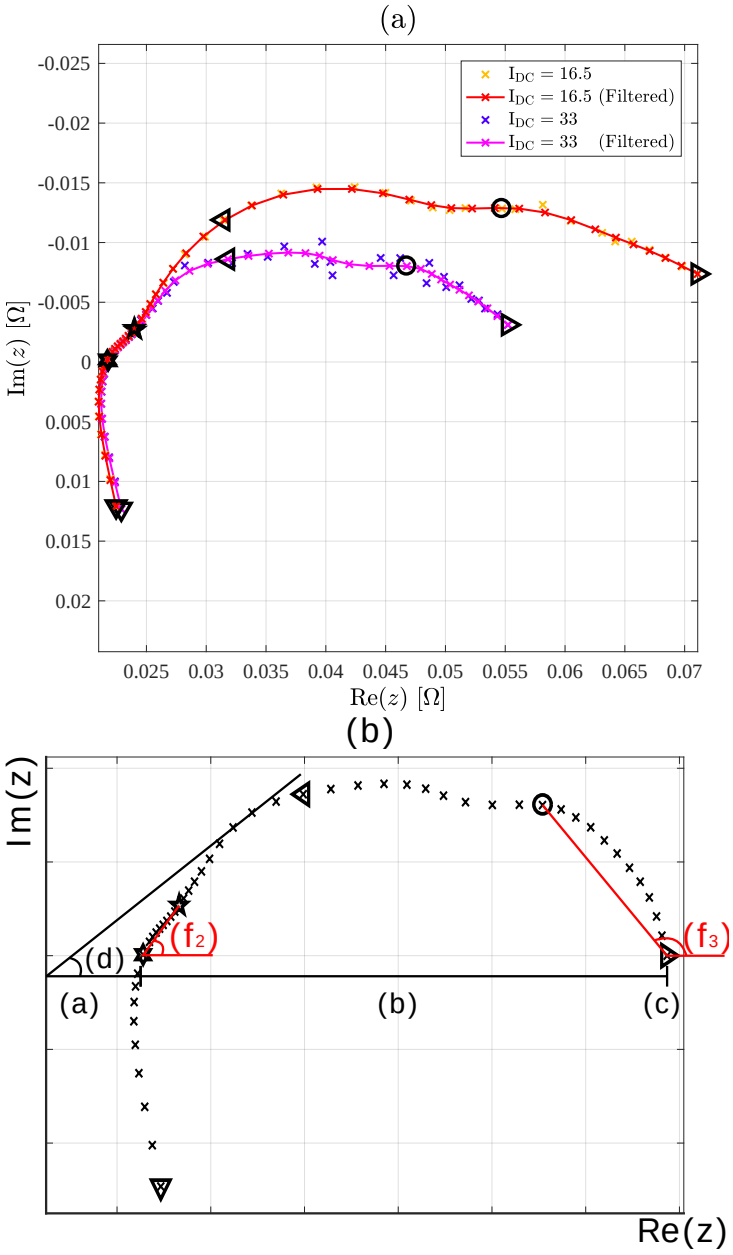

Figure 5: **(a)** Impedance spectra for 16.5 and 33 A at day 2, before and after preprocessing. **(b)** Typically features found in the literature ((a)-(d)) and the two features (f_2 , f_3) used for this work.

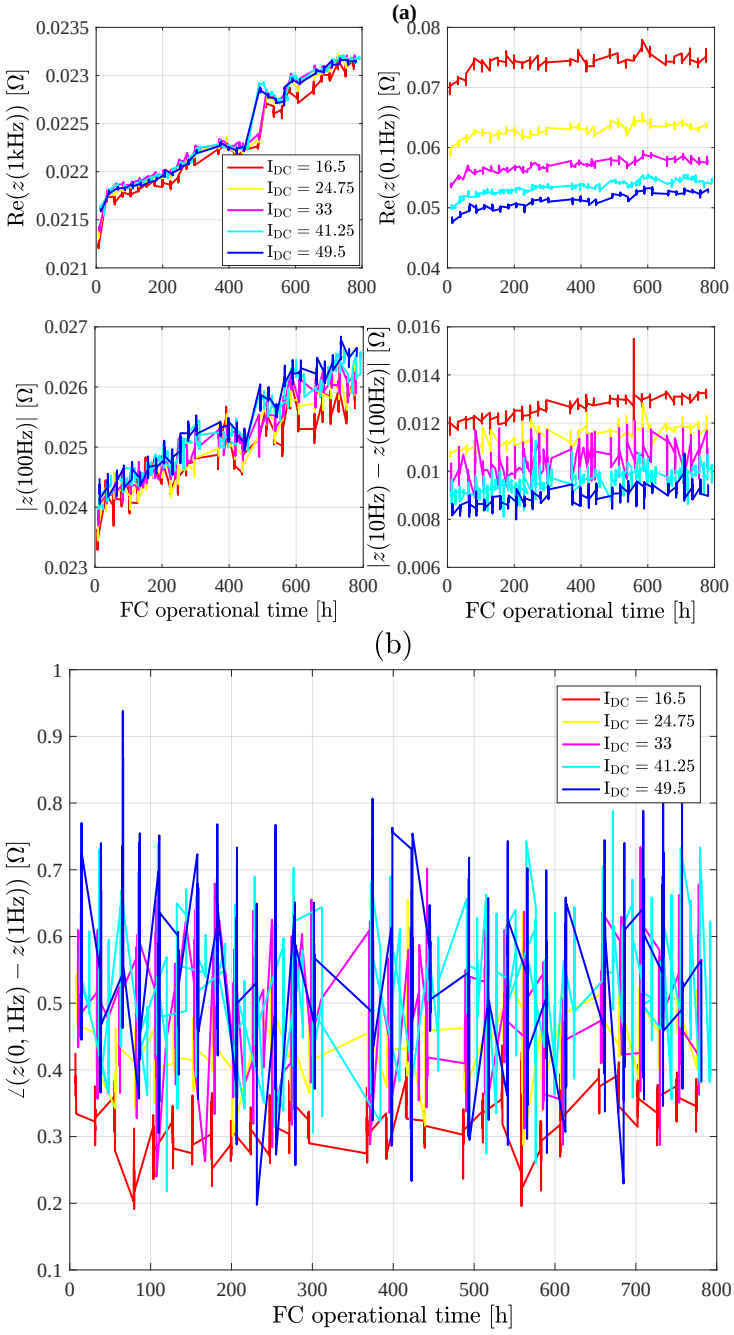

Figure 6: **(a)** Selection of features that change with degradation. All data for normal operation. **(b)** The feature f_3 for normal operational data, as function of the fuel cell operational time.

Table 3: Description of the three features, which is used as input to the ANN classifier.

Feature No.	**Description**
f_1	DC component of fuel cell current
f_2	$\angle\left(z(100\text{Hz}) - z(1\text{kHz})\right)$
f_3	$\angle\left(z(0.1\text{Hz}) - z(1\text{Hz})\right)$

faults considered in this work are listed in Table 1, and are for HTPEM applications. Some of the features above like the series resistance are therefore not useful for this algorithm. In addition, it can be seen that some extracted features change with degradation. This is illustrated in Figure 6(a), where 4 different extracted features are plotted with respect to degradation. In Figure 6(a), the top left is the internal series resistance (represented as the high frequency intercept) plotted with respect to fuel cell operational time, and the top right is the real value of the 0.1 Hz impedance point plotted. In Figure 6(a), the two bottom figures shows how the internal magnitude of the spectrum changes relatively to the operational time. It can be seen that the features shown in Figure 6(a), is changing with the operational time and thereby the degradation. It is not desirable to use features, that change with time, since the design of thresholds become difficult. When features change with time, the fault detection becomes more prone to false alarm or false detection.

A self-cognizant diagnostic methodology could solve this problem, by adapting to the change in features as result of degradation. Alternatively, a set of features that are constant for healthy operation and independent of degradation could be chosen, if possible.

Different methods to extract features from the impedance spectrum have been analyzed in this work, and three features were found to be independent of degradation and suitable for detecting the faults listed in Table 1. The methods suggested for feature extraction are listed in Table 3 as f_2 and f_3. The features f_2 and f_3 are angles between the frequencies decades 1 kHz to 100 Hz (f_1) and 1 Hz to 0.1 Hz (f_2). Since the features are angles of the spectrum, they are relative and do not change with respect to degradation. The feature f_1 is illustrated in Figure 6(b), as a function of the fuel cell operational time. In Figure 6.b it can also be seen that the feature f_1 is dependent on the fuel cell current and for this reason is the DC component of fuel cell current chosen as the third feature (f_1).

The behavior of the features f_2 and f_3 under normal and faulty conditions,

Table 4: Based on empirical analysis, how the features f_2 and f_3 changes, for the faults ϕ_1 - ϕ_5.

	ϕ_0	ϕ_1	ϕ_2	ϕ_3	ϕ_4	ϕ_5
f_2	-	-	-	$\uparrow$	$\downarrow$	-
f_3	-	$\uparrow$	$\downarrow$	-	-	$\downarrow$

is shown in Figure 7(a), for the entire data set at 16.5 A. As stated in Table 4, it can be seen that faults ϕ_3 and ϕ_4 are correlated with feature f_2 and the faults ϕ_1, ϕ_2 and ϕ_5 are correlated with feature f_3. Furthermore, it can be observed that a high methanol vapour in the anode gas (ϕ_4), is quite close to the normal operation data set. Thus, it is expected that that fault is harder to detect and isolate.

In Figure 7(b), the entire feature space with the entire data set is plotted. Here, it can be seen that the value of the features f_2 and f_3 changes with f_1, and therefore, it is necessary to include the DC component of the fuel cell current as a feature.

3.3. ANN classifier and the training

As fault detection and isolation classifier, a feed forward neural network is trained for the task. In Figure 8, an overview of the offline training is illustrated. Firstly, the experimental data from the experiment described in section 2.2, is labeled with a fault identifier (ϕ_0-ϕ_5) and the features (f_1 - f_3) are calculated for each of the 2010 EIS measurements. Next, the data set is divided into training data, validation data and test data. The test data is manually selected for ensuring that each fault case is equally represented. For each day at non-healthy operation two EIS measurements are reserved for testing at each current set point, and for each day at healthy operation one EIS measurement is reserved for testing at each current set point. The remaining data set is split randomly with 85 % for training and 15 % for validation. An overview of the allocation of the overall data is given in Table 5.

The training data is used in the training process of the ANN classifier, the validation data is used as a stop criteria for the training algorithm and the test data is used for human expert approval of the ANN classifier performance.

The feed forward ANN consists of one hidden layer with 10 neurons and with a tansig transfer function and an output layer with one outlet for each of the fault cases, with a softmax transfer function. No normalization of any of the inputs is performed.

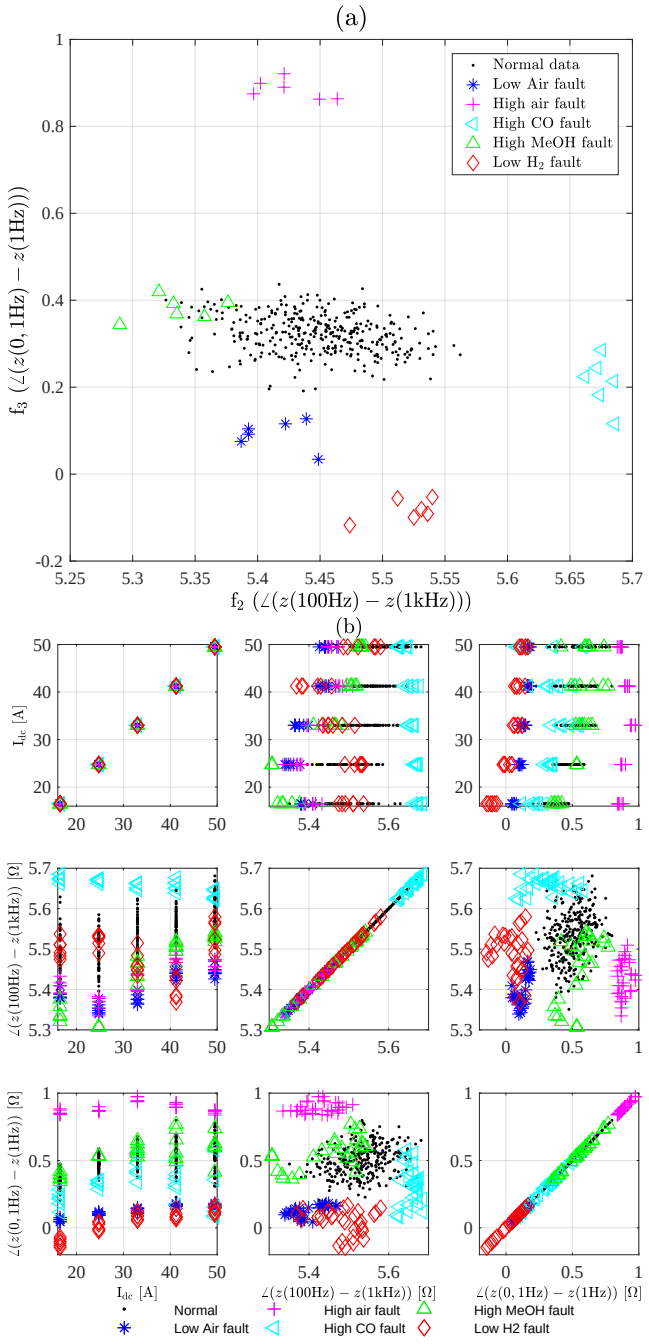

Figure 7: **(a)** Feature space $\{f_2\ ,\ f_3\}$ for the entire experiment at 16.5 A. **(b)** Feature space $\{f_1\ ,\ f_2\ ,\ f_3\}$ for the entire experiment.

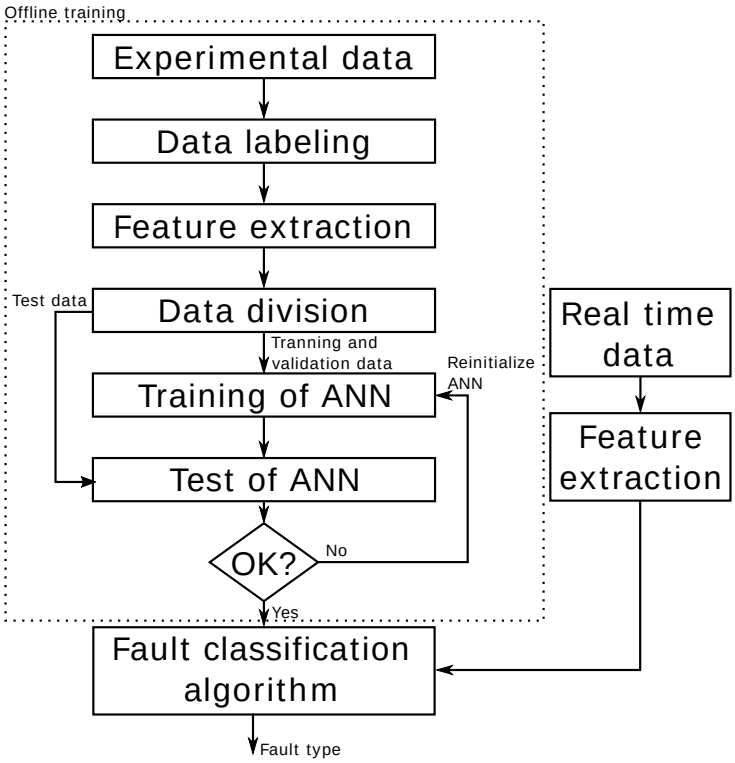

Figure 8: Offline procedure for the training of artificial neural network in the dashed square. For the online procedure, an EIS measurement is acquired, the feature extraction is calculated, and the features is used for input to the artificial neural network.

As training the scaled conjugate gradient optimization algorithm is utilized. As stop criteria for the training there are three options; 10 number of validation checks, where the ANN performance has not increased, the gradient becomes less than 10^{-6} or the performance becomes 0, where the performance is calculated as the Cross-Entropy.

4. Results and discussion

4.1. Training results accuracy and performance evaluation

The proposed ANN classifier methodology presented in the previous section, in combination with the proposed features, has in general proven to be well suited for fault detection and isolation, of the five faults (ϕ_1-ϕ_5) listed in Table 1.

Table 5: In percentage, how the entire dataset (2010 EIS measurements) is divided in the training, validation and test data subsets. Test dataset in selected, and the remaining data in randomly divided into training and validation data subsets.

	% of data
Training data	76 %
Validation data	14 %
Test data	10 %

Table 6: The result of the test data, listed in a confusion matrix. The results are listed in %. Global accuracy is 94.6 %.

		Target class					
		ϕ_0	ϕ_1	ϕ_2	ϕ_3	ϕ_4	ϕ_5
ANN output class	ϕ_0	98	0	0	0	70	0
	ϕ_1	0	100	0	0	0	0
	ϕ_2	0	0	100	0	0	0
	ϕ_3	0	0	0	100	0	0
	ϕ_4	2	0	0	0	30	0
	ϕ_5	0	0	0	0	0	100

The results of the test data (10% of the entire dataset) is listed in a confusion matrix between the ANN output and the actual target class, in Table 6. It can be seen that the faults ϕ_1, ϕ_2 and ϕ_3 and ϕ_5 have 100 % success rate. As it can be seen in Table 6, the ANN classifier has problems distinguishing between high methanol content fault and normal operation data. This is supported by Figure 2(a), where it can be seen that the impedance spectrum of high methanol vapour concentration in the anode gas fault (ϕ_4), is quite close to the impedance spectrum of the normal operation data (ϕ_0).

To improve detectability of fault ϕ_4, the methanol concentration could be increased. However, a methanol vapour concentration of 5% is considered a well-established fault and would not be considered as early detection. Furthermore, it is expected that a higher than 5% methanol vapour concentration would yield a impedance signature comparable to the high CO concentration fault (ϕ_3), and therefore, a higher than 5% methanol vapour concentration fault would only move the problem to distinguishing between high CO and high methanol concentrations.

The global accuracy of the test data classification using the proposed methodology is 94.6 %. This is good in line with previously reported values in the

literature, for LTPEM fuel cell FDI. Hissel et al. [25] reported a 89 % accuracy and Zheng et al. [19] reported a 100 % accuracy, both using a Fuzzy Clustering Algorithm. Onanena et al. [17] did a comparison of k-nearest neighbor and linear discriminant analysis with two different ways of feature extraction, which yielded a 93.9 % - 99.6 % accuracy for different methods.

4.2. Discussion

One of the benefits to this methodology, compared to using the parameters of an equivalent electrical circuit, is that it is not necessary to acquire the entire spectrum, but only impedance at four frequencies. To acquire an incomplete impedance spectrum is less time consuming than acquiring the full spectrum, which is an advantage since there are less risk that the fuel cell moves away from steady state operation. In this work, the entire impedance spectrum was acquired, and therefore, if only the relevant frequencies were measured, the pre-processing part of the methodology would need to be changed, e.g. by calculating the average of the impedance at the neighboring frequency points.

One of the major issues with EIS as reported in literature is complex data processing and time consuming process. Here in the present work the frequency domain is reduced and hence the data processing and the measurement time is relatively smaller. The accuracy level of the measurements in separating out the different faulty conditions are quite high which makes the process more promising and efficient. The FDI methodology from the present study could be easily implemented in the existing fuel cell system with minor modification provided the training is carried out offline. The study takes into account the degradation of the cell which makes the algorithm robust and minimal human interference as required in some others FDI methods proposed in the literature's.

This work builds on a data driven method, and there is no knowledge of how the methodology would perform if utilized on a different stack from another production batch. Therefore, for deploying this methodology in the field, a larger database with impedance data from different production batches is needed, since there is no information of the impedance variance from stack to stack in the literature.

Furthermore, this analysis was carried out on a 10 cell short stack, but normally a fuel cell of this type is deployed in the field in a 60 or 120 cells configuration. The experimental procedure would therefore need to be reinitialized for a full-size stack. Moreover, the impedance spectrum of full-size HTPEM

stack is not reported in literature, for the faults considered in this work. This could be subject of future studies.

The experiments for this work were performed on laboratory scale, with a Gamry galvanostat for impedance measurements. This implementation is quite expensive, and is therefore not suited for in-field implementation. However, some EU projects work on implementing the EIS characterization method on the onboard DC/DC converter (D-code project Grant: 256673). This requires great attention to the bandwidth of the DC/DC converter and requirements to the onboard computer. In this work all data processing was done offline, which would not be the case for a system in the field.

Based on this work, there is no evidence how the algorithm will perform for faults at intermediate fault amplitude. For-example, a larger concentration of CO (ϕ_3) could resemble the low anode stoichiometry fault (ϕ_5) or a lower concentration of CO could resemble the high methanol vapour concentration fault (ϕ_4). This could be subject of future studies.

5. Conclusions

In this work a methodology for fault detection and isolation of low and high cathode stoichiometry, high CO concentration in the anode gas, high methanol vapour concentration in the anode gas and low anode stoichiometry was proposed. The fault detection and isolation methodology is data driven based on EIS impedance spectrum.

The fault detection and isolation is divided into 4 steps; acquiring of EIS measurement, pre-processing of data, feature extraction and artificial neural network classification of fault class. The pre-processing of the impedance spectrum is conducted by a zero phase Butterworth filter, which is used to remove outliers. The extracted features used in this work are the DC component of the fuel cell current, and two angles between the impedance at 100 Hz and 1 kHz and between 0.1 Hz and 1 Hz.

A broad selection of features is analyzed with respect to degradation, and it is found that the selected features are robust towards degradation. Therefore, there is no need to retrain the artificial neural network classifier.

The experimental data foundation is based on a 35 day experiment, where the first week is fault free and hereafter a new fault is introduced on the last day of the week, for the remainder 3 weeks. This results in 2010 unique EIS measurements under the influence of degradation.

The proposed fault detection and isolation methodology is based on an artificial neural network classifier, which is trained on 76 % of the entire data-set and validated on 14 % of the data-set. 10 % of the data-set is used for testing the algorithm.

Overall global accuracy on the test data is 94.6 %, which is considered a good result, and it can be concluded that the artificial neural network together with the suggested features, is feasible for fault detection and isolation. The achieved accuracy for faults related to CO pollution, anode- and cathode stoichiometry is 100 % success rate. It can be concluded that the proposed algorithm has difficulties distinguishing between the high methanol vapour concentration in the anode gas fault and normal operational data.

Acknowledgments

The work was supported by Innovation Fund Denmark in the frame of the 4M Centre. The authors would also like to acknowledge SerEnergy A/S for supplying the short-stack for experimental work.

References

References

[1] M. Becherif, H. S. Ramadan, K. Cabaret, F. Picard, N. Simoncini, O. Bethoux, Hydrogen Energy Storage: New Techno-Economic Emergence Solution Analysis, Energy Procedia 74 (0) (2015) 371–380. doi:10.1016/j.egypro.2015.07.629.

[2] J. Andrews, B. Shabani, Re-envisioning the role of hydrogen in a sustainable energy economy, International Journal of Hydrogen Energy 37 (2) (2012) 1184–1203. doi:10.1016/j.ijhydene.2011.09.137.

[3] G. Gahleitner, Hydrogen from renewable electricity: An international review of power-to-gas pilot plants for stationary applications, International Journal of Hydrogen Energy 38 (5) (2013) 2039–2061. doi:10.1016/j.ijhydene.2012.12.010.

[4] G. Krajačić, R. Martins, A. Busuttil, N. Duić, M. da Graça Carvalho, Hydrogen as an energy vector in the islands' energy supply, International Journal of Hydrogen Energy 33 (4) (2008) 1091–1103. doi:10.1016/j.ijhydene.2007.12.025.

[5] D. Teichmann, W. Arlt, P. Wasserscheid, Liquid Organic Hydrogen Carriers as an efficient vector for the transport and storage of renewable energy, International Journal of Hydrogen Energy 37 (23) (2012) 18118–18132. doi:10.1016/j.ijhydene.2012.08.066.

[6] Q. Li, R. He, J. Jensen, N. Bjerrum, Approaches and recent development of polymer electrolyte membranes for fuel cells operating above 100 C, Chemistry of materials (2003) 4896–4915doi:10.1021/cm0310519.

[7] S. S. Araya, F. Zhou, V. Liso, S. L. Sahlin, J. R. Vang, S. Thomas, X. Gao, C. Jeppesen, S. K. Kær, A comprehensive review of PBI-based high temperature PEM fuel cells, International Journal of Hydrogen Energy 41 (46) (2016) 21310–21344. doi:10.1016/j.ijhydene.2016.09.024.

[8] G. A. Olah, A. Goeppert, G. K. S. Prakash, Chemical recycling of carbon dioxide to methanol and dimethyl ether: From greenhouse gas to renewable, environmentally carbon neutral fuels and synthetic hydrocarbons, Journal of Organic Chemistry 74 (2) (2009) 487–498. doi:10.1021/jo801260f.

[9] U.S. DOE., The Fuel Cell Technologies Office Multi-Year Research, Development, and Demonstration Plan, Tech. rep., U.S. Department of Energy (2016).
URL `https://energy.gov/eere/fuelcells/fuel-cells`

[10] D. Hissel, M. Pera, Diagnostic & health management of fuel cell systems: Issues and solutions, Annual Reviews in Control 42 (2016) 201–211. doi:10.1016/j.arcontrol.2016.09.005.

[11] C. Cadet, S. Jemeï, F. Druart, D. Hissel, Diagnostic tools for PEMFCs: from conception to implementation, International Journal of Hydrogen Energy 39 (20) (2014) 10613–10626. doi:http://dx.doi.org/10.1016/j.ijhydene.2014.04.163.

[12] R. Petrone, Z. Zheng, D. Hissel, M. C. Péra, C. Pianese, M. Sorrentino, M. Becherif, N. Yousfi-Steiner, A review on model-based diagnosis methodologies for PEMFCs, International Journal of Hydrogen Energy 38 (17) (2013) 7077–7091. doi:10.1016/j.ijhydene.2013.03.106.

[13] Z. Zheng, R. Petrone, M. C. Péra, D. Hissel, M. Becherif, C. Pianese, N. Yousfi Steiner, M. Sorrentino, A review on non-model based

diagnosis methodologies for PEM fuel cell stacks and systems, International Journal of Hydrogen Energy 38 (21) (2013) 8914–8926. doi:10.1016/j.ijhydene.2013.04.007.

[14] P. Polverino, C. Pianese, M. Sorrentino, D. Marra, Model-based development of a fault signature matrix to improve solid oxide fuel cell systems on-site diagnosis, Journal of Power Sources 280 (2015) 320–338. doi:10.1016/j.jpowsour.2015.01.037.

[15] T. Génevé, J. Régnier, C. Turpin, Fuel cell flooding diagnosis based on time-constant spectrum analysis, International Journal of Hydrogen Energy 41 (1) (2016) 516–523. doi:10.1016/j.ijhydene.2015.10.089.

[16] G. Mousa, J. Devaal, F. Golnaraghi, Diagnosis of hydrogen crossover and emission in proton exchange membrane fuel cells, International Journal of Hydrogen Energy 39 (35) (2014) 20116–20126. doi:10.1016/j.ijhydene.2014.09.116.

[17] P. A. R. Onanena, L Oukhellou, E Côme, D Candusso, D Hissel, Fault-diagnosis of PEM fuel cells using electrochemical spectroscopy impedance, Power Plants and Power Systems Control (2012) 651–656doi:10.3182/20120902-4-FR-2032.00114.

[18] A. Debenjak, M. Gašperin, B. Pregelj, M. Atanasijević-Kunc, J. Petrovčič, V. Jovan, Detection of flooding and drying inside a PEM fuel cell stack, Strojniski Vestnik/Journal of Mechanical Engineering 59 (1) (2013) 56–64. doi:10.5545/sv-jme.2012.640.

[19] Z. Zheng, M. C. Péra, D. Hissel, M. Becherif, K. S. Agbli, Y. Li, A double-fuzzy diagnostic methodology dedicated to online fault diagnosis of proton exchange membrane fuel cell stacks, Journal of Power Sources 271 (2014) 570–581. doi:10.1016/j.jpowsour.2014.07.157.

[20] C. Jeppesen, M. Blanke, F. Zhou, S. J. Andreasen, Diagnosis of CO Pollution in HTPEM Fuel Cell using Statistical Change Detection, IFAC-PapersOnLine 48 (2015) 547–553. doi:10.1016/j.ifacol.2015.09.583.

[21] C. de Beer, P. Barendse, P. Pillay, B. Bullecks, R. Rengaswamy, Electrical circuit analysis of CO poisoning in high temperature PEM fuel cells for rapid fault diagnostics, 2013 IEEE Energy Conversion Congress and Exposition 51 (1) (2013) 4623–4630. doi:10.1109/ECCE.2013.6647320.

[22] R. Chattot, S. Escribano, Ageing studies of a PEM Fuel Cell stack developed for reformate fuel operation in μCHP units: Development of an accelerated degradation procedure, International Journal of Hydrogen Energy 0 (2014) 1–8. doi:10.1016/j.ijhydene.2015.01.066.

[23] R. Onanena, L. Oukhellou, D. Candusso, F. Harel, D. Hissel, P. Aknin, Fuel cells static and dynamic characterizations as tools for the estimation of their ageing time, International Journal of Hydrogen Energy 36 (2) (2011) 1730–1739. doi:10.1016/j.ijhydene.2010.10.064.

[24] P. Moçotéguy, B. Ludwig, J. Scholta, R. Barrera, S. Ginocchio, Long term testing in continuous mode of HT-PEMFC based H3PO 4/PBI celtec-PMEAs for μ-CHP applications, Fuel Cells 9 (4) (2009) 325–348. doi:10.1002/fuce.200800134.

[25] D. Hissel, D. Candusso, F. Harel, Fuzzy-clustering durability diagnosis of polymer electrolyte fuel cells dedicated to transportation applications, IEEE Transactions on Vehicular Technology 56 (5 I) (2007) 2414–2420. doi:10.1109/TVT.2007.898389.

[26] S. M. Rezaei Niya, M. Hoorfar, Study of proton exchange membrane fuel cells using electrochemical impedance spectroscopy technique - A review, Journal of Power Sources 240 (2013) 281–293. doi:10.1016/j.jpowsour.2013.04.011.

[27] J. R. Vang, S. J. Andreasen, S. S. Araya, S. K. Kær, Comparative study of the break in process of post doped and sol-gel high temperature proton exchange membrane fuel cells, International Journal of Hydrogen Energy 39 (27) (2014) 14959–14968. doi:10.1016/j.ijhydene.2014.07.017.

[28] N. V. Dale, M. D. Mann, H. Salehfar, A. M. Dhirde, T.-H. Han, ac Impedance Study of a Proton Exchange Membrane Fuel Cell Stack Under Various Loading Conditions, Journal of Fuel Cell Science and Technology 7 (3) (2010) 031010. doi:10.1115/1.3207871.

[29] A. V. Oppenheim, W. S. Ronald, J. R. Buck, Discrete-Time Signal Processing, 2nd Edition, Prentice Hall, 1999.

[30] E. Alpaydin, Introduction to Machine Learning, 2nd Edition, The MIT Press, 2010.

[31] N. Fouquet, C. Doulet, C. Nouillant, G. Dauphin-Tanguy, B. Ould-Bouamama, Model based PEM fuel cell state-of-health monitoring via ac

impedance measurements, Journal of Power Sources 159 (2) (2006) 905–913. doi:10.1016/j.jpowsour.2005.11.035.

[32] Z. Zheng, R. Petrone, M. C. Pera, D. Hissel, M. Becherif, C. Pianese, Diagnosis of a commercial PEM fuel cell stack via incomplete spectra and fuzzy clustering, IECON Proceedings (Industrial Electronics Conference) (2013) 1595–1600doi:10.1109/IECON.2013.6699371.

ISSN (online): 2446-1636
ISBN (online): 978-87-7112-918-2

AALBORG UNIVERSITY PRESS